ADVANCED OXIDATION PROCESSES FOR TREATMENT OF PHARMACEUTICAL WASTEWATER

Thesis
Submitted in Partial
Fulfillment of the Requirements for the Degree of
DOCTOR OF PHILOSOPHY

by

Ardhendu Sekhar Giri

Under Supervision
of
Dr. Animes K Golder

Department of Chemical Engineering
Indian Institute of Technology Guwahati
October 2014

ABSTRACT

Pharmaceutically active compounds (PhACs) are mostly released into the environment for decades without proper treatment and toxicity assay. Typical PhACs include antibiotics, analgesics, anti-depressants, beta-blockers, and hormones & hormone mimics. Recently, efforts have been made to quantify the impact of these compounds on the ecosystem and public health. Advanced oxidation processes (AOPs) seem to be promising for the decomposition of PhACs and personal care products from industrial and municipal wastewater.

The decomposition behavior of three PhACs i.e., chloramphenicol (CHPL), ciprofloxacin (CIP) and dipyrone (DIPY) at higher concentration were investigated in Fenton process (FP), photo-Fenton process (PFP), UV-photolysis (UVP) and UV-TiO_2 photocatalysis (UVPC).

The study on CHPL aimed on the formation of Fe^{2+}-chloramphenicol complex (FeCHPLCOM) and degradation of CHPL-FeCHPLCOM mixture. LC-MS spectra evidenced for formation of charge transfer FeCHPLCOM at 1:1 CHPL to Fe^{2+} ratio. CHPL acted as a bidented ligand coordinated with Fe^{2+}. IR study uncovered that ligand to metal bonding weakened the stretching frequency of both O-H bond and –C=O group through coordination with Fe^{2+}. The enhanced FeCHPLCOM degradation (13.4% more) was found in photo-assisted Fenton reaction. The asymmetry centres of CHPL with weakly bonded hydrogen atoms of high nucleophilic character were the most preferred sites of $HO^{\bullet}$ attack. CHPL was oxidized through segmentation of the aliphatic chain attached to benzene ring under acidic conditions (pH 3). The toxicity of CHPL to *Escherichia coli* (*E. coli*) XL 10GOLD decreased significantly after 45 min of decomposition with the order as, PFP>FP>UVP.

Maximum CIP cleavage of 74.4, 78.4 and 52.7% was achieved in FP, PFP and UVP at pH 3.5 with an initial concentration of 15 mg/L. The mean oxidation number of carbon (MONC) determined in terms of COD and TOC value was well accordance to that of from the oxidation number of individual carbon atom. MONC increased to 1.68, 2.1, 1.42 from the initial value of 1.28 in FP, PFP and UVP, respectively. The result can be corroborated by the refractory nature of the quinolone moiety and oxidation of greater numbers of products in PFP. A simple 2^{nd} order kinetic model was proposed for the oxidation of CIP and degradation products (DP_s) with respect to $HO^{\bullet}$ concentration. The concentration of $HO^{\bullet}$ radical was measured by N, N-dimethyl phenyl hydrazine method using dimethyl sulphoxide as a probe. CIP and DP_s fairly followed the 2^{nd} order kinetic equation. The initial concentration of $HO^{\bullet}$

was found to be 11.67, 11.91 and 11.08 µM in FP, PFP and UVP. The rate constants of 3.13×10^3 and 4.89×10^3, 4.37×10^3 and 5.09×10^3, 3.53×10^3 and 3.91×10^3 1/M.s were estimated for CIP and DP_s in FP, PFP and UVP, respectively. Total twenty six intermediates appeared in the mass spectra with six common products in all three processes. The breakage of piperazine ring was more effective in CIP oxidation due to high nucleophilic character of lone pair of electron present on nitrogen atom. CIP decomposition in PFP gave the lowest antimicrobial activity with 24.3 to 30.5 % lower *E. coli* death compared to FP and UVP.

DIPY is very quickly hydrolyzed to 4-methylaminoantipyrine (4-MAA) in an acidic solution. Maximum 4-MAA removal of 94.1, 96.4, 74.4 and 71.2% were achieved in FP, PFP, UVP and UVPC, respectively, against mineralization of 49.3, 58.2, 47 and 24.6%. The proposed mechanisms suggest that the cleavage of three methyl moieties followed by pyrazolinone ring breakage led to formation of various intermediates with low errors (-0.86 to 0.46 g/mole). The intermediates primarily were hydroxylated and carboxylic derivatives. BOD_5 to COD ratio of $\geq$0.4 was resulted in all oxidation processes with the highest value in PFP. The collapse of Fe(III)-chelates under UV irradiation gave higher biodegradability. The ease of biodegradability was found to be, PFP>>FP>UVP>UVPC. 4-MAA solution of 50 mg/L caused the complete suppression of *E. coli* growth.

An equimolar molar mixture (each of 0.05 mM) of CHPL, CIP and DIPY (CCD) was investigated and compared with single drug treatment at the same concentration. The degradation efficiency was likely hindered (maximum 12.5 %) in CCD treatment due to formation of common ions like Cl^-, F^-, NH_4^+ and NO_3^-. Addition of the same ion i.e. Cl^- and F^- could release upon cleavage of CHPL and CIP in CCD mixture suppressed the decomposition efficiency by about 6.5, 11.9, 15.9 and 5.9, 12.4, 20.8 % in FP, PFP and UVP, respectively. The major intermediates appeared in the mass spectra in combination of ion chromatograph were used to validate the routes of CCD decomposition and evolution of inorganic ions. A reciprocal relation between the biodegradability index and antimicrobial activity was observed for all the PhACs used in the present work irrespective to the process of oxidation. It varied from 0.29 to 1.51 and 86.7 to 35.2 % (death of *E. coli*), respectively.

TABLE OF CONTENTS

CERTIFICATE

*This is to certify that the thesis entitled "**Advanced Oxidation Processes for Treatment of Pharmaceutical Wastewater**", being submitted by **Mr. Ardhendu Sekhar Giri,** to the Indian Institute of Technology Guwahati, India, for the award of Doctor of Philosophy, is a record of bonafide research work carried out by him under my guidance and supervision. The work embodied in this thesis has not been submitted for any other degree or diploma. In my opinion, the thesis is up to the standard of fulfilling the requirements of the doctoral degree as prescribed by the regulations of this Institute.*

Date:

Dr. Animes K Golder
[Thesis Supervisor]
Associate Professor
Department of Chemical Engineering
Indian Institute of Technology Guwahati

Dedication

To My Parents and Family

ACKNOWLEDGEMENT

The doctoral work has been an unforgettable experience for me and it would not possible without these people.

First and foremost, I would like to thank my thesis supervisor **Dr. Animes K Golder**, for giving me an opportunity to work in a very interesting area of research. I am very grateful to Dr. Golder for his continuous guidance, important advices and stimulating discussions. In spite of his busy schedule, he always happily spends time to analyze problems and gave needed suggestions for the betterment of my work. Some of his notable qualities such as, patience during work, his depth of perfection and attractive presentation skills, will always continue to inspire me. The experience of working with him will have far-reaching influence in my future life. I consider it an honor to work under him.

I am thankful to all the Professors of Chemical Engineering Department at IIT Guwahati. I am also thankful to Prof. Mahamad Jawed, Civil Engineering Department at IIT Guwahati, instructor of the course titled 'Physicochemical Properties of Wastewater' for teaching many fundamental topics related my research work. I would like to thank my doctoral committee members, Prof. Bishnupada Mandal, Dr. Chandan Das, Department of Chemical Engineering and Prof. Mahamad Jawed**,** Department of Civil Engineering, for their valuable suggestions and efforts which made my thesis successful.

It is a pleasure to acknowledge to Prof. Aloke Kumar Ghoshal, Prof. Pallab Ghosh, Dr. Mihir Kumar Purkait, Dr. Ashok Kumar Das Mahapatra, and Dr. Kaustubha Mohanty for their encouragement and supporting me during this work.

My sincere thanks to Dr. Mahesh Kumar Gagrai and Dr. Kartick Mondal, for their co-operative assistance in learning the basics concepts and provided me constant source of encouragement throughout my Ph.D.

I am also thankful to my senior research colleagues Dr. Samen Jana, Dr. Vijay Sing, Dr. Avijit Ghosh, Dr. Soumay Sasmal, Dr. Rajen Kundu and Mr. Amaresh Sahoo.

I would like to thank my fellow research scholars Mrs. Chitrita Kumdu, Mr. Mriganka Sekhar Manna, Mr. Sanjib Barma, Mr. Rajeev Parmar, Mr. Soumyadeep Chakraborty, Mr. Dhamodharan K., Mr. Kulkarni Vihangraj Vijaykumar, Mr. Md. Palashuddin Sk and Mr. Gaurav Kumar.

I am particularly grateful to my batch mates Mr. Anand Babu Desamala, Mr. Ruhit Jyoti Konwar, Mr. Sriharsha Emani, Mr. Yennam Rajesh and Mr. M. Shivaih for their help and support.

I am also thankful to present research group members Mr. Arijit Das., Mr. Raj Kumar Das, Mr. Ch Venkatanarasimha Rao, Mr. Suman Saha, Mr. Sujoy Bose, Mr. Kibrom Albel Gebru, Mr. Amit Kumar Behera, Mr. Satyadip Chakraborty, Mrs. Versha Rani, and last but not the least Mrs. M. Malika.

I cannot forget to thank my friends Mr. Sankar Chakma, Mr. Arya Das, Mr. Arnab Ghosh, Mr. Sayantan Samanta, Mr Somnath Mondal, for the lovely support in making my stay at IIT Guwahati memorable.

After all I would like to thank all departmental and office stuffs for helping me in many ways for my research work.

Deep heartedly, I thank my parents and my family members for their encouragement, blessings and motivation at each and every step.

Last, but not least, I thank the Almighty God for giving me strength to overcome difficulty, which crossed my way to be a pole star.

I dedicate this thesis to *My Family.*

ARDHENDU SEKHAR GIRI

LIST OF FIGURE CAPTIONS

LIST OF TABLE CAPTIONS

Mr. ARDHENDU SEKAR GIRI

Date of Birth: **18th February 1982**
Email: **a.giri@iitg.ernet.in**

Educations:

Ph.D. pursuing
Department of Chemical Engineering
Indian Institute of Technology, Guwahati
Guwahati, Assam, India
200- 2014
Marks obtained: 7.5 (CPI), 1st Class

M. Tech in Chemical Engineering
Department of Chemical Engineering
University of Calcutta
Kolkata, West Bengal, India
2007-2009
Marks obtained: 71.1%, 1st Class

B. Tech in Chemical Engineering
Department of Chemical Engineering
University of Calcutta
Kolkata, West Bengal, India
2004-2007
Marks obtained: 64.5%, 2nd Class

B.S. in Chemistry honors
University of Calcutta
Department of Chemistry
Asutosh College
Kolkata, West Bengal, India
2000-2004
Marks obtained: 59.8%, 2nd Class

Higher Secondary in Science
W.B.C.H.S, West Bengal, India
2000
Marks obtained: 73.4%, 1st Class

Secondary Education
W.B.B.S.E, West Bengal, India
1998
Marks obtained: 69%, 1st Class

Publications

Journal papers:

1. **A.S. Giri** and A. K. Golder, "Formation of Fe(II)-Chloramphenicol Chelate and its Decomposition in Fenton and Photo-Fenton: Identification and biodegradability assessment of primary by products", ***Ind. Eng. Chem. Res.***, **DOI: 10.1021/ie501508d**.
2. **A.S. Giri** and A. K. Golder, "Fenton, Photo-Fenton, H_2O_2-photolysis and TiO_2 photo-catalysis for Dipyrone oxidation: Drug removal, mineralization, biodegradability and degradation mechanism", ***Ind. Eng. Chem. Res.***, 2014, 53 (4), 1351-1358.
3. **A.S. Giri** and A. K. Golder, "Ciprofloxacin degradation from aqueous solution by Fenton oxidation: Reaction kinetics and degradation mechanisms", ***RSC Adv.,*** 2014, 4, 6738-6745.
4. **A.S. Giri** and A. K. Golder, "Kinetics and Mechanisms of Ciprofloxacin Cleavage in Light Assisted Fenton Reaction***", International Journal of Recent Research in Science and Technology,*** 2014, 6(1), 78-82
5. **A.S. Giri** and A. K. Golder, "Drug mixture decomposition in photo-assisted Fenton process: comparison to singly treatment, evolution of inorganic ions and toxicity assay" (Under review).
6. **A.S. Giri** and A. K. Golder, "Synthesis and characterization of ZnO-TiO_2 Nano composites for Ciprofloxacin degradation: Determination of intermediates and reaction pathways" (To be submitted).
7. Ch.V. Rao, **A.S. Giri**, V.V. Goud and A.K. Golder, "Degradation of brilliant green dye in Fenton oxidation: Influence of Fe(II)/ Fe(III) and Decomposition mechanism", ***CLEAN- Soil Air Water*** (Revised manuscript submitted).

Conference publications:

1. **A.S. Giri** and A.K. Golder, "Degradation of pharmaceutical from wastewater: Oxidative Fenton process", Chemical Engineering Congress (CHEMCON-2011), 27-30th December, 2011, Bangalore, India.
2. **A.S. Giri** and A.K. Golder, "Fenton Oxidation Process for the removal of an antimicrobial drug from wastewater", 2nd International Conference on Advanced Oxidation Processes (AOP 2012), 5-8th October, 2012, Kottayam, Kerala.
3. **A.S. Giri** and A.K. Golder, "Oxidative degradation of Dipyrone from wastewater using Fenton reagent", Indian Chemical Engineering Congress (CHEMCON-2012), 27-30th December, 2012, Dr. B.R. Ambedkar National Institute of Technology, Jalandhar, Punjab, India.
4. **A.S. Giri** and A.K. Golder, "Dynamics of Photo Fenton Process for Dipyrone Degradation and Hydroxyl Radical Quantification", International Exhibition and Conference on Water Technologies and Environmental Technology and renewable Energy (OMICS group), 11-14th February, 2013, Bombay Exhibition Centre, Mumbai.
5. **A.S. Giri** and A.K. Golder, "Mechanism and identification of reaction byproducts for the degradation of Chloramphenicol drug in heterogeneous photo-catalytic Process", International Conference on Chemical and Bioprocess Engineering (ICCBPE-2013), 16-17th November, 2013, Department of Chemical Engineering, National Institute of Technology Warangal, Andhra Pradesh, India.

6. **A.S. Giri** and A.K. Golder , "Mechanism and identification of reaction byproducts for the degradation of an antibiotic drug in heterogeneous photo-catalysis using TiO_2", International Conference on Frontiers in Chemical Engineering (ICFCE-2013), 9-11th December, 2013, NIT Rourkela, Orissa, India.
7. **A.S. Giri** and A.K. Golder, "Photolytic decomposition of aqueous Ciprofloxacin: Transformation products and mechanisms", Indian Chemical Engineering Congress (CHEMCON-2013), 27-30th December, 2013, Institute of Chemical Technology, Mumbai, India.
8. **A.S. Giri** and A.K. Golder, "Kinetics and mechanisms of Ciprofloxacin cleavage in light assisted Fenton reaction", Emerging Challenges and Issues in Environmental Protection, 23-24th January, 2014, Raipur Institute of Technology, Raipur (C.G.), India.

Symposium:

1. **A.S. Giri** and A.K. Golder, "Degradation of dipyrone in water by photo-assisted Fenton reaction: treatment of solid waste and toxicity study", presented in RECYCLE-2014 in Civil Engineering Department, 6th April, 2014, IIT Guwahati, Assam, India.
2. **A.S. Giri** and A.K. Golder, "Degradation of Dipyrone in water by heterogeneous photo catalytic reaction: Degradation mechanism and reaction pathways", presented in Reflux-1.0 in Chemical Engineering Department, 27-29th March, 2013, IIT Guwahati, Assam, India.
3. **A.S. Giri** and A.K. Golder, "The fate of Chloramphenicol during degradation from wastewater using Fenton oxidation process", Presented in an one day symposium on 'environment and us' on World Environment Day, IIT Guwahati, Assam, India, 5th June 2012, Technical Session 2, Poster 2A (2012).

Awards:

1. Best presentation award for the paper entitled "Mechanism and identification of reaction byproducts for the degradation of an antibiotic drug in heterogeneous photo-catalysis using TiO_2", in International Conference on Frontiers in Chemical Engineering (ICFCE-2013), 9-11th December, 2013, NIT Rourkela, Orissa, India.
2. Best presentation award for the paper entitled "Degradation of dipyrone in water by heterogeneous photo catalytic reaction: Degradation mechanism and reaction pathways", in Reflux-2.0-Annual Chemical Engineering Symposium, Department of Chemical Engineering, 29-30th March, 2014, IIT Guwahati, Assam, India.

CHAPTER 1

Introduction and Literature Survey

This chapter introduces the problem, includes literature survey and outlines the research objectives.

1.1 Overview

Pharmaceutically active compounds (PhACs) are generally designed to produce a biological activity on humans and animals. Manufacturing processes of PhACs lead to release of toxic organic compounds and their metabolites into the environment. The side effects of pharmaceuticals on human and animal health are usually investigated through the safety and toxicology studies (Stumpf et al., 1999). PhACs can create a biological activity well below the concentrations usually used in the safety tests. Many PhACs and their metabolites are nowadays are detected not only in wastewater but also in drinking water. More recently, significant concentrations of antidepressant drugs are found in the tissue of brook trout, a freshwater food fish, exposed to wastewater that had gone through primary treatment (Huber et al., 2005). Also the breakdown products and the combinations of different biologically active compounds may have unanticipated effects on the environment. Large amounts of veterinary medicines, such as antibiotics, antifungal and parasiticidal agents also contribute to the stress on the environment. They often directly enter into soils and surface water. Whereas, human medicines usually enter through the water treatment facilities, excretion and disposal of unused drugs into sewage systems or landfills.

In India, pharmaceutical wastewater is released indiscriminately into the environment without proper or any treatment. Proper removal of PhACs present in water and wastewater has an important role in the prevention of diseases both in humans and animals. PhACs are structurally complex organic compounds and also possess some inherent characteristics. For

this reason, treatment of pharmaceutical wastewater using conventional treatment processes namely, adsorption, membrane based separations, ion-exchange and biological treatment are not that efficient for the industrial applications (Murphy et al., 2005). Environmental researchers are continuously working to develop technically, environmentally and economically sound treatment techniques.

1.1.1 Environmental impact of pharmaceuticals waste

In the past few years, several attempts have been made to quantify the impact of PhACs on the environment. Low levels of PhACs are detected in surface, ground and drinking water resources apart from wastewater effluent throughout the Globe (Kolpin et al., 2002). PhACs include antibiotics, analgesics, anti-depressants, beta-blockers, and hormones & hormone mimics. PhACs undergo additional transformations within a wastewater treatment plant (WWTP). However, the removal efficiency is highly variable and it can be substantially less than 100%. Many PhACs may be accumulated to the measurable levels in aquatic ecosystems due to their relatively long environmental half-life (Carballa et al., 2005). Individual PhACs are generally measured at concentrations less than one part per billion, while the combined concentrations even exceed parts per million ranges (Kolpin et al., 2002). PhACs are designed to be highly active and interactive with receptors in humans and animals or they are toxic towards health threatening organisms such as bacteria, fungi and parasites. Many smaller animals have receptor systems similar to humans and bigger animals. Moreover, various types of organisms capable of affecting human and animal health are also targeted by PhACs. It is therefore possible that PhACs may affect the aquatic and terrestrial organisms (Adams et al., 2002). They are usually exposed to waste PhACs for a long duration. For this reason, researchers have started to investigate the effects caused by long-term low-level exposure of organisms to PhACs (Ahmed et al., 1999).

Analgesic and anti-inflammatory drugs are ubiquitous in effluents of municipal WWTPs. They are among the major pharmaceutical pollutants in recipient water at concentrations even up to µg/L. For an example, diclofenac is found in WWTP effluent concentration as high as 1.4 µg/L (Ternes et al., 2003). Most of the members of this group are acidic in nature because they contain carboxylic moieties and one or two phenolic hydroxyl groups. Antibiotics are common medicines to prevent or treat bacterial infections. In addition, they are used in veterinary applications as food additives at sub-therapeutic doses to improve feed efficiency and promote growth (Ellis et al., 2006). Carballa et al. (2005) reported that wide application of antibiotics may lead to bacterial resistances. The occurrence of antibiotics

in sewage sludge of WWTPs and surface is well reported (Li et al., 2013; Gulkowska, et al., 2008). Common PhACs present in various industrial effluents is summarized in Table 1.1.

Table 1.1. Common PhACs in wastewater and typical applications (Yang et al., 2006).

Sub-group	Compounds	Common uses
Analgesics	Acetaminophen Acetylsalicylic acid Dipyrone	Antipyretic, Pain reliever
Anti-epileptic drugs	Carbamazepine	Anticonvulsant
Antihyper-lipidemics	Fenofibric acid	Lipid regulator
Antibiotics	Chloramphenicol Ciprofloxacin Erythromycin Sulfamethoxazole	To treat bacterial infection
Polycyclic musks	Acetyl-hex methyl-tetrahydro-napthalene (AHTN)	Fragrance
Cyclopentabenzopyran	Diclofenac Ibuprofen	Anti-inflammatory

1.1.2 Sources of PhACs in water and wastewater

Agriculture and agriculture industry: Variety of PhACs made from recombinant proteins potentially has greater efficacy and fewer side effects than small organic molecules (Kulakovskaya et al., 2012). Recombinant proteins are most commonly produced using bacteria or yeast (Conesa et al., 2010). However, the production of recombinant proteins or their metabolic products using pharmings does not require expensive infrastructure. Also the production capacity can be quickly scaled up to meet the demand. It is estimated that the expense of producing a recombinant protein via pharming will be less than 70% of the current cost (Hartmann et al., 1997). Agriculture industry uses large amount of water and also causes extensive pollution, primarily by introducing nonpoint-source of contaminants. Runoff from agricultural fields often contains eroded soil, fertilizers, pharmaceuticals and pesticides that together form a major source of water pollution (Giri et al., 2011).

Health care facilities: Huge amounts of erythromycin (ERE) and vancomycin (VRE) are isolated from urban and hospital wastewater (Nie et al., 2013). It appears that they could pass through WWTPs and be transferred to surface water (Filiz et al., 2010). Antibiotics and disinfectants are supposed to disturb the wastewater treatment processes and the microbial ecology in surface water (Kim et al., 2010). About 40 PhACs including antidepressants, non-

steroidal anti-inflammatories, analgesics, hypolipidemics, alpha- and beta-blockers, anti-cancer drugs, anti-fungal agents, opiates, antibiotics, anti-coagulants, diuretics, anti-anginals and anti-diabetics are detected by Chang and co-workers (2010) in hospitals effluents. Unregulated disposal of unused and expired medicines are the primary inception of PhACs into the environment from hospitals and health care facilities (Chang et al., 2010). Another important source of PhACs is rejection of syringe into the hospital drain off after application on the patient's body (Huseyin et al., 2006).

Surface water and ground water: The residues of pharmaceutical products can enter into the aquatic environment due to incomplete elimination in WWTPs (Goutama et al., 2007). The typical concentration of pharmaceutical substances in water and solid wastes is summarized in Table 1.2. However, the concentration in untreated industrial wastewater varies from parts per billion to parts per million levels. The occurrence of pharmaceuticals in the environment is illustrated in Figure 1.1. The typical values of different parameters of pharmaceutical industry wastewater are shown in Table 1.3.

Table 1.2. Concentrations of pharmaceuticals in water and solid wastes (Stasinakis et al., 2008).

Parameters	Typical values
Drinking water, µg/L	0.3
Surface water, µg/L	2
Ground water, µg/L	1
Municipal sewage (treated), µg/L	10
Biosolids (treated), µg/kg	10000
Agricultural soils, µg/kg	10

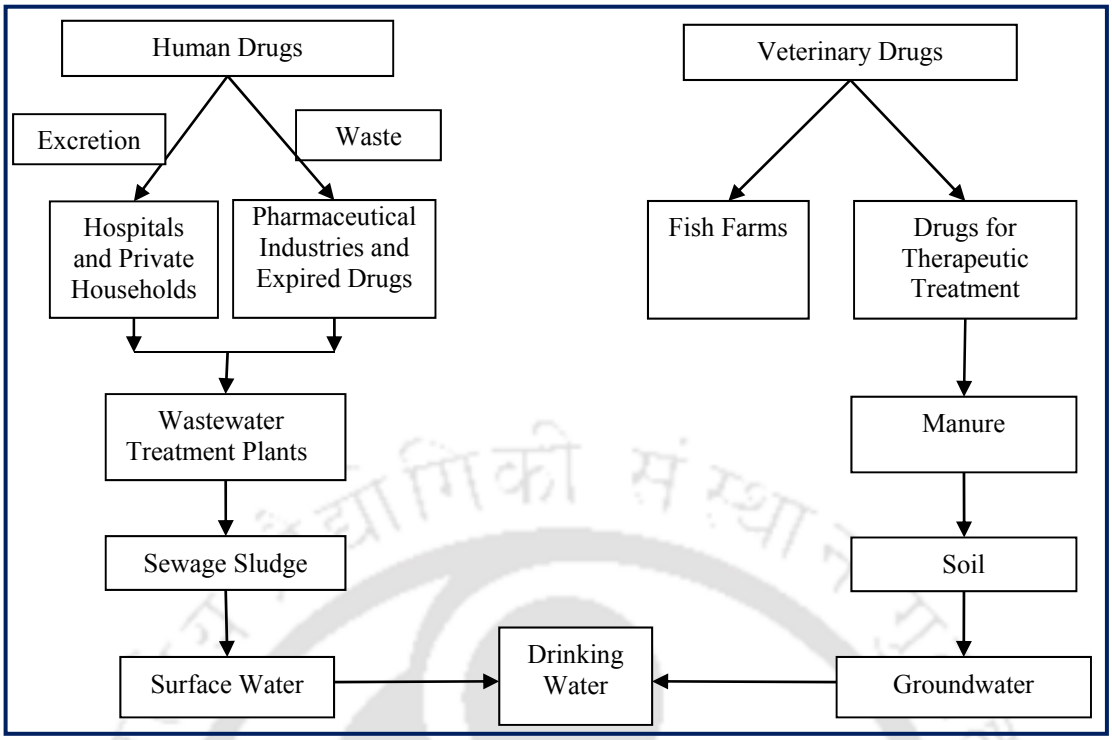

Figure 1.1. Pathways for inception of pharmaceuticals and their metabolites in the environment (Heberer et al., 2002).

Table 1.3. Characteristics of pharmaceutical industry wastewater producing allopathic medicines (Yeole et al., 1996; Mayabhate et al., 1988; Kolpin et al., 2002).

Parameters	Typical values
pH	6.5–7.0
BOD, mg/L	1,200–1,700
COD, mg/L	2,000–3,000
BOD/COD	0.57–0.6
Suspended solids, mg/L	300–400
Volatile acids, mg/L	50–80
Alkalinity as $CaCO_3$, mg/L	50–100
Phenols, mg/L	65–72

1.1.3 Present Indian scenario: Pharmaceutical wastewater pollution

In India, huge pharmaceutical industries have led to severely contaminated wastewater downstream from drug factories. It is laden with around 150 times the highest levels of contamination found in USA (Wen et al., 2014; Rodriguez et al., 2013). Annually, around 0.33 million ton of pharmaceutical waste is generated in India. Unfortunately, for most of the cases contaminated water is directly disposed off in to the receiving water bodies without suitable treatment and / or water treatment facilities are not equipped to treat/ filter out $PhAC_S$. The foremost reason is very high treatment cost.

Very recently, the most adverse effects of pharmaceutical waste and wastewater contamination in Patancheru (Andhra Pradesh, India) have come in public domain. The Patancheru Industrial Development Area (IDA) is a part of the catchment of Nakkavagu, a tributary of Manjira river. The area covers about 120 km^2 within Patancheru. More than 400 industries are functioning in this area dealing with the production of pharmaceuticals, paints and pigments, metal treatment and steel rolling, cotton & synthetic yarn and engineering goods (Walling et al., 1975). Aqueous effluents, mostly untreated, are discharged into various unlined channels and streams. Common Effluent Treatment Plant (CETP) of Patancheru, is situated adjacent to Peddavagu and wastewater discharged into the Peddavagu stream from CETP was found to have a total dissolved solids (TDS) concentration ranging from 4000 to 5000 mg/L.

Extremely high levels of PhACs are found in treated wastewater plant where about 90 drug factories dispose-off the pharmaceuticals residues. The combined industrial estates in Bollaram and Patancheru generate cumulatively about 8×106 L effluents per day which are directly discharged into surrounding land, irrigation fields and surface water bodies (Mayabhate et al., 1988).

High concentration of antibiotics is detected in streams, lakes and well water near pharmaceutical factories in Hyderabad, India. There are about 100,000 to 1,000,000 times higher than concentrations measured in typical water samples. Most of the world's supply of generic antibiotics is produced in Hyderabad (Shrivastava et al., 2010). It poses direct risks to human health via contaminated drinking water, and they may also foster conditions for pathogens to develop antibiotic resistances. Bigger pharma companies (the names withheld here) are also equally responsible for polluting the nearby areas. Most of these industries have pharmaceutical units that manufacture bulk drugs like sulphamethoxazole, ibuprofen, trimethoprim and paracetamol. There are around 40 industries in this area and no proper

waste disposal facilities are built. Almost all the companies are wantonly disposing off the waste in nearby land and water bodies.

There are thousands of pharmaceutical industries across the entire country, disposing off million gallons of untreated wastewater every. There is an urgent need of research on pharmaceutical waste/ wastewater specifically in Indian context and it has commercial relevance also.

1.2 Techniques for Treatment of Pharmaceutical Wastewater

1.2.1 Adsorption technique

The efficiency of adsorption process is studied by numerous workers for treatment of wastewater containing PhACs. The extent of adsorption depends on the nature of adsorbent especially its porosity and surface area (Goutama et al., 2007). Dutta et al. (1997) investigated both adsorption and desorption efficiency of 6-aminopenicillanic acid (6-APA) in aqueous effluent using activated carbon (AC). They found that adsorption process is highly reversible and the extent of reversibly adsorbed 6-APA is around 93%. Snyder et al. (2007) showed that both powdered activated carbon (PAC) (5 mg/L) and granular activated carbon (GAC) can remove greater than 90% of estrogens. However, dissolved organic compounds, surfactants and humic acids compete with binding sites and can block the pores within AC structures (Snyder et al., 2007). A filtration step prior to treatment of micro pollutants using PAC is important to increase removal efficiency (Hartig et al., 2001; Deegan et al., 2011). It reduces carbon demand due to reduced blocking of micropores by high molecular weight compounds. Thus, PAC is only suitable for the treatment of pre-treated wastewater or with a low organic loading (Deegan et al., 2011). The general difficulty with PAC treatment lies in separating the fine carbon particles. An additional step of separation is usually needed such as sedimentation, which necessitates the use of precipitants, or via (membrane) filtration.

1.2.2 Membranes processes

Different types of membranes and membrane based separation methods are used for the removal of PhACs from wastewater like MBR (membrane bioreactor), MBR/RO (MBR followed by reverse osmosis), UF/RO (ultra-filtration followed by RO) (Snyder et al., 2007). Maeng et al., (2013) reported that PhACs like naproxen, acetaminophen, ibuprofen, and caffeine can be significantly removed using MBR and the degradation efficiency can be as high as 75%. In MBRs, however, due to its enhanced sludge retention time (SRT), the

adaptation of microorganisms to less degradable compounds can occur. It would make possible to degrade such compounds in MBRs. MBR treatment has a better performance (removal >80%) than the conventional processes for diclofenac, ketoprofen, ranitidine, gemfibrozil, bezafibrate, pravastatin and ofloxacin. Chang et al., (2008) obtained about 95% COD and 99% BOD reduction from a 10 m^3 per day capacity MBR operated at a pharmaceutical facility. Nano filtration (NF) and RO membranes are more efficient in eliminating PhACs having different physico-chemical properties. The removal using NF is mostly over 85%, with the exception of gemfibrozil (50.2%), bezafibrate (71.8%), atenolol (66.6%), mefenamic acid (30.2%) and acetaminophen (43%) (Castiglioni et al., 2006). Snyder et al., (2007) detected pentoxifylline, iodopromide, dimethyltoluamide (DEET), meprobamate, phosphanetriyltripropanoic acid (TCEP), gemfibrozil, musk ketone and oxybenzone in the permeate stream of different configurations of the filtration processes. Short circuiting of membrane or failure of membrane support is responsible for the reduction of permeate quality. However, the retentate must be treated further to degrade the more concentrated form of PhACs.

1.2.3 Biological treatment

Biological processes use bacteria and other microorganisms to remove contaminants by assimilating them and it has long been a support of wastewater treatment in chemical industries. The main key factor for any biological system is an adequate supply of oxygen as cells need not only organic materials as food but also oxygen to breathe. A wide range of natural and xenobiotic chemicals in pharmaceutical wastewater are recalcitrant and non-biodegradable in nature. Anaerobic processes are not always effective in removing such substances (Deegan et al., 2011). Conventional activated sludge treatment (AST) with a long hydraulic retention time (HRT) generally is the choice for pharmaceutical industry wastewater **(**Alaton et al., 2002; Oz et al., 2004). It needs a lower capital cost than advanced treatment methods and a limited operational requirement. However, it suffers from the production of large amounts of sludge (Snyder et al., 2009). Removal efficiencies are likely to decrease due to development of more resistant microorganisms towards many PhACs (Khetan and Collins, 2007). Ibuprofen, naproxen, bezafibrate and estrogens (estrone, estradiol and ethinylestradiol) showed a high degree of removal while sulfamethoxazole, carbamezapine and diclofenac displayed limited removal efficiency (Clara et al., 2005). A number of studies are carried out using sequence batch reactors (SBRs) and MBRs to improve the efficiency of AST (Clara et al. 2005; Radjenovic et al. 2007). Ileri et al., (2003)

achieved removal efficiency of 82% biochemical oxygen demand (BOD), 88% chemical oxygen demand (COD), 96% NH_3 and 98% suspended solids (SS) from domestic and pharmaceutical wastewater in a SBR operated for 4 h aeration followed by 60 min sedimentation. In an another study, slightly lower COD removal efficiencies between 63-69% are reported (Aguado et al., 2008). MBRs are known to be effective for the removal of bulk organics and can replace traditional methods when operated in combination with a conventional AST (Noble, 2006). The main advantage of MBRs over AST is that they require less space (Yang et al., 2006), and can also treat variable wastewater compositions (Chang et al., 2008). Biologically active filters are also used for pharmaceutical wastewater treatment and are capable of removing PhACs (Aziz et al., 1980). Important literatures for removal of PhACs using different treatment processes are summarized in Table 1.4.

Table 1.4. Performance of traditional techniques for treatment of pharmaceutical effluents.

PhACs	Operating conditions	Process	Key findings	Source
Ibuprofen (IBP)	Activated carbon 0.03 g/L Initial conc. 50 mg/L pH 7.6 Contact time 24 h Temp 25°C	Adsorption/ Ion exchange	Highest removal efficiency of 87% Ibuprofen possibly form a mono layer on the surface of adsorbent	Melillo et al., 2004
Carbamazepine	Initial conc. 20 mg/L pH 6.0 Contact time 2 h Flow rate 1.5 mL/min Temp 25±2°C Organic polymer resin		Maximum drug uptake of 89% A steady-state approximation was applied using quasi-equilibrium modelling	Li et al., 2011
Sulfamethoxazole (SMX)	Initial conc. 50 mg/L pH 5.3 Reaction time 8 h Flow 1.5 mL/min Temp 25°C Organic polymer resin		Maximum removal efficiency of 85%	Barlas et al., 2009
Ibuprofen Diclofenac Ketoprofen Naproxen	Initial conc. 1000 mg/L Pore size 0.4 µm pH 2 Reaction time 9 h Temp 25°C	MBR using Microfiltration (MF)	Concentration of ibuprofen decreased to 10 ng/L Ibuprofen is considerably biodegradable Poor removal of clofibric acid as it contains chlorine in the structure	Kimura et al., 2005
Diazepam Diclofenac Gemfibrozil Hydrocodone Iopromide	Initial conc. 5µg/L pH 2-9.5 HRT 32 h Membrane area 32.5 m^2 Cross flow velocity 2-5 m/s Pore size 0.2 µm Operating pressure 1-10 psi Temp 20-25°C	MBR followed RO	Combined process showed better efficiency than individual process Upto 90% removal in combined process	Snyder et al., 2005

Cyclophosphamide (CP)	Initial conc. 5µg/L pH 7-8 SRT 50 days HRT 48 h Working volume 20 L Cross flow velocity 4-5 m/s Pore size 0.2 µm Temp 25-32°C	MBR	CP cannot be used as the primary source of energy/carbon due to low concentration CP and COD removal upto 80 and 90%	Delgado et al., 2009
Ampicillin	Initial conc. 3.2 mg/L pH 6.8 HRT 1.25 day Temp 20-25°C	Biological treatment	Removal efficiency of 67.8% First order rate constant and half-life of 0.06 1/day and 4.8 days	Adams et al., 2002
Aureomycin	Initial conc. 1 mg/L pH 6.6 HRT 2.5 days Temp 20-25°C		Removal efficiency of 51.5% Rate constant of 0.53 1/day Half-life is 7.5 days	Balciolu et al., 2002

1.2.4 Advanced oxidation processes (AOPs)

Advanced Oxidation Processes (AOPs) are based on the generation of very reactive radicals, such as hydroxyl radicals ($HO^{\bullet}$) which are able to react with most of the organic compounds and initiate their degradation. The pollutants and by-products are degraded through a series of complex reactions. In the first step, $HO^{\bullet}$ radicals react with organic compounds either by H abstraction, double bond addition, or electron transfer leading to formation of organic radicals. The latter species react with dissolved oxygen to form peroxyl ($ROO^{\bullet}$) radicals which undergo rapid decomposition. The overall process leads to partial or total mineralization of pollutants **(**Oppenlander et al., 2003).

1.2.4.1 Fenton Processes (FP)

Fenton's reagent, a mixture of ferrous iron (catalyst) and hydrogen peroxide (H_2O_2) is known for formation of $HO^{\bullet}$ radical, a strong oxidizing agent ($E^0 = 2.8$ vs. NHS). The mechanism of FP is studied by several workers (Chang et al., 2008; Chamarro et al., 2001). The main reactions occurring in Fenton oxidation of organics are appended bellow (Eqs 1.1 to 1.4):

$$Fe^{2+} + H_2O_2 \rightarrow Fe^{3+} + OH^- + HO^{\bullet} \quad (1.1)$$

$$Fe^{2+} + HO^{\bullet} \rightarrow Fe^{3+} + OH^- \quad (1.2)$$

$$HO^{\bullet} + RH \rightarrow H_2O + R^{\bullet} \quad (1.3)$$

$$R^{\bullet} + Fe^{3+} \rightarrow R^{+} + Fe^{2+} \quad (1.4)$$

where, $R^{\bullet}$ is alkyl free radical.

The major parameters affecting FP are solution pH, amount of ferrous ion, concentration of H_2O_2, initial concentration of pollutants/ PhACs and presence of other background ions (Gogate and Pandit, 2004a). The optimum pH for FP generally ranges from 2 to 4. At pH>4, Fe^{2+} ions are unstable and they are easily transformed to Fe^{3+} forming complexes with hydroxyl ion. Moreover, under alkaline conditions H_2O_2 loses its oxidative power as it breakdowns to water (Chang et al., 2008). Adjustment of effluent pH is usually needed before addition of Fenton reagent. Increase of ferrous ions and H_2O_2 concentration boosts up the degradation rate (Li et al., 2012). The use of excess amount of H_2O_2 can deteriorate the overall degradation efficiency of FP coupled with biological treatment due to toxic nature of H_2O_2 to microorganisms (Gogate and Pandit, 2004b). Fenton oxidation of organics/PhACs can be inhibited by phosphate, sulfate, fluoride, bromide and chloride ions. The inhibition may be due to precipitation of iron, scavenging of $HO^{\bullet}$ radicals or coordination with Fe^{3+} to form a less reactive complex (Pignatello et al., 2006).

1.2.4.2 Photo-Fenton Processes (PFP)

Photo-Fenton process ($H_2O_2/Fe^{2+}/UV$) involves formation of $HO^{\bullet}$ radicals through photolysis of hydrogen peroxide (H_2O_2/UV) along with the Fenton reaction (H_2O_2/Fe^{2+}). In presence of UV irradiation, ferric ions (Fe^{3+}) are also photo-catalytically converted to ferrous ions (Fe^{2+}) with formation of additional $HO^{\bullet}$ radicals (Eq. 1.5) (Moraes et al., 2004).

$$Fe(OH)_2^{+} + h\nu \rightarrow Fe^{2+} + HO^{\bullet} \qquad (1.5)$$

Likewise, PFP gives faster rates and higher degree of mineralization compared to conventional FP (Pignatello et al., 2006). The reaction can be driven by low energy photons and it also can be achieved using solar irradiation (Lin et al., 1997). The employment of solar light significantly reduces the operational cost. Another important advantage of PFP is that iron-organic complexes formed during Fenton oxidation can be broken under the illumination of UV light (Miralles-Cuevas et al., 2014).

1.2.4.3 UV/H_2O_2 photolysis (UVP)

UVP includes H_2O_2 injection with continuous mixing in a reactor equipped with UV irradiation system (wavelength 200 to 280 nm). UV light is used to cleave O-O bond of H_2O_2 forming $HO^{\bullet}$ radicals. The reactions describing UVP are presented below (Eqs. 1.6 to 1.11) (Buxall et al., 2003):

$$H_2O_2 + h\nu \rightarrow 2HO^{\bullet} \quad (1.6)$$

$$H_2O_2 + HO^{\bullet} \rightarrow HO_2^{\bullet} + H_2O \quad (1.7)$$

$$H_2O_2 + HO_2^{\bullet} \rightarrow HO^{\bullet} + H_2O + O_2 \quad (1.8)$$

$$2HO^{\bullet} \rightarrow H_2O_2 \quad (1.9)$$

$$2HO_2^{\bullet} \rightarrow H_2O_2 + O_2 \quad (1.10)$$

$$HO^{\bullet} + HO_2^{\bullet} \rightarrow H_2O + O_2 \quad (1.11)$$

Reaction 1.6 is rate limiting because the rates of other reactions are much higher. In UVP, a higher initial H_2O_2 concentration produces higher $HO^{\bullet}$ radical concentration (Eq. 1.6), which decomposes the target compounds. However, an optimal H_2O_2 concentration exists because overdosing of H_2O_2 leads to reaction with $HO^{\bullet}$ radicals leaving off $HO_2^{\bullet}$ (Eq. 1.7). UVP is quite efficient in mineralizing PhACs (Buxall et al., 2003). A disadvantage of UVP is that it cannot utilize solar light as the source of UV illumination. The required UV irradiation for the photolysis of H_2O_2 is not available in the solar spectrum (Haddad et al., 2014). H_2O_2 has poor UV absorption characteristics and input irradiation to the reactor is wasted if the water matrix absorbs UV light. Performance of UVP for treatment of pharmaceutical effluents is summarized in Table 1.7.

1.2.4.4 UV/TiO_2 photo catalysis (UVPC)

Photocatalysis is the acceleration of a photoreaction using a catalyst in presence of light/photon. It is a well-recognized approach where light energy is employed to excite the semiconductor material producing electron (e^-_{cb})/hole (h^+_{vb}) pair (Eq. 1.12) which eventually involves in the detoxification of pollutants (in water or air). e^-_{cb} from the valence band (VB) is promoted to the conduction band (CB) of the semiconductor and a h^+_{vb} is created in the VB. The photo generated e^- migrates to the surface without recombination can reduce and oxidize the contaminants adsorbed on the surface of the semiconductor (Chen and Mao, 2007). e^-_{cb} react with surface adsorbed molecular oxygen to yield superoxide radical anions

(Eq. 1.13), while h^+_{vb} react with water to form $HO^{\bullet}_{ad}$ radicals on the surface of the catalyst (Eq. 1.14) (Gurkan et al., 2012).

$$TiO_2 + h\nu \rightarrow e^-_{cb} + h^+_{vb} \quad (1.12)$$

$$e^-_{cb} + O_2 \rightarrow O_2^{-\bullet} \quad (1.13)$$

$$h^+_{vb} + H_2O \rightarrow H^+ + HO^{\bullet}_{ad} \quad (1.14)$$

TiO_2 is widely used as a photocatalyst due to high photo-catalytic activity, low cost, low toxicity, high oxidation power, easy availability and chemical stability under UV light (λ<380 nm) (Leonidas et al., 2007). TiO_2 has two common crystal structures i.e., rutile and antase. TiO_2 Degussa 25 consisting of 20% rutile and 80% anatase is considered as a standard photocatalyst.

Organic compounds can undergo oxidative degradation through reactions with h^+_{vb}, $HO^{\bullet}_{ad}$, and $O_2^{-\bullet}$ radicals as well as through reductive cleavage by e^-_{cb}. The key advantages of UVPC are treatment at ambient conditions, lower mass transfer limitations using nanoparticles and possibility of use of solar irradiation. UVPC is capable for destruction of a wide range of organic chemicals into harmless compounds such as CO_2 and H_2O (Chatterjee and Dasgupta, 2005). The major factors affecting UVPC are initial pollutant load, amount of catalyst, reactor design, irradiation time, temperature, solution pH, light intensity and presence of ionic species. The use of excess catalyst may reduce the amount of photon transfer into the medium due to opacity offered by the catalyst particles (Gogate and Pandit, 2004a). The design of reactor should assure uniform irradiation of the catalyst (Ray et al., 1999).

1.3 Advantages and Limitations of AOPs

AOPs using H_2O_2 and Fe^{2+} suffer from the requirement of acidic conditions, interference by inorganic ions, iron-organic complexation and formation of iron sludge. Some of the above limitatins can be overcome when heterogeneous photocatalytic treatments like UVPC is used. However, uniform illumination of UV light and separation of catalyst particles could limit the application (Yang et al., 2008). Application of artificial UV light increases the cost of treatment and also poses health hazard to the working personnel.

The typical advantages of iron based AOPs are:

i. The process is capable to destroy a wide variety of organic compounds even without formation of toxic intermediates (Heeb et al., 2014).

ii. It offers a cost-effective source of $HO^{\bullet}$ radicals using easy-to-handle reagents (Swancutt et al., 2010).

iii. In FP and PFP, both oxidation and coagulation take place simultaneously (Xing et al., 2009).

iv. Effective in destruction of refractory PhACs to improve biodegradability and produce an effluent that can be treated biologically as a finishing step (Bel et al., 2009).

1.3.1 Treatment of Pharmaceutical Wastewater using AOPs: Literature Survey

Lin et al., (1997) used Fenton's reagent in treatment of refractory high-strength pharmaceutical, landfill leachate, dying, and semi-conductor wastewater. Effluent laden with amoxicillin showed very low biodegradability in presence of organic solvents and dissolved salts. It hinders direct biological and membrane-based treatments. In another study, they reported that employment of FP for complete oxidation of pharmaceuticals increases the reagent cost prohibitively because of the quantity required. Zhang (2005) showed that TOC removal efficiency is around 30% in 1 h reaction time and it can be reached upto 50.6% in 3 h. Further increase in reaction time, there was not much variation in TOC removal. Nie et al., (2014) observed inhibitory effect of inorganic species like Cl^- for decomposition of chloramphenicol. It effects PFP because Cl^- acts as a $HO^{\bullet}$ radical scavenger. The negative effect of Cl^- is due to formation of Fe(III)-chlorocomplexes. Highest COD removal efficiency of 65% is achieved with H_2O_2/Fe^{2+} molar ratio of 155 (0.3 M H_2O_2 and 0.002 M Fe^{2+}) (Tekin et al., 2008). They reported that the optimal pH is around 3.5. The oxidation rate falls as coagulation is initiated at pH>7 and precipitated sludge can be removed at this pH. Canonica et al. (2008) conducted photodegradation of selected pharmaceuticals using a monochromatic irradiation varying pH from 3 to 9 and temperature between 10 and 40°C. The reaction rate follows the first order kinetics. Moraes et al., (2004) determined the quantum yields for cleavage of hydrocarbon at different pH and temperatures at 254 nm. They showed that the rate constants are related to the functional groups attached the quinolone core. Some of the intermediate compounds formed during amoxicillin oxidation are resistant to mineralization using Fenton's reagent. The highest TOC removal is 37%. H_2O_2 and Fe^{2+} requirements increase at higher antibiotic concentration for effective mineralization. Iomeprol, diatrizoate

and iopamidol give slightly higher oxidation efficiency (7 to 11%) in ozonation process in comparison to UVP (Ternes et al., 2003).

The common AOPs include FP, PFP, UVP and UVPC. The key results for treatment of aqueous effluents containing PhACs are summarized in Tables 1.5 to 1.8. 'Initial conc.' in the Tables indicates the initial concentration of the contaminant(s).

Table 1.5. Fenton process (FP) for removal of PhACs.

PhACs	Operating conditions	Key findings	Source
Trichloroethylene (TCE)	Fe^{2+} 1.0 mM H_2O_2 0.25 mM Initial conc. 32.85 mg/L pH 3.0 Time 40 min Volume 40 mL Temp 20 ºC	Maximum 78% TCE removal at pH 3 Lowest degradation of 22% attained at neutral pH	Teel et al., 2001
Metronidazole	Fe^{2+} 11.76 µM H_2O_2 29.4 µM Initial conc. 1.02 mg/L pH 3.5 Time 15 min Volume 350 mL Temp 25 ºC	Metronidazole degradation followed second order kinetics Half-life ($t_{1/2}$) decreased with increasing ferrous ion concentration	Shemer et al., 2006
Amoxicillin Ampicillin Cloxacillin	H_2O_2/Fe^{2+} molar ratio 20 Initial conc. 104 mg/L pH 3.5 Time 30 min Volume 1000 mL Temp 60 ºC	COD removal of 62 % in 30 min Biodegradability improved from 0.09 to 0.49	Elmolla et al., 2009
	Fe^{2+} 0.45 mM H_2O_2 11.76 mM Initial conc. 60 mg/L pH 3.5 Time 15 min Volume 1000 mL Temp 23-25 ºC	Maximum 90% drug removal COD and TOC removal of about 81 and 37% within 15 min	Ay et al., 2010
Ciprofloxacin (CIP)	Fe^{2+}/H_2O_2 molar ratio 10 and 15 Initial conc. 18.22 mg/L pH 3.2 Time 2.5 min Volume 200 mL Temp 24 ºC	CIP degradation followed second-order kinetics Four major peaks with m/z 348, 362, 330, and 263 were identified during CIP degradation	Xiao et al., 2010
Carbamazepine	Fe^{2+} 0.139 mM Fe^{3+} 0.0168 mM H_2O_2 0.0125 mM Initial conc. 5 mg/L pH 3.52 Time 120 min Volume 250 mL Temp25 ºC	Total carbamazepine degradation was obtained under optimal condition A nonlinear polynomic regression well fitted (R^2=0.9) to calculate final drug removal	Dominguez et al., 2011
Diuron	Fe^{2+} $/H_2O_2$ molar ratio 25 Initial conc. 39.6 mg/L pH 3.0	Mineralization reached to 89% Absolute rate constant found as	Oturan et al., 2011

	Time 3 h Volume 400 mL Temp 25 ºC	$(4.75\pm0.20)\times10^{9}$ L/mol.s	
Acetaminophen (ACTP)	Fe^{2+} 0.1 mM H_2O_2 15 mM Initial conc. 125.1 mg/L pH 2.0 Time 90 min Volume 10 mL Temp 25 ºC	About 72% drug removal in 90 min Maximum ACTP degradation efficiency was found to be 84%	Su et al., 2012
Flumequine	Fe^{2+} 5 mM H_2O_2 10 mM Initial conc. 0.5 mg/L pH 2.8 Time 15 min Volume 190 mL Temp 25 ºC	Four by-products identified by mass spectrometry They reported 50% growth inhibition of *E. coli*	Rodrigues-Silva et al., 2013
Acetaminophen (ACTP)	Fe^{2+} 0.06 mM H_2O_2 19.87 mM Initial conc. 5 mg/L pH 3.2 Time 120 min Volume 400 mL Temp 25 ºC	Maximum removal efficiency of 96% Maximum COD removal of 28% Oxalic acid caused highest decrease in degradation efficiency	Luna et al., 2014
Carbamazepine (CBZ)	Fe^{2+} 0.05 mM H_2O_2 0.05 mM Initial conc. 118 mg/L pH 3.0 Time 120 min Volume 10 mL Temp 25 ºC	Drug decomposition of 60% in 5 min In presence of vanadium (V) ions only 21% CBZ lost after 120 min	Karpinska et al., 2014

Table 1.6. Photo-Fenton process (PFP) for removal of PhACs.

PhACs	Operating conditions	Key findings	Source
Diclofenac	Fe^{3+}/H_2O_2 molar ratio 10 Initial conc. 35.53 mg/L pH 2.8 UV 254 nm Time 60 min Volume 1400 mL Temp 50 ºC	Activation energy (E_a) for diclofenac disappearance found as 16.08 kJ/mol Residual H_2O_2 in solution was around 38-40%	Ravina et al., 2002
Sulfamethoxazole (SMX)	Drug:Fe^{2+}:H_2O_2 molar ratio 1:(1.5-5): 0.05 Initial conc. 200 mg/L pH 2.8 UV 254 nm Volume 2000 mL Temp 25 ºC	About 75% SMX removal obtained BOD_5/COD raised from 0 to 0.3	Gonzalez et al., 2007

Ibuprofen (IBP)	Fe^{2+} 1.2 mM H_2O_2 0.32 mM Initial conc. 179.5 mg/L pH 3.0 UV 254 nm Time 120 min Volume 30 mL Temp 30 ºC	Only 40% degradation reported within 2 h Photolability of Fe(III)-IBP coordinated complex promoted in decarboxylation of IBP	Mendez-Arriaga et al., 2010
Sulfamethazine (SMT)	Fe^{2+} 0.68 mM H_2O_2 17.6 mM Initial conc. 50 mg/L pH 5.37 UV 254 nm Time 240 min Volume 1000 mL Temp 18-19 ºC	TOC removal of 50% achieved in 45 min First-order rate constant found as 0.0253 1/min	Perez-Moya et al., 2010
Caffeine	Fe^{2+} 0.18 mM H_2O_2 14.7 mM Initial conc. 17 mg/L pH 2.9 UV 254 nm Time 15 min Volume 2000 mL Temp 25 ºC	TOC reduction was within 75% A hybrid discrete-continuous dosage scheme proposed using two factors in an experimental design (2^2)	Yamal-Turbay et al., 2012
Paracetamol	Fe^{2+} 0.05 mM H_2O_2 3.5 mM Initial conc. 50 mg/L pH 2.5 UV <290 nm Intensity 250 W/m^2 Time 300 min Volume 39 mL Temp 25 ºC	Maximum 79% TOC reduction in 300 min using $FeSO_4$ Toxicity for *Vibrio fischeri* and *Daphnia magna* decreased from 100% to less than 40%	Trovo et al., 2012
Flumequine	Fe^{2+} 0.25 mM H_2O_2 10 mM Initial conc. 0.5 mg/L pH 2.8 UV 254 nm Time 60 min Volume 190 mL Temp 25 ºC	Decomposition efficiency > 94% in 60 min Intermediates with m/z of 244, 238, 220 and 202 were detected Antimicrobial activity reduced by 67%	Rodrigues-Silva et al., 2013
Chloramphenicol (CHPL)	Fe^{2+} 0.172 mM H_2O_2 11.76 mM Initial conc. 200 mg/L pH 2.6 UV 41.5 W/m^2 Time 6.5 min Volume 5000 mL Temp 25-30 ºC	About 92% dissolved organic carbon (DOC) removal Mean oxidation number of carbon (MONC) increased from +0.48 to +1.59	Trovo et al., 2013
Diphenhydramine (Antihistamine drug)	Fe^{2+} 1.9 mM H_2O_2 16 mM Initial conc. 100 mg/L pH 2.8 UV 350 nm Time 60 min Volume 75 mL Temp 25 ºC	Catalyst prepared at 180 ºC at 4:1 molar ratio of NaOH and $FeCl_3$ Maximum TOC reduction found as 82%	Luisa et al., 2014

ß-blockers (Atenolol and Metoprolol)	Fe^{2+} 0.09 mM H_2O_2 2.94 mM Initial 20 mg/L pH 7.0 UV 290 nm Time 60 min Volume 1000 mL Temp 35 ºC	Followed pseudo-first order kinetics with rate constant ('k') as 0.061 1/min Metoprolol's intermediates moderately toxic than atenolol's intermediates	Veloutsou et al., 2014

Table 1.7. UV/H_2O_2 photolysis (UVP) processes for removal of PhACs.

PhACs	Operating conditions	Key findings	Source
Paracetamol	H_2O_2 5 mM Initial conc. 37.8 mg/L pH 3.0 UV 254 nm Time 4 h Temp 27 ºC	About 40% drug removal reached in 4 h Intermediates concentration not influenced by HO· radicals production	Andreozzi et al., 2003
Naproxen, Iohexol, Carbamazepine, Ciprofloxacin, Ketoprofen, Clofibric acid	H_2O_2 0.294 mM Initial conc. 1 to 3 µM pH 7.0 UV 254 nm Time 60 min Temp 25 ºC	Medium pressure lamps were more efficient to maximize degradation of the selected group of compounds Overall degradation rate constants attenuated due to screening of UV light and HO· radical scavenging	Pereira et al., 2007
Dipyrone (Antipyretic)	H_2O_2 10 mM Initial conc. 10-50 mg/L pH 3.4- 5.4 UV 290 nm Time 160 min Temp 25-30 ºC	4-FAA and 4-AAA showed slower photo degradation with $t_{1/2}$ of 24 and 28 h, respectively	Gomez et al., 2008
	H_2O_2 10 mM Initial conc. 15 mg/L pH 7.0 UV 250 nm Time 60 min Temp 100-120 ºC	^{1}HNMR signals of degradation products evidence the presence of aromatic protons HO· radical took part in hydroxylation reaction as obtained by ^{1}HNMR signals	Santos et al., 2010
Clofibric acid, Diclofenac, Fenoprofen, Isopropylantipyrine, Ketoprofen	H_2O_2 1.47 mM Initial conc. 1000 mg/L pH < 5.7 UV 254 nm Time 30 min Temp 25±2 ºC	Removal efficiency > 85% Followed first-order kinetics	Lia et al., 2008
Antipyrine (AP)	H_2O_2 1.06 mM Initial conc. 5 mg/L pH 7.2 UV 254 nm at Time 30 min Temp 50±2 ºC	k_{obs} decreased from 1.99 to1.27 1/h with increasing [HCO_3^-] from 0 to 200 mM AP firstly attacked by •OH radical at C=C position in the pentacyclic ring	Tan et al., 2013

Naproxen (NAP)	H_2O_2 0.27 mM Initial conc. 23 mg/L pH 7.0 UV 254 nm Time 5 min Temp 25 ºC	Significant quantity of carbon (35-75%) found in solution even after maximum degradation Aromatic photoproducts completely decomposed in 30 min using UV+vacuum and in 40 min using UV	Arany et al., 2013
Clofibric acid, Diclofenac, Naproxen, Benzafibrate, Ketoprofen, Ibuprofen (IBP),	H_2O_2 0.03 mM Initial conc. 0.1 mg/L pH 5.8 to 6.5 UV 254 nm Time 120 min Temp 20 ºC	Average removal efficiency about 89.3% Followed first-order kinetics with 'k' from 0.018 to 0.043 1/min	Yuan et al., 2013
Ciprofloxacin (CIP)	H_2O_2 0.15 mM Initial conc. 20 mg/L pH 7.0 UV 300 nm Time 30 min Temp 21±1 ºC	Maximum removal efficiency > 61% They identified 11 intermediates during CIP degradation	Haddad et al., 2014
Chloramphenicol (CHPL)	H_2O_2 5 mM Initial conc. 96.9 mg/L pH 5.5 UV 254 nm Time 20 min Temp 25 ºC	Maximum removal efficiency found to be 96% Mineralization was 47.2%	Zourro et al., 2014

Table 1.8. UV/TiO_2 photocatalysis (UVPC) for removal of of PhACs.

PhACs	Operating conditions	Key findings	Source
Dipyrone	TiO_2 0.2 g/L Initial conc. 5 mg/L pH 2.8 UV intensity 30 W/m^2 Time 120 min Temp 40 ºC	Removal efficiency >50% Followed first-order kinetics (k = 0.069 1/min)	Leonidas et al., 2007
Acetaminophen (ACTP), ß-blocker atenolol	TiO_2 0.2 g/L Initial conc. 10 mg/L pH 6.8 UV 250 nm Time 10 h Temp 25 ºC	Removal efficiency >90% Concentration of NH_4^+ and NO_3^- was detected as 0.35 and 0.18 mg/L	Radjenovic et al., 2009
Ciprofloxacin (CIP)	TiO_2 0.5 g/L Initial conc. 40.4 mg/L pH 6.0 UV intensity 175 J/cm^2 Time 8 h Temp 37 ºC	Inhibition of growth of *E. coli* by 50% Degradation products retain negligible toxicity relative to the parent compound	Paul et al., 2010

Chloramphenicol (CHPL)	TiO_2 0.94 g/L Initial conc. 19.97 mg/L pH 6.4 UV 254 nm Time 60 min Temp 25 ºC	Removal efficiency > 85.9% Second-order polynomial model well fitted the experimental results	Zhang et al., 2010
Ciprofloxacin (CIP), Moxifloxacin (MOX)	TiO_2 0.5 g/L Initial conc. 15 mg/L pH 7 UV 365 nm Time 40 min Volume 200 mL Temp 25 ºC	Fastest degradation at pH 10 and 7 Followed first-order rate with 'k' as 0.072 and 0.058 1/min for CIP and MOX	Doorslaer et al., 2011
Cefazolin	TiO_2 0.1- 1 g/L Initial conc. 47.7 mg/L pH 6.4 UV 365 nm Time 45 min Volume 600 mL Temp 23 ºC	53% degradation obtained in 60 min Higher photocatalytic activity of cefazolin for N-doped TiO_2 compared to Degussa P25	Gurkan et al., 2012
Ibuprofen	TiO_2 0.1-1 g/L Initial conc. 10 to 100 mg/L pH 9.0 UV 362 nm Time 30 min Volume 250 mL Temp 37 ºC	Additional oxygen enhanced photocatalytic reaction Intermediates formed by radical polymerization leads to catalyst deactivation	Choina et al., 2013
Propranolol	TiO_2 0.4 g/L Initial conc. 50 mg/L pH 7.0 UV 360 nm Time 360 min Volume 10 L Temp 25 ºC	About 99 and 58.1% removal of drug and TOC BOD_5/COD signified more biodegradable intermediates	Cruz et al., 2013
Lorazepam	TiO_2 0.2 g/L Initial conc. 0.2 mg/L pH 7.2 UV 30 W/m^2 Time 60 min Volume 850 mL Temp 35 ºC	pK_a value of 12.46 TiO_2 absorbed about 100% of solar UV photons	Sousa et al., 2013
Ceftiofur sodium (CFS)	TiO_2 1 g/L Au^{3+} 20 mg/L Initial conc. mg/L pH 7 UV nm Time 120 min Volume 100 mL Temp 80 ºC	Au–TiO_2 exhibited 95% degradation within 2 h under UV-irradiation About 51% TOC reduction with Au-TiO_2 nanoparticles	Pugazhenthiran et al., 2014

1.3.2 Knowledge gap and Objectives of the work

AOPs are promising for the decomposition of PhACs and personal care products from industrial and municipal wastewater (Stumpf et al., 1999). AOPs undergo through different reacting systems such as homogeneous or heterogeneous phases and in light or dark. They have common characteristics of formation of hydroxyl free radicals ($HO^{\bullet}$) (Alaton et al., 2002; Buxton et al., 1988). It causes consecutive unselective degradation of organic materials. Complete mineralization occurs even at very low concentration and the byproducts formed may be environmentally non-hazardous (Liu et al., 2013).

Biological treatment is recognized as the cheapest available technology to remove and degrade organic contaminants. However, AST gives very inefficient degradation of PhACs because they are usually resistant to biodegradation and characterized by low BOD/COD ratio (Tekin et al., 2008). Partial Fenton oxidation yields more biodegradable products together with the destruction of inhibitory effect towards microorganisms in the downstream biological treatment. It also increases the overall treatment efficiencies compared to the efficiency of individual process. AOPs can be employed for the detoxification of PhACs until the biodegradability is improved to a level amicable for subsequent biological treatment (Stumpf et al., 1999).

Likewise, it also can increase the overall treatment efficiencies compared to the efficiency of each individual process. However, there many questions still unanswered for the treatment of pharmaceutical effluents include (i) kinetic modelling, (ii) iron-organic chelation, (iii) decomposition mechanism, (iv) biodegradability improvement and, (v) antimicrobial activity.

Three pharmaceutical compounds (also stated as drug) i.e., chloramphenicol (CHPL), ciprofloxacin (CIP) and dipyrone (DIPY) were selected for this study based on their consumption, occurrence and possible iron-complexation. AOPs investigated are Fenton process (FP), photo-Fenton process (PFP) and UV-photolysis (UVP). The decomposition behaviour of DIPY in UV/TiO_2 photocatalysis (UVPC) is also studied.

Therefore, the objectives of the dissertation are:

i. To investigate the performance of AOPs for the decomposition of selected pharmaceuticals and to find out the proper treatment conditions

ii. To determine the concentration of hydroxyl radical ($HO^{\cdot}$) and to develop the kinetic model of drug and degradation product degradation

iii. To uncover the decomposition behaviour of PhACs-iron chelates and its impact on the mineralization efficiency

iv. To identify the intermediates formed during treatment and to validate the proposed mechanism of drug cleavage

v. To investigate the influence of foreign anions to understand drug mineralization when treating the mixture of PhACs

vi. To study the performance of FP, PFP, UVP and UVPC on biodegradability and antimicrobial activity

References

Adams, C., Wang, Y., Loftin, K. and Meyer, M., "Removal of antibiotics from surface and distilled water in conventional water treatment processes", *J. Environ. Eng.,* **128,** 253-260 (2002).

Aguado, D., Montoya, T., Borras, L., Seco, A. and Ferrer, J., "Using SOM and PCA for analysing and interpreting data from a pharmaceutical removal from a P-removal SBR", *Eng. Appl. Artif. Intel.,* **21 (6),** 919- 930 (2008).

Ahmed, A., Daschner, F. D. and Kummerer, K., "Biodegradability of cefotiam, ciprofloxacin, meropenem, penicillin G, and sulfamethoxazole and inhibition of waste water bacteria", *Arch. Environ.Contam. Toxicol.,* **37,** 158-163 (1999).

Alaton, I. and Balcioglu, I. A., "Biodegradability assessment of ozonated raw and biotreated pharmaceutical wastewater", *Arch. Environ. Contam. Toxicol.,* **43,** 425-431 (2002).

Andreozzi, R., Caprio, V., Marotta, R. and Radovnikovic, A., "Ozonation and H_2O_2/UV treatment of clofibric acid in water: a kinetic investigation", *J. Haz. Mater.,* **103 (3),** 233-246 (2003).

Arany, E., Szabo, R. K., Alapi, L. A. T., Mazellierd, I. I. P., Dombi, A. and Schrantza, K. G., "Degradation of naproxen by UV, VUV photolysis and theircombination", *J. Hazard. Mater.,* **162,** 151-157 (2013).

Ay, F. and Kargi, F., "Advanced oxidation of amoxicillin by Fenton's reagent treatment", *J. Hazard. Mater.,* **179,** 622–627 (2010).

Aziz, J. A. and Tebbutt, T. H. Y., "Significance of COD, BOD and TOC correlations in kinetic models of biological oxidation", *Water Res.,* **14,** 319-322 (1980).

Balciolu, I. A. and Otker, M., "Treatment of pharmaceutical wastewater containing antibiotics by O_3 and O_3 /H_2O_2 processes", *Chemosphere,* **50(1),** 85–95 (2002).

Bel, E. D., Dewulf, J., Witte, B. D., Langenhove, H. V. and Janssen, C., "Influence of pH on the sonolysis of ciprofloxacin: Biodegradability, ecotoxicity and antibiotic activity of its degradation products", *Chemosphere,* **77**, 291-295 (2009).

Boxall, A. B. A., "The environmental side effects of medication", *EMBO reports,* **5,** 1110–1116, (2003).

Buxton, G. V., Greenstock, W., Helman, P. and Ross, A. B., "Critical review of rate constants for reactions of hydrated electrons, hydrogen atoms and hydroxyl radicals in aqueous solution", *J. Phys. Chem. Ref. Data,* **17,** 513-886 (1988).

Canonica, S., Meunier, L. and Gunten, U. V., "Phototransformation of selected pharmaceuticals during UV treatment of drinking water", *Water Res.,* **42,** 121-128 (2008).

Carballa, M., Omil, F. and Lema, J. M., "Removal of cosmetic ingredients and pharmaceuticals in sewage primary treatment", *Water Res.,* **39,** 4790-4796 (2005).

Castiglioni, S., Bagnati, R., Fanelli, R., Pomati, F., Calamari, D. and Zuccato, E., "Removal of pharmaceuticals in sewage treatment plants in Italy", *Environ. Sci. Technol.,* **40,** 357-363 (2006).

Chamarro, E., Marco, A. and Esplugas, S., "Use of Fenton reagent to improve organic chemical biodegradability', *Water Res.,* **35 (4),** 1047-1051 (2001).

Chang, C., Chang, J., Vigneswaran, S. and Kandasamy, J., "Pharmaceutical wastewater treatment by membrane bioreactor process: a case study in southern Taiwan", *Desalination,* **234 (1-3),** 386-392 (2008).

Chang, C. Y., Hsieh, Y. H., Cheng, K. Y., Hsieh, L. L., Cheng, T. C. and Yao, K. S., "Effect of pH on Fenton process using estimation of hydroxyl radical with salicylic acid as trapping reagent", *Water Sci. Technol.,* **23,** 34-39 (2008).

Chang, X., Meyer, M. T., Liu X., Zhao, Q., Chen, H. and Chen, J., "Determination of antibiotics in sewage from hospitals, nursery and slaughter house, wastewater treatment plant and source water in Chongqing region of Three Gorge Reservoir in China", *Environ. Pollut.,* **158,** 1444-1450 (2010).

Chatterjee, D. and Dasgupta, S., "Visible light induced photocatalytic degradation of organic pollutants", *J. Photochem. Photobiol.,* **6,** 186-205 (2005).

Chen, X. and Mao, S. S., "Titanium Dioxide Nanomaterials: Synthesis, Properties, Modifications, and Applications", *Chem. Rev.,* **107,** 2891-2959 (2007).

Choina, J., Kosslick, H., Fischer, C., Flechsig, G., Frunza, L. and Schulz, A., "Photocatalytic decomposition of pharmaceutical ibuprofen pollution in water over titania catalyst", *Appl. Catal., B* **129,** 589-598 (2013).

Cruz, N. D., Dantas, R. F., Gimenez, J. and Esplugas, S., "Photolysis and TiO_2 photocatalysis of the pharmaceuticals propanlol solar and artificial light", *Appl. Catal., B* **130-131**, 249-256 (2013).

Clara, M., Strenn, B., Gans, O., Martinez, E., Kreuzinger, N. and Kroiss, H., "Removal of selected pharmaceuticals, fragrances and endocrine disrupting compounds in a membrane bioreactor and conventional wastewater treatment plants", *Water Res.,* **39 (19),** 4797-4807 (2005).

Conesa, C, Calvo, M. and Sanchez, L., "Recombinant human lactoferrin: A valuable protein for pharmaceutical products and functional foods", *Biol. Adv.,* **28,** 831–838 (2010).

Deegan, A. M., Shaik, B., Nolan, K., Urell, K., Oelgemoller, M., Tobin, J. and Morrissey, A., "Treatment options for wastewater effluents from pharmaceutical Companies", *Int. J. Environ. Sci. Tech.,* **8 (3),** 649-666 (2011).

Delgado, J., Briones, J. and Sierra J., "Emerging therapies for patients with advanced chronic lymphocytic leukaemia", *Blood Reviews,* **23,** 217-224 (2009).

Doorslaer, X. V., Demeestere, X., Philippe, M., Heynderickx, H. and Dewulf, V. L., "UVA and UVC induced photolytic and photocatalytic degradation of aqueous ciprofloxacin and moxifloxacin: Reaction kinetics and role of adsorption", *Appl. Catal., B* **101**, 540-547 (2011).

Dutta, M., Baruah, R. and Dutta, N., "Adsorption of 6-aminopenicillanic acid on activated carbon", *Sep. Purif. Tech.,* **12 (2),** 99-108 (1997).

Elmolla, E. and Chaudhuri, M., "Optimization of Fenton process for treatment of amoxicillin, ampicillin and cloxacillin antibiotics in aqueous solution", *J. Hazard. Mater.,* **170,** 666-672 (2009).

Ellis, J., "Pharmaceutical and personal care products (PPCPs) in urban receiving waters", *Environ. Pollut.,* **144,** 184-189 (2006).

Filiz, A. and Fikret, K., "Advanced oxidation of amoxicillin by Fenton's reagent treatment", *J. Hazard. Mater.,* **179,** 622-627 (2010).

Gautama, A. K. and Sabumona, P. C., "Preliminary study of physico-chemical treatment options for hospital wastewater", *J. Environ. Manage.,* **83,** 298-306 (2007).

Giri, R., Ozaki, H., Takayanagi, Y., Taniguchi, S. and Takanami, R., "Efficacy of ultraviolet radiation and hydrogen peroxide oxidation to eliminate large number of pharmaceutical compounds in mixed solution", *Int. J. Environ. Sci. Tech.,* **8 (1),** 19-30 (2011).

Gogate, P.R. and Pandit, A. B., "A review of imperative technologies for wastewater treatment I: oxidation technologies at ambient conditions", *Adv. Environ. Res.,* **8,** 501-551, (2004a).

Gogate, P. R. and Pandit, A. B., "A review of imperative technologies for wastewater treatment II: hybrid methods", *Adv. Environ. Res.,* **8,** 553-597, (2004b).

Gomez, J. M., Sirtory, C., Mezcua, M., Fernandez, A. R. and Aguera, A., "Photodegradation study of three dipyrone metabolites in various water systems: Identification and toxicity of their photodegradation products", *Water Res.,* **42,** 2698-2706 (2008).

Gonzalez, O., Sans C. and Esplugas S. "Sulfamethoxazole abatement by photo-Fenton Toxicity, inhibition and biodegradability assessment of intermediates", *J. Hazard. Mater.,* **146**, 459-464 (2007).

Gurkan, Y. Y., Turkten, N., Hatipoglu, A. and Cinar, Z., "Photocatalytic degradation of cefazolin over Ndoped TiO_2 under UV and sunlight irradiation: Prediction of the reaction paths via conceptual DFT", *Chem. Eng. J.*, **184**, 113-124 (2012).

Gulkowska, A, Leung, H. W., So, M. K., Taniyasu, S., Yamashita, N. and Yeung, L. W. Y., "Removal of antibiotics from wastewater by sewage treatment facilities in Hong Kong and Shenzhen, China", *Water Res.,* **42,** 395-403 (2008).

Haddad, T. and Kummerer, K., "Characterization of photo-transformation products of the antibiotic drug Ciprofloxacin with liquid chromatography–tandem mass spectrometry in combination with accurate mass determination using an LTQ-Orbitrap", Chemosphere, http://dx.doi.org/10.1016/j.chemosphere.2014.02.013.

Hartig, C., Ernst, M. and Jekel, M., "Membrane filtration of two sulphonamides in tertiary effluents and subsequent adsorption on activated carbon", *Water Res.,* **35 (16),** 3998-4003 (2001).

Hartmann, T., Kummerer, K. and Hartmann, A., "Biological degradation of cyclophosphamide and its occurrence in sewage water", *Ecotoxic. Environ. Safe.,* **36,** 174-179 (1997).

Heberer, T., "Occurrence, fate, and removal of pharmaceutical residues in the aquatic environment. a review of recent research data", *Toxicol. Lett.,* **131,** 5-17 (2002).

Heeb, M. B., Criquet, J., Zimmermann-Steffens, G. S. and Gunten, U. V., "Oxidative treatment of bromide-containing waters: Formation of bromine and its reactions with inorganic and organic compounds d A critical review", *Water Res.,* **48,** 15-42 (2014).

Huber, M. M., Gobel, A., Joss, A., Hermann, N., Loffler, D., Mc Ardell, C. S., Ried, A., Siegrist, H., Ternes, T. and von-Gunten, U., "Oxidation of pharmaceuticals during ozonation of municipal wastewater effluents: A Pilot study", *Environ. Sci. Technol.,* **39,** 4290-4299 (2005).

Huseyin, T., Okan, B., Selale, S. and Tolga, H., "Use of Fenton oxidation to improve the biodegradability of a pharmaceutical wastewater", *J. Hazard. Mater.,* **136,** 258–265 (2006).

Ileri, R., Sengil, I., Kulac, S. and Damar, Y., "Treatment of mixed pharmaceutical industry and domestic wastewater by sequencing batch reactor", *J. Environ. Sci. Heal. A.,* **38 (10),** 2101-2111 (2003).

Karpinska, A., Sokoł, A. and Karpinsk, J., "Studies on the kinetics of carbamazepine degradation in aqueousmatrix in the course of modified Fenton's reactionsAgnieszka", *J. Pharm. Bio. Anal.,* http://dx.doi.org/10.1016/j.jpba.2014.06.033.

Khetan, S. and Collins, T., "Human pharmaceuticals in the aquatic environment: A challenge to green chemistry", *Chem. Rev.,* **107 (6),** 2319-2364 (2007).

Kim, I. and Tanaka, H., "Use of ozone-based processes for the removal of pharmaceuticals detected in a wastewater treatment plant", *Water Environ. Res.,* **82(4),** 294-301 (2010).

Kimura, K., Hara, H. and Watanabe, Y., "Removal of pharmaceutical compounds by submerged membrane bioreactors (MBRs)", *Desalination,* **178,** 135-140 (2005).

Kolpin, D. W., Furlong, E. T., Meyer, M. T., Thurman, E. M., Zaugg. and Buxton, H. T., "Pharmaceuticals, hormones and other organic wastewater contaminants in U.S. streams, 1999–2000: A national reconnaissance", *Environ. Sci. Technol.,* **36,** 1202–1211 (2002).

Kulakovskay, T. V., Vladimir, M. and Kulaev, S., "Inorganic polyphosphate in industry, agriculture and medicine: Modern state and outlook", *Process Biochem.,* 47, 1-10 (2012).

Li, X., Zhou, Q., Wei, S., Ren, W. and Sun, X., "Adsorption and desorption of carbendazim and cadmium in typical soils in northeastern China as affected by temperature", *Geoderma,* **160,** 347–354 (2011).

Li, W., Nanaboina, V., Zhou, Q. and Korshin, G. V., "Effects of Fenton treatment on the properties of effluent organic matter and their relationships with the degradation of pharmaceuticals and personal care products", *Water Res.,* **46 (2),** 403-412 (2012).

Li, W., Shi Y., Lihong, G., Liu, J. and Y Cai., "Occurrence, distribution and potential affecting factors of antibiotics in sewage sludge of wastewater treatment plants in China", *Sci. Total Environ.,* **445–446,** 306–313 (2013).

Lia, K., Hokanson, D. R., Crittendena, C. R., Rhodes, R. and Minakata, T. D., "Evaluating UV/H_2O_2 processes for pharmaceuticals removal: Effect of pretreatment options and light sources", *Water Res.,* **42,** 5045-5053 (2008).

Lin, S. H. and Lo, C. C., "Fenton process for treatment of desizing wastewater", *Water Res.,* **31,** 2050-2056 (1997).

Liu, H., Chen, Q., Yu, Y., Liu, Z. and Xue, G., "Influence of Fenton's reagent doses on the degradation and mineralization of H-acid", *J. Hazard. Mater.,* **263**, 593-599 (2013).

Luna, M. D. G., Veciana, M. L., Colades, J. I., Su, C. C. and Lu, M. C. "Factors that influence degradation of acetaminophen by Fenton processes*", J. Taiwan Inst. Chem. Eng.,* **45,** 565–570, (2014).

Luisa, M., Martinez, P., Pereira, N., Lima, R., Joaquim, L., Faria, H. T. and Gomes, A. M. T., "Degradation of diphenhydramine by photo-Fenton using magnetically recoverable iron oxide nanoparticles as catalyst," *Chem. Eng. J.*, http://dx.doi.org/10.1016/j.cej.2014.04.117.

Leonidas, A., Perez-Estrada, S. M., Aguera, A. and Fernandez-Alba, A. R., "Degradation of dipyrone and its main intermediates by solar AOPs Identification of intermediate products and toxicity assessment", *Catal. Today*, **129**, 207–214 (2007).

Maeng, S. K., Choi, B. G., Lee, K. T. and Song, K. G., "Influences of solid retention time, nitrification and microbial activity on the attenuation of pharmaceuticals and estrogens in membrane bioreactors", *Water Res.*, **47,** 3151-3162 (2013).

Mayabhate, S. P., Gupta, S. K. and Joshi, S. G., "Biological treatment of pharmaceutical wastewater", *Water Air Soil. Poll.*, **38,** 189-197 (1988).

Mendez-Arriaga, F., Esplugas, S. and Gimenez, J., "Degradation of the emerging contaminant ibuprofen in water by photo-Fenton", *Water Res.*, **44,** 589-595 (2010).

Miralles-Cuevas, S., Oller, I., Sanchez Perez, J. A. and Malato, S., "Removal of pharmaceuticals from MWTP effluent by nanofiltration and solar photo-Fenton using two different iron complexes at neutral pH", *Water Res.*, **64,** 23-31 (2014).

Moraes, J. E. F., Quina, F. H., Nascimento, C. A. O., Silva, D. N. and Chiavone-Filho, O., "Treatment of saline wastewater contaminated with hydrocarbons by the photo-Fenton Process", Environ. Sci. Technol., **38,** 1183-1187 (2004).

Murphy, R. J., Jones, D. E. and Stessel, R. I., "Relationship of microbial mass and activity in biodegradation of solid waste", *Waste Manage. Res.*, **13,** 485-497 (2005).

Nie, X. P., Liu, B. Y., Yu, H. J., Liu, W. Q. and Yang, Y. F., "Toxic effects of erythromycin, ciprofloxacin and sulfamethoxazole exposure to the antioxidant system in Pseudokirchneriella subcapitata", *Environ. Pollut.*, **172,** 23-32 (2013).

Nie, M., Yang, Y., Zhang, Z., Yan, C., Wang, X., Li, H. and Dong, W., "Degradation of chloramphenicol by thermally activated persulfate in aqueous Solution", *Chem. Eng. J.*, DOI: http://dx.doi.org/10.1016/j.cej.2014.02.047 (2014).

Noble, J., "MBR technology for pharmaceutical wastewater treatment", *Membr. Technol.*, **9,** 7-9 (2006).

Oppenlander, T., "Photochemical purification of water and air", *Membr. Tech.*, **11,** 17-29 (2003).

Oturan, M. A., Oturana, N., Mohamed, C., Edelahia, F. I. and Kacemib, E. K., "Oxidative degradation of herbicide diuron in aqueous medium by Fenton's reaction based advanced oxidation processes", *Chem. Eng. J.*, **171,** 127–135 (2011).

Paul, T., Dodd, M. C. and Strathmann, T. J., "Photolytic and photocatalytic decomposition of aqueous ciprofloxacin: Transformation products and residual antibacterial activity", *Water Res.*, **44,** 3121-3132 (2010).

Perez, M., Torrades, F., Domenech, X. and Peral, J., "Removal of organic contaminants in paper pulp effluents by AOPs: an economic study", *J. Chem. Technol. Biotechnol.*, **77(5),** 525-532 (2010).

Pugazhenthiran, N., Murugesan, S., Sathishkumar, P. and Anandan, S., "Photocatalytic degradation of ceftiofur sodium in the presence of gold nanoparticles loaded TiO_2 under UV-visible light", *Chem. Eng. J.*, **241**, 401-409 (2014).

Pereira, V. J., Linden, K. G. and Weinberg, H. S., "Evaluation of UV irradiation for photolytic and oxidative degradation of pharmaceutical compounds in water", *Water Res.,* **41(19),** 4413-4423 (2007).

Pignatello, J. J., Oliveros, E. and Mackay, A., "Advanced oxidation processes for organic contaminant destruction based on the Fenton reaction and related chemistry", *Crit. Rev. Environ. Sci. Technol.,* **36,** 1-84, (2006).

Plant, L. and Jeff, M., "A potent force to destroy organics in wastewater using hydrogen peroxide", *Chem. Eng. J.,* **31,** 16-20 (1994).

Radjenovic, J., Petrovic, M. and Barcelo, D., "Analysis of pharmaceuticals in wastewater and removal using a membrane bioreactor", *Anal. Bioanal. Chem.,* **387 (4),** 1365-1377 (2009).

Ravina, M., Campanella, L. and Kiwi, J., "Accelerated mineralization of the drug Diclofenac via Fenton reactions in a concentric photo-reactor", *Water Res.,* **36,** 3553–3560, (2002).

Ray, A. K., "Design, modeling and experimentation of a new large-scale photocatalytic reactor for water treatment", *Chem. Eng. Sci.,* **54,** 3113-3125, (1999).

Rodriguez, E. M., Marquez, G., Leon, E. A., Alvarez, P. M., Amat, A. M. and Beltrán, F. J., "Mechanism considerations for photocatalytic oxidation, ozonation and photocatalytic ozonation of some pharmaceutical compounds in water", *J. Environ. Manage.,* **127,** 114-124 (2013).

Santos, J. L., Aparicio, I., Callejon, M. and Alonso, E., "Occurrence of pharmaceutically active compounds during 1-year period in wastewater from four wastewater treatment plants in Seville (Spain)," *J. Hazard. Mat.,* **164 (2–3),** 1509–1516 (2010).

Shrivastava, A., Rathore, K. S, Solanki, N.S. and Shrivastavay, A. K., "Pharmaceuticals as pollutants treatment from the wastewater", *J. Pharm. Sci. Tech.,* **2(3),** 163-170 (2010).

Snyder, S., Adham, S., Redding, A., Cannon, F. and Carolis, J., "Role of membranes and activated carbon in the removal of endocrine disruptors and pharmaceuticals" *Desalination,* **202 (1-3),** 156-181 (2007).

Stumpf, M., Ternes, T.A., Wilken, R. D., Rodrigues, S. V. and Baumann, W., "Polar drug residues in sewage and natural waters in the state of Rio de Janeiro, Brazil", *Sci. Total Environ.,* **225,** 135-141 (1999).

Shemer, H., Kunukcu, Y. K. and Linden, K. G., "Degradation of the pharmaceutical metronidazole via UV, Fenton and photo-Fenton processes", *Chemosphere,* **63,** 269–276 (2006).

Su, C. C., Chang C. T., Luzvisminda M., Lu M. C., "Degradation of acetaminophen by Fenton and electro-Fenton processes in aerator reactor", *Sep. Purif. Technol.,* **99,** 8–13 (2012).

Sousa, M. A., Goncalves C., Joao H. O. S. Pereira., Vıtor J. P., Rui A. R. and Alpendurada M. F., "Photolytic and TiO_2-assisted photocatalytic oxidation of the anxiolytic drug lorazepam (Lorenino pills) under artificial UV light and natural sunlight: A comparative and comprehensive study", *Solar Energy,* **87,** 219-228 (2013).

Swancutt, K. L., Dail, M. K., Mezyk, S. P. and Ishida, K. P., "Absolute kinetics and reaction efficiencies of hydroxyl-radical-induced degradation of methyl isothiocyanate (MITC) in different quality waters", *Chemosphere,* **81,** 339-344 (2010).

Tekin, H., Bilkay, O., Selale, S. and Tolga, H., "Use of Fenton oxidation to improve the biodegradability of a pharmaceutical wastewater", *J. Hazard. Mater.,* **136,** 258–265 (2008).

Ternes, T. A., Stuber, J., Herrmann, N., McDowell, D., Ried A., Kampmann, M. and Teiser, B., "Ozonation: a tool for removal of pharmaceuticals, contrast media and musk fragrances from wastewater", *Water Res.,* **37,** 1976-1982 (2003).

Teel, A. L., Warberg, C. R., Atkinson, D. A. and Watts, R. J., "Comparison of mineral and soluble iron Fenton's catalysts for the treatment of trichloroethylene", *Water Res.,* **35 (4),** 977-984 (2001).

Trovo, A. G., Nogueira, R. F. P., Aguera, A., Fernandez-Alba, A. R. and Malato, S., "Paracetamol degradation intermediates and toxicity during photo-Fenton treatment using different iron species", *Water Res.,* **46,** 5374-5380 (2012).

Trovo, A. G., Paiva, A. B. de. V., Machado, A. E. H., Carlos A. and Santos, R. O., "Degradation of the antibiotic chloramphenicol by photo-Fenton process at lab-scale and solar pilot plant: Kinetic, toxicity and inactivation assessment", *Solar Energy,* **97**, 596-604 (2013).

Tan, C., Gao N., Deng, Y., Zhanga, Y., Suia, M., Denga, J. and Zhou, S., "Degradation of antipyrine by UV, UV/H_2O_2 and UV/PS", *J. Hazard. Mater.,* **260,** 1008– 1016 (2013).

Veloutsou, S., Bizani E. and Fytianos K., "Photo-Fenton decomposition of b-blockers atenolol and metoprolol; study and optimization of system parameters and identification of intermediates", *Chemosphere,* **107,** 180–186 (2014).

Walling, C., "Fenton's reagent revisited on metal-ligand interaction study", *Americ. Chem. Res.,* **8,** 125-129 (1975).

Wen, Z. H., Chen, L., Meng, X. Z., Duan, Y. P., Zhang, Z. S. and Zeng, E. Y., "Occurrence and human health risk of wastewater–derived pharmaceuticals in a drinking water source for Shanghai, East China", *Sci. Total Environ.,* **490,** 987-993 (2014).

Yang, W., Cicek, N. and Ilg, J., "State-of-the-art of membrane bioreactors: Worldwide research and commercial applications in North America", *J. Membr. Sci.,* **270 (1-2),** 201-211 (2006).

Yang, L., Yu, L. E, Ray and M. B., "Degradation of paracetamol in aqueous solutions by TiO_2 photocatalysis", *Water Res.,* **42,** 3480–3488, (2008).

Yeole, T. Y., Gadre, R. V. and Ranade, D. R., "Biological treatment of a pharmaceutical waste", *Indian J. Environ. Health.,* **38, (2),** 95-99 (1996).

Yuan, H., Zhou, X. and Zhang, Y., "Degradation of Acid Pharmaceuticals in the UV/H_2O_2 Process: Effects of Humic Acid and Inorganic Salts," *CLEAN-Soil Air Water,* **348**, 342-347 (2013).

Xiao, X., Zeng, X., Ann A. and Lemley T., "Species-Dependent Degradation of Ciprofloxacin in a Membrane Anodic Fenton System", *J. Agric. Food Chem.,* **58,** 10169–10175 (2010).

Xing, Z. P. and Sun, D. N., "Treatment of antibiotic fermentation wastewater by combined polyferric sulfate coagulation, Fenton and sedimentation process", *J. Hazard. Mater.,* **168,** 1264-1268 (2009).

Zhang, H. and Huang, C. H., "Aquatic photochemistry of fluoroquinolone antibiotics", *Environ. Sci. Technol*., **39,** 4474-4483 (2005).

Zhang, J., Fu, D., Xu, Y. and Liu, C., "Optimization of parameters on photocatalytic degradation of chloramphenicol using TiO_2 as photocatalyist by response surface methodology", *J. Environ. Sci.*, **22(8),** 1281-1289 (2010).

Zuorro, A., Fidaleo, M., Fidaleo, M. and Lavecchia R., "Degradation and antibiotic activity reduction of chloramphenicol in aqueous solution by UV/H_2O_2 process", *J. Environ. Manage.*, **133,** 302-308 (2014).

CHAPTER 2

Materials and Methods

This chapter details the experimental investigations, procedures and the methods of analyses followed throughout the study. It includes determination of drug concentration, total organic carbon (TOC), chemical oxygen demand (COD), biochemical oxygen demand (BOD), liquid chromatography-time-of-flight mass spectrometry (LC-TOF-MS), ion chromatography, Fourier transformed infrared (FTIR) spectroscopy and antimicrobial activity test. Specifications of all reagents and chemicals are documented in this chapter. Any specific change or deviation from what is stated here is detailed in the respective section(s) / chapter(s).

2.1 Chemicals and Reagents

HPLC grade CHPL (purity > 99% w/w), CIP (purity > 98% w/w) and DIPY (purity > 99% w/w), were procured from Sigma Aldrich (China). The chemical structure of the pharmaceuticals is illustrated in Figure 2.1. Other chemicals and reagents were procured mostly form Merck, Mumbai (India), Loba-Chemie, Mumbai (India) and Himedia (India).

Escherichia coli (*E. coli*) XL 10GOLD was collected from the Department of Biotechnology, Indian Institute of Technology Guwahati. Yeast (99% w/w purity) and tryptone (98% w/w purity) were obtained from Himedia (India). Mili-Q water (model: Elix 3, Millipore, USA) was used to prepare all reagents and solutions. All the plastic wares used were made of polypropylene procured from Tarson Products Pvt. Ltd., Kolkata (India).

Glassware with low coefficient of thermal expansion was obtained from Borosil, Mumbai (India). The chemical and reagent details are listed in Table 2.1.

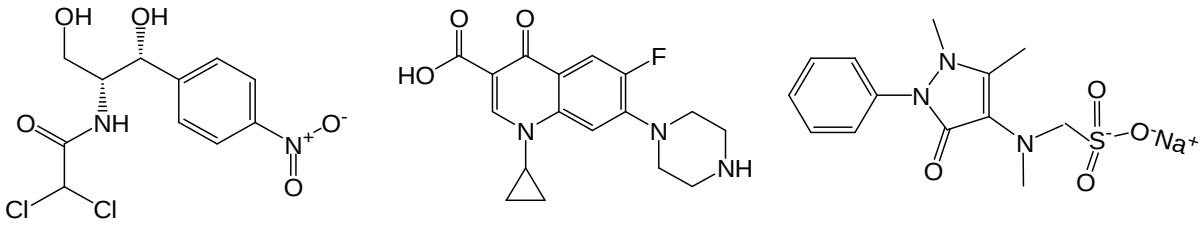

(a) (b) (c)

Figure 2.1. Chemical structure of chosen pharmaceuticals. (a) Chloramphenicol [2,2-dichloro-N-((1R,2R)-1,3-dihydroxy-1-(4-nitrophenyl)propan-2-yl) acetamide], (b) Ciprofloxacin [1-cyclopropyl-6-fluoro-4-oxo-7-(piperazin-1-yl)-quinoline-3-carboxylic acid], (c) Dipyrone [(2,3-dihydro- 1,5-dimethyl- 3-oxo- 2-phenyl-1-pyrazol-4-yl) methyl amino] methane sulfonate.

Table 2.1. List of chemicals/reagents used to prepare model effluent and reagents/ solutions.

Reagents/chemicals	**Purity (%)**	**Grade**	**CAS**	**Make**
Ethanol (C_2H_5OH)	99.9	AR	GB678-90	ChangshuYangyuan chemicals (China)
Tryptone	98	HPLC	ATTCC 25922	Himedia (India)
Yeast	98	AR	ATCC 16404	
Acetonitrile	99	AR	75-05-8	Loba-Chemie, Mumbai (India)
Calcium chloride ($CaCl_2 \cdot 2H_2O$)	95	AR	10043-52-4	
Formic acid (HCOOH)	98	AR	64-18-06	
Oxalic acid	99	AR	6153-56-6	
Sodium hydrogen carbonate ($NaHCO_3$)	99.5	AR	144-55-8	
Sodium nitrate ($NaNO_3$)	99	AR	7631-99-4	
Sodium oxalate (0.1 N)	99	AR	141-33-14	
Titanium dioxide (TiO_2)	99.5	AR	13463-67-7	
Agar solution	99	AR	10-29-2	Merck (India)
Ammonium Fluoride (NH_4F)	98	AR	7703-87-3	
Barium dichloride ($BaCl_2$)	98	AR	80-06-1	
Buffer solution pH 4.0 (phthalate)	99	AR	91-05-11	
Buffer solution pH 7.0 (phosphate)	99	AR	99-62-00	
Dimethyl sulphoxide (DMSO)	99	AR	67-68-5	
Dinitrophenyl hydrazine (DNPH)	99	AR	7758-99-7	
Dipotassium hydrogen phosphate(K_2HPO_4)	99	AR	10361-37-2	
Di-sodium hydrogen orthophoaphate (Na_2HPO_4)	99	AR	7758-79-4	
Ferroin solution ($C_{36}H_{24}FeN_6^{2+}$)	0.1	AR	14634-91-4	

Ferrous ammonium sulphate (FAS) ($Fe(NH_4)_2(SO_4)_2$)	98.5	AR	7783-85-9	
Formaldehyde (HCHO)	37-41	AR	50-00-0	
Hydrogen peroxide (H_2O_2)	50	AR	3722-44-1	
Hydroxyl-ammonium chloride	99	AR	10361-37-2	
Iron (III) chloride	96	AR	7705-08-0	
L-Glutamic acid	99	AR	56-86-0	
Magnesium chloride ($MnC1_2.4H_2O$)	97	AR	7791-18-6	
Mercury(II) chloride	98.5	GR	66-09-13	
Mercuric sulphate ($HgSO_4$)	98	AR	7783-35-9	
Methanol (CH_4OH)	99	AR	67-56-1	
Magnesium sulphate ($MgSO_4.7H_2O$)	99.5	AR	10034-99-8	
Molybdenum trioxide (MoO_3)	99.5	GR	5758	
Ortho-phosphoric acid	85	AR	7664-38-2	
Potassium bromide (KBr)	99.5	GR	03-02-7758	
Potassium dichromate ($K_2Cr_2O_7$)	99	AR	7778-50-9	
Potassium hydrogen phthalate($C_8H_5KO_4$)	99	AR	877-24-7	
Potassium iodide (KI)	99	GR	7681-11-0	
Potassium nitrate (KNO_3)	99	AR	7757-79-1	
Silver sulphate (Ag_2SO_4)	99	AR	10294-26-5	
Sodium acetate (CH_3COONa)	99	AR	127-09-3	
Sodium chloride (NaCl)	99.5	GR	7647-14-5	
Sodium carbonate (Na_2CO_3)	98	AR	14-05-11	
Sodium thiosulphate ($Na_2S_2O_3$)	98	AR	53-67-1	
Sucrose ($C_{12}H_{22}O_{11}$)	99	AR	57-50-1	
Sulphuric acid (H_2SO_4)	98	AR	7664-93-9	
Triethylamine (TEA)	99	AR	121-44-1	
Vitamin B_{12} ($C_{63}H_{88}CoN_{14}O_{14}P$)	97	AR	68-19-9	
Zinc sulphate ($ZnSO_4.7H_2O$)	99	AR	7446-20-0	
Chloramphenicol (CHPL)	98	HPLC	56-75-7	Sigma Aldrich (China)
Ciprofloxacin (CIP)	98	HPLC	85721-33-1	
Dipyrone (DIPY)	98	HPLC	68-89-3	
Pyridine-2,6-Dicarboxylic Acid	99	AR	499-83-2	SRL (India)
Tartaric acid	99	AR	147-71-7	
Escherichia coli (*E. coli*)	98	AR	T0910	Hi Tech (Chandigarh)

2.2 Analytical Methods

2.2.1 High Performance Liquid Chromatography (HPLC) for concentration determination of drug and iron-CHPL complex

C_{18} HPLC column (150 mm length, ∅ 3.5 mm) was used for the determination of concentration of drugs. HPLC instrument (model: 26462, Simadzu, Japan) equipped with UV-visible detector was employed for the chromatographic measurement. The mobile phase used for CHPL was a mixture of oxalic acid (0.01 M) and acetonitrile (60:40 v/v) at a flow rate of 0.4 mL/min and wavelength 362 nm (Liu et al., 2013). Acetonitrile (98% purity, v/v), water and tri-ethylamine (98% purity, v/v) at the flow rate of 1 mL/min (20:80:0.1 v/v/v) was used as the mobile phase for CIP at a wavelength of 280 nm (Hubicka et al., 2013).pH was adjusted to 3.0 using 5% (v/v) o-phosphoric acid. Methanol and water at the flow rate of 0.5 mL/min (80:20 v/v) was used for DIPY determination. The scanning was performed at a wavelength of 254 nm (Feldmann et al., 2008). In case of CHPL, CIP and DIPY (CCD) mixture, methanol and water (70:30 v/v) at a flow rate of 0.4 mL/min was used as the mobile phase and the scanning was performed at a wavelength of 236 nm. The suspended particle appeared, if any, were removed by filtration using 0.45 µm cellulose acetate filter (make: Pall India Pvt. Ltd., India; serial no. 08091ID0683).

The calibration curve was obtained in the range of 5 to 100 mg/L for CHPL and DIPY. The fitted equation was found as Peak-area = 688.1[CHPL] + 3917 (R^2 = 0.99) andPeak-area= 766.2[DIPY] + 6681 (R^2 = 0.99), respectively. The calibration of CIP was derived with concentration range from 1.0 to 12 mg/L and the calibration curve was obtained as Peak-area= 1288.4[CIP] + 562.5 (R^2 = 0.98).

A calibration curve for the determination of concentration of iron-CHPL complex (FeCHPLCOM) was prepared with a fixed dose of CHPL (100 mg/L) at different concentration of Fe^{2+} ranging from 0.5 to 2.0 mM. The complexation reaction was allowed for 10 min. The concentration of free CHPL was determined from its calibration curve without iron in solution corresponding to the retention time of 7.9 min (Table 2.2). The concentration of FeCHPLCOM was found out from the mass balance and a calibration equation was generated against peak area at 4.3 min of retention time. A linear relation as Peak-area= 214543.1[FeCHPLCOM] + 15406 with R^2 = 0.99 was obtained.

The slope and intercept of linearly fitted calibration equation for HPLC analyses are shown in Table 2.2.

Table 2.2. Parameters of calibration equation for determination of CHPL, CIP, DIPY and FeCHPLCOM concentration.

Compound	Retention time, min	Slope, (mV/mg/L)	Intercept, mV	R^2
CHPL	7.9	688.1	3917	0.99
CIP	6.1	1288.7	562.5	0.99
DIPY	11.7	766.2	6681	0.99
FeCHPLCOM	4.3	214543.1	15406	0.99

2.2.2 TOC determination

Total organic carbon (TOC) analyser of O.I. Analytical (model: 1030C Aurora, USA) was employed for determination of TOC before and after the experiments. Non-dispersive infrared method was adopted for the detection (NDIR). TOC was obtained by considering total inorganic carbon (TIC), purgeable organic carbon (POC), non-purgeable organic carbon (NPOC) and total carbon (TC) as outlined in Table 2.3.

TOC concentration of sample was calculated by comparing carbon content in potassium hydrogen phthalate (KHP) used as standard organic compound. The calibration curve was determined as $\text{Peak-area} = 26737.6[\text{TOC (mg/L)}] + 53123.4$ with $R^2 = 0.99$ in the range of 0.5 to 25 mg/L of TOC using KHP.

Table 2.3. Procedure for determination of TOC.

Procedure	Description
TC	Sample was oxidized using persulfate oxidation technique at 100 °C. To determine TC, sample was mixed with a pre-programmed volume of H_3PO_4 and $Na_2S_2O_8$. Combined sample was heated to the method temperature, allowing the carbonates and bicarbonates to dissociate to CO_2, and hydroxyl radicals oxidize organics to CO_2. TC was sent to the detector upon completion of the reaction. A stream of N_2 is passed through the reaction chamber carrying CO_2 to the non-dispersive infrared (NDIR) detector where the mass of carbon was quantified.

TIC	Inorganic carbon concentration was eliminated by acidification and sparging. Acidified (H_3PO_4) sample (pH ≤ 2) was heated to the 'method temperature', allowing carbonates and bicarbonates to dissociate to CO_2.
TIC +NPOC	After TIC, the system was ready for TOC analysis. It determined TOC by measuring CO_2 released by chemical oxidation of organic carbon present in the sample. Sodium persulfate ($Na_2S_2O_8$), a strong oxidizer, was used. Oxidant quickly reacts with organic carbon at100°C to CO_2. After completion of reaction, CO_2 was purged from the solution and routed to the NDIR detector. Results were reported as mg/L or µg/L of TOC.
NPOC Dissolved organic carbon (DOC) + Suspended organic carbon (SOC)	To remove TIC prior to NPOC analysis, a specified sample volume was transferred to the reaction chamber with 5 mL H_3PO_4. Acidified sample (pH ≤ 2) was sparged with a stream of N_2 as bicarbonates in the sample dissociate to CO_2. System determined TOC by measuring CO_2 released by chemical oxidation of organic carbon in the sample. After completion of reaction, CO_2 was purged from the solution and routed to the NDIR detector. TOC in calculated as mg/L or µg/L of TOC.
TOC Purgeable organic carbon (POC) + NPOC	TOC was obtained by subtracting TC from TIC.

2.2.3 Measurement of COD

COD was determined according to HACH method. A closed reflux digester of HACH (model: DRB 200, USA) was used for digestion. The digestion solution (0.25 N $K_2Cr_2O_7$) was prepared by dissolving 4.9 g $K_2Cr_2O_7$ in 500 mL DI water followed by addition of 167 mL concentrated H_2SO_4 and 33.3 g $HgSO_4$. The final volume was adjusted to 1 L. $K_2Cr_2O_7$ was dried at 103^oC for 2 h prior to preparation of reagent. Acid reagent solution was made

using 5.5 g Ag_2SO_4 per kg of concentrated sulphuric acid. It was kept for two days for the dissolution. Ferrous ammonium sulphate (FAS) of 0.25N was prepared by dissolving 39.2 g in 1 L of DI water with 20 mL of concentrated H_2SO_4 (APHA, 1998).

COD digestion vessel of 10 mL capacity was employed as the reaction chamber. A sample of 2.5 mL was added with 3 mL acid reagent followed by 1.5 mL of digestion solution. A second digestion vessel with the same quantity of these reagents and DI water instead of the sample was used as the blank. They were then kept in the COD digester at 150ºC for 120 min. The digested samples were then cooled down to room temperature and titrated with standard FAS using Ferroin as an indicator. The end point of titration was identified with the change in colour from bluish green to reddish brown. The volume of FAS consumed in titration was used for COD calculation using Eq. 2.1. COD measurement method adopted was suitable in the range from 0 to 1500 mg/L.

$$\text{COD} = \frac{(a-b)\times N\times 800}{\text{sample volume}}\ , \text{ mg/L} \qquad (2.1)$$

Where,

a = volume of FAS used in blank run, mL

b = volume of FAS used in sample run, mL

N = normality of FAS titrant

Sample volume = actual volume of sample used before dilution, mL

2.2.4 5-day BOD measurement

Biochemical oxygen demand (BOD) is usually defined as the amount of oxygen required by microorganisms while stabilizing decomposable organic matter under aerobic conditions. The term ‘decomposable’ may be interpreted as meaning that the organic matter can serve as food for microorganisms and energy is derived from its oxidation (Sawyer et al. 2003).Sample solution pH was neutralized to around 7 by using 1 molar NaOH or H_2SO_4. DI water was used for preparing dilution water and this was aerated to saturate it with oxygen before use. Appropriate quantity of phosphate buffer, magnesium sulphate, calcium chloride and ferric chloride were added to dilution water. 2 mL of sewer wastewater was added per litre of dilution water for ‘seeding’ purpose. Two sets of 300 mL BOD bottles were filled up. The BOD measurement is based upon the difference of dissolved oxygen (DO) of the first set, immediately measured and after incubating, it for 5 days at 20°C. Similarly, two measurements were performed for analysis of blank (APHA, 1998).

Dissolved oxygen (DO) was measured using a precision DO meter (model: HI 2400, Hanna Instruments, USA). Table 2.4 was used to prepare the dilution water for BOD determination.

Table 2.4. Typical volume of sample and dilution water for 5-days BOD tests (Sawyer and McCarty, 1978).

Anticipated range of BOD_5, mg/L	Sample volume, mL	Dilution water, mL
0-7	300	0
6-21	100	200
12-42	50	250
30-105	20	280
60-210	10	290
120-420	5	295
300-1050	2	298
600-2100	1	299

2.2.5 Derivatization procedure and determination of $HO^{\bullet}$ concentration

Sample was added into glass vial with previously added DMSO reagent (250 mM) at 1:0.4 (v/v). It was then mixed with 5 mL 2, 4-di-nitrophenylhydrazine (DNPH)-phosphate buffer reagent. It was prepared by mixing phosphate buffer of 2.5 mL at pH 4 with 6 mM of 0.2 mL DNPH (prepared in ethanol) and diluted to 5 mL with DI water. Hydrazone coloured derivative formed by the reaction between HCHO and DNPH is shown in Figure 2.2. The reaction mixture was analyzed by HPLC at a fixed wavelength of 365 nm at room temperature (Tai et al., 2004). An eluent phase of 40:60 (v/v) water/methanol at 0.5 mL/min was employed. The retention time of HCHO-DNPH coloured derivative at this condition was found as 7.8 min. The reactions involved for the formation of HCHO using DMSO and $HO^{\bullet}$ are shown through Eqs. (2.2) to (2.5). The amount of HCHO is formed at the stoichiometric ratio of 1:2.17 with respect to $HO^{\bullet}$ (Lindsey et al., 2000). The linear calibration equation as $\text{Peak-area} = 2350.7[HCHO - DNPH] + 587763.6$ (R^2 = 0.97) was obtained for determination of HCHO-DNPH.

$$2(CH_3)_2SO + 2OH^{\bullet} \rightarrow 2CH_3SO_2H + 2CH_3^{\bullet} \quad (2.2)$$

$$2CH_3^{\bullet} + 2H{-}R \rightarrow 2CH_4 + 2R^{\bullet} \quad (2.3)$$

$$2CH_3^{\bullet} + 2O_2 \rightarrow 2CH_3OO^{\bullet} \quad (2.4)$$

$$2CH_3OO^{\bullet} \rightarrow HCHO + CH_3OH + O_2 \quad (2.5)$$

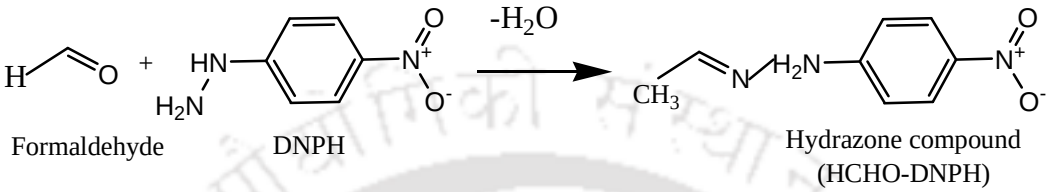

Figure 2.2. Formation of hydrazine colour derivative by the reaction between HCHO and DNPH.

2.2.6 Liquid chromatography-mass spectrometry (LC-MS)

HPLC method outlined earlier was adopted for subsequent sample introduction to MS detector. The chromatographic separation was performed using a YMC Hydrosphere C_{18} 150 mm×4.6 mm (5 µm particle size) reverse phase analytical column (Wilmington, NC, US) following a YMC Hydrosphere 10 mm×4 mm (5 µm particle size) guard column. The mobile phase flow rate was 0.8 mL/min. H_2O and acetonitrile with 0.1% (v/v) formic acid was employed as the mobile phase for all experiments. A linear gradient from 95 to 50% water for 15 min was used. A 10 µL of both sample and calibration solution were injected into the column using an AS 3000 auto injector (Thermo Finnigan, USA). Atmospheric pressure chemical ionization method in positive ion mode over the mass range of 100 to 500 amu was adopted. N_2 at a flow rate of 400 L/hfor drying and 150 L/h for sheathing were purged. The source temperature at 120°C and a cone voltage of 25 V were maintained to determine the mass (mass to charge ratio, m/z) of the parent ion and isotope. A cone voltage of 75 V was used for the fragmentation of the daughter ions. The electrospray source voltage was held at 3.5 kV and the temperature was maintained at 200°C.

2.2.7 Determination of inorganic ions

Inorganic ions released during mineralization of CCD mixture were measured by ion chromatography (model: 792 IC, Metrohm, India). Analyses were performed by injecting 25 µL aliquot of samples. Cl^-, F^- and NO_3^- concentration was determined with an ANION METROSEP A sup 5 column IC (250 mm in length with 4 mm in id). NH_4^+ was measured with a CATION METROSEP C_2 250 column IC (250 mm in length with 4 in mm id). The circulating phase with a flow-rate of 0.7 mL/min was composed of 1.0 mM $NaHCO_3$ and 3.2 mM Na_2CO_3 (1:1) for anion determination. It was pyridine dicarboxylic acid (0.75 mM) and tartaric acid (4.0 mM) at 1:1 (v/v) for cation. The flow rate was 1 mL/min.

2.2.8 FTIR spectroscopic analysis

The presence of different organic functional groups was confirmed by acquiring the FTIR spectra using KBr pellet method. KBr salt was dried in a hot air oven (model: MTC 1201, Sonu Instrument Manufacturing Company India) at 105°C. KBr to sample in the ratio of 99:1 (w/w) was grinded in a clean mortar and pestle for homogenization. It was then transferred to the pellet casting die. The pressure of 5 to 7 tons was imposed to create a thin pellet. The background correction was done with pure KBr pellet by scanning from 450 to 4500 1/cm with a resolution of 5 1/cm. The mixed sample was scanned in the same range. The number of scans was 45 for each specimen for noise reduction. A FTIR spectrophotometer (model: IR affinity 1, of Shimadzu, Japan) was employed for this work.

2.2.9 UV-Vis spectroscopy

UV-Vis spectra were acquired by employing a spectrophotometer (model: UV-2300, Thermo Scientific, India) with an optical path length of 1 cm. Concentration of H_2O_2 was determined using colorimetric method. The colour of aqueous H_2O_2 solution was developed in acidic reagent of $Ti_2(SO_4)$. The intensity of H_2O_2-Ti(IV) yellow colour complex was measured at 420 nm (Nicoll et al., 1955).

2.2.10 Antimicrobial activity test

The antimicrobial activity of drugs and its degradation products were evaluated by recording the number of colony forming unit (CFU) of *E. coli* bacteria. It was inoculated in Luria-Bertani (LB) media (yeast extract 5, tryptone 10 and NaCl 10 are in g/L) (Liang et al., 2013).

The media pH was adjusted to 7.2 using 1M NaOH and autoclaved (model: 7407PAD, Medica Instrument Mfg. Co., India) for 20 min at 15 lbs pressure (121°C). 50 µL initial cultured of *E. coli* was added to 5 mL media and incubated for 24 h at 37°C on an orbital shaker at 180 rpm (model: ORBITEK^{R}, Scigenics Biotech, India). The growth media with harvested cells analysed into 3 parts. 1 mL diluted growth media was added on the agar plate (Sisto et al., 2014) and the number of CFU was counted after 24 h of incubation at 37°C. The second sample was diluted at different proportions and the absorption intensity was recorded at 621 nm. A calibration curve was prepared by plotting the number of CFU/mL against the absorption intensity.

The third sample was centrifuged at 2000 rpm for 15 min. The supernatant was discarded and the harvested bacterial cells were washed in deionized water. It was then suspended in 50 mL LB media and further diluted to have CFU/mL of ~2×10^{8}. 1 mL of media and 5 mL sample was mixed and incubated for 24 h at 37°C (Livard et al., 2013). The corresponding absorbance was recorded and converted to CFU/mL from the calibration curve.

The details of various instruments used in different parts of this work are summarized in Table 2.5.

Table 2.5. Instrumental details for analysis of water quality parameters and experimental work.

Instrument	Model and make	Purpose	Detection/ working/performance range
Analytical balance	Model: BSA 224S-CW Make: Sartorius, India	Weight measurement	0 to 220 g Resolution: 0.1 mg
Centrifuge	Model: HA01-10092 Make: Remi, India	Sludge separation	Maximum speed: 8000 rpm
DO meter	Model: HI2400 Make: Hanna Instruments, USA	Dissolved oxygen	DO: 0 to 45 mg/L
COD digester	Model:DRB 200 Make: HACH, USA	Chemically oxygen demand determination	0-1500 mg/L
FTIR spectrometer	Model: IR affinity 1 Make: Shimadzu, Japan	Functional group characterization	Frequency: 350 to 7500 cm^{-1}
Hot air oven	Model: ISO 9001-2008 Make: Navyug, India	Moisture removal	Temperature: 30 to 250°C
HPLC instrument	Model: LC-20AD Make: Simadzu, Japan	Concentration determination	0.01 to 1µg/mL
Ion chromagraphy	Model: 792 IC Make: Metrohm, Switzerland	Inorganic ion determination	5 µg/L to 50 mg/L
TOC analyser	Model: 1030C Aurora	Total organic carbon	50 ±1 to 2 µg/L

	Make: O.I. Analytical, USA	determination	
Liquid chromatography mass spectrometer	Model: YMC Make: Wilmington, USA	Mass analysis	50-1000, m/z
Magnetic stirrer	Model: Spinot 6020 Make: Tarson, India	Mixing/agitation	Stirrer speed: 100 to 1000 rpm
Micropipette	Model: T100 & T1000 Make: Tarsons products Pvt Ltd., India	µL range liquid dispensing for analytical work	Capacity T100:10 to 100 µL T1000:100 to 1000 µL
Microwave oven	Model: MH-2046HB Make: LG Electronics, India	Microwave assisted drying of glasswere	Frequency: 2450 MHz (fixed) Microwave: 800 W (fixed)
Millipore water purification unit	Model: Elix 3 Make: Millipore, USA	Preparation of all reagent and test solutions	TOC: <30 µg/L Pyrogens (endotoxins):<0.001 EU/mL Water resistivity (@ 25 °C): >5 MΩ cm
Orbital shaker	Model: LSI-3016R Make: Lab Tech, Korea	Agitation	Maximum speed: 350 rpm Temperature: ± 0.5°C
pH meter	Model: pH 510 Make: Eutech Instruments, Singapore	pH measurement	pH: 0 to 14 Resolution: 0.01 pH
Ultrasonic bath	Model: Lab Companion UC-02 Make: Jeiotech, Korea	Mixing	Frequency (sound wave): 40 kHz (fixed) Ultrasonic power: 70 W (fixed)
UV-vis spectrophotometer	Model: Spectrascan UV-2300 Make: Thermofisher Scientific, India	Absorbance measurement	Wavelength: 190-1100 nm Resolution: 0.05 nm

2.3 Experimental procedure

Fenton process (FP): Batch experiment was conducted for the degradation study with continuous stirring. A 1000 mL capacity cylindrical borosilicate vessel (Ø 10.5 cm) was used as the reactor. 0.05 N H_2SO_4 was used for the adjustment of drug solution pH prior to addition of catalyst. $[Fe(NH_4)_2(SO_4)].7H_2O$ was added (Serra et al., 2011) and mixed for about 10 min at 260 rpm using a magnetic stirrer (model: Spinot 6020, Tarson, India; stirring bar: Ø 0.8 mm, length 40 mm) and solution pH was recorded. After that desired amount of H_2O_2 was added to drug-Fe^{2+} solution to obtain the final volume of 400 mL. The initial concentration of CHPL, CIP and DIPY were of 100, 15 and 50 mg/L, respectively (Trovo et al., 2014; Assumpcao et al., 2013; Yang et al., 2006). Equimolar concentration of CCD mixture was used for mixed drug system. The concentration of each drug was 0.05 mM, calculated based on DIPY concentration, for CCD mixture.

pH was varied from 2.0 to 4.0, 2.0 to 4.5 and 2.0 to 4.0 for CHPL, CIP and DIPY, respectively. Fe^{2+} doses were of 0.5 to 2.0, 0.5 to 1.8 and 1.0 to 3.0mM. The subsequent H_2O_2

was in the range of 5.0 to 25, 10 to 10 and 5.0 to 25mM. CCD experiment was conducted at fixed pH, Fe^{2+} and H_2O_2 of 3.5, 2.25 mM and 22.5 mM, respectively.

10 mL sample was taken out at different time intervals and 0.1 N NaOH was immediately to stop the reaction at 10:1 (v/v). NaOH addition increased pH at around from 12.0. Conversion of Fe^{2+} to Fe^{3+} is extremely fast at such high pH (Stumm et al., 1981). Sludge was separated out by centrifugation at 2000 rpm for 30 min and clear supernatant was heated at 70°C to destroy residual H_2O_2, if any (Luis et al., 2009) for drug degradation experimentation. After that drug concentration, COD and TOC were determined. FTIR spectra, mass spectra, ion-chromatograph and antimicrobial activity test were usually carried out at the beginning and end of the experimental run. The sample was subjected for an additional step of filtration using 0.45µm cellulose filter (make: Pall India Pvt. Ltd., India; serial no. 08091ID0683).

Photo-Fenton process (PFP): PFP was performed in similar manner under UV light irradiation. An UV lamp (wavelength: 362 nm, intensity: 12 W/m^2) of obtained from Hong Kong Jie Meng International Lighting Ltd Company (China) was employed for this work. The intensity of UV light was selected based on the earlier study (Zuorro et al., 2014). The UV-lamp was fixed just on the top of solution at about 5 cm above. The solution temperature was controlled with proper cooling arrangement (25±2°C). The other experimental condition was similar to FP.

UV/H_2O_2 photolysis (UVP): UVP experiment was conducted with a fixed concentration of H_2O_2 under UV irradiation without Fe^{2+}. Optimized value of pH and H_2O_2 in FP or PFP was adopted for UVP.

UV/TiO_2 photo catalysis (UVPC): TiO_2 of rutile type crystal was used for the decomposition of DIPY. Like FP, PFP and UVP, the test was performed with 400 mL DIPY solution and pH was adjusted to the desired value. The same UV lamp was employed for all photo experiments. TiO_2 was then added and mixed for about 10 min to achieve DIPY adsorption on the catalyst surface. Catalyst dose and pH were varied from 0.5 to 2.5 g/L and 2 to 4.5, respectively. UV light was irradiated and sample was withdrawn at different time intervals. Catalyst particle was separated by centrifugation followed by filtration. The sample was analysed as outlined before. All the experiments were performed in duplicate and the average values are reported.

References

APHA, *Standard Methods for the Examination of Water and Wastewater*, American Public Health Association, 20th ed., Washington (1998).

Assumpcao, M. H. M. T., Moraesa, A., Souzaa, R. F. B. D., Reisb, R. M., Rochab, R. S., Gaubeura, I., "Degradation of dipyrone via advanced oxidation processes using a cerium nanostructured electrocatalyst material", *Appl. Catal. A.,* **462-463,** 256-261 (2013).

Feldmann, D. F., Zuehlke, S. and Heberer, T., "Occurrence, fate and assessment of polar metamizole(dipyrone) residues in hospital and municipal wastewater", *Chemosphere,* **71,** 1754-1764 (2008).

Hubicka, U., Żmudzk, P., Talik, P., Zuromska-Witek, B., and Krzek, J., "Photodegradation assessment of ciprofloxacin, moxifloxacin, norfloxacin and ofloxacin in the presence of excipients from tablets by UPLC-MS/MS and DSC", *Chem. Cent. J.*, **7,** 133-137 (2013).

Levard, C., Mitra, S., Yang, T., Jew, A. D., Badireddy, A. R., Gregory. V. and Brown, G. E., "Effect of chloride on the dissolution rate of silver nanoparticles and toxicity to E. coli", *Environ. Sci. Technol.*, **47,** 5738-5745 (2013).

Liang, B., Cheng, H. Y., Kong, D.Y., Gao, S. H., Sun, F., Cui, D., Kong, F. Y., Zhou, A. J., Liu, W. Z., Ren, N. Q., Wu, W. M., Wang, A. J. and Lee, D. J., "Accelerated reduction of chlorinated nitroaromatic antibiotic chloramphenicol by biocathod", *Environ. Sci. Technol.*, **47,** 5353-5361 (2013).

Lindsey, E. M. and Tarr, A. M., "Quantitation of hydroxyl radical during Fenton oxidation following a single addition of iron and peroxide", *Chemosphere*, **41(3),** 409-417 (2000).

Luis, A. D., Lombranda, J. I., Varona, F. and Menendez, A., "Kinetic Study and hydrogen peroxide consumption of phenolic compounds oxidation by Fenton's reagent", *Korean J. Chem. Eng.*, **26(1),** 48-56 (2009).

Nicoll, W. D. and Smith, A. F., "Stability of dilute alkaline solutions of hydrogen peroxide", *Ind. Eng. Chem. Res.*, **47(12),** 2448-2554 (1955).

Sawyer, C. N. and McCarty, P. L., *Chemistry for Environmental Engineering*, McGraw-Hill, 3rd ed., USA (1978).

Sawyer, C. N., McCarty, P. L. and Parkin, G. F., *Chemistry for Environmental Engineering and Science*, Tata McGraw-Hill Publishing Company Limited, 5th ed., New Delhi (2003).

Serra, A., Dom, X.,Brillas, E. and Peral, J., "Life cycle assessment of solar photo-Fenton and solar photoelectro-Fenton processes used for the degradation of aqueousamethylphenylglycine", *J. Environ. Monit.*, **13**, 167-174 (2011).

Sisto, F., Bonomi, A., Cavicchini, L., Cocce, V.,Scaltrito, M. M.,Bondiolotti, G., Alessandri, G., Parati, E. and Pessina, A., "Human mesenchymal stromal cells can uptake and release ciprofloxacin, acquiring in vitro anti-bacterial activity", *Cytotherapy*, **16,** 181-190 (2014).

Stumm, W. and Morgan, J. J., *Aquatic Chemistry*, John Wiley, 2nd ed., New York (1981).

Tai, C., Peng, J. F., Liu, J. F., Jiang, G. B. and Zou, H., "Determination of hydroxyl radicals in advanced oxidation processes with dimethyl sulfoxide trapping and liquid chromatography", *Anal. Chim.Acta.,* **527,** 73-80 (2004).

Trovo, A. G., Paiva, A. B. de. V., Machado, A. E. H., Carlos, A. and Santos, R. O., "Degradation of the antibiotic chloramphenicol by photo-Fenton process at lab-scale and solar pilot plant: Kinetic, toxicity and inactivation assessment", *Solar Energy*, **97,** 596-604 (2013).

Yang, W., Cicek, N. and Ilg, J., "State-of-the-art of membrane bioreactors: Worldwide research and commercial applications in North America", *J. Membr. Sci.,* **270 (1-2),** 201-211 (2006).

Zuorro, A., Fidaleo, M., Fidaleo, M. and Lavecchia R., "Degradation and antibiotic activity reduction of chloramphenicol in aqueous solution by UV/H_2O_2 process", *J. Environ. Manage.*, **133,** 302-308 (2014).

CHAPTER 3

Chloramphenicol Degradation: Formation of Fe^{2+}-Chloramphenicol Chelate, Reaction Pathways and Toxicity Assay

Formation of Fe^{2+}-chloramphenicol complex (FeCHPLCOM) and degradation of chloramphenicol (CHPL) and FeCHPLCOM mixture at high concentration are focused in this chapter. The antimicrobial activity of CHPL and its degradation products are also covered.

3.1. Introduction

Chloramphenicol (CHPL) is a broad-spectrum antibiotic exhibiting the activity against both gram-positive and gram-negative bacteria. It imparts the action through inhibition of microorganism protein synthesis. CHPL was found between 0.001 and 0.031 mg/L in surface water at different places of Singapore and Korea. In effluents of STP, it was detected between 2.08 and 26.6 mg/L in China (Trovo et al., 2013). Traditionally, CHPL is biosynthesized by the soil organism, *Streptomyces venezuelae* and several other *Actinomycetes* as well (Aouiche et al., 2012). CHPL is a suspected carcinogen. The drug is banned for use in food-producing animals in the European Union and in many other countries, including USA, Canada, Australia, Japan, and China due to its linkage with the development of aplastic anemia in humans (Wongtavatchai et al., 2004). A monitoring study focusing on the detection of veterinary drugs in manure, groundwater, soil, and plants, confirmed the presence of low levels of CHPL in plants and soil (<1 μg/kg) (Hu et al., 2010). In Asian countries including

China, CHPL was detected as 26-2430 ng/L in influent and 3-1050 ng/L in STP effluent (Lin et al., 2011; Sui et al., 2008; Xu et al., 2007). CHPL concentration in sewage was observed as high as 47.4 µg/L in Guiyang, China (Liu et al., 2009). In India, the Marine Products Export Development Authority has banned the use of CHPL in food producing animals in 2002 (MPEDA, 2002). As expected that CHPL resistant bacteria/genes were found in numerous water streams (Parsley et al., 2010).

Antibiotics act as a ligand for the formation of ligand to metal charge transfer (LMCT) complex (Lai et al., 1995). 3d-transition metals could coordinate through carbonyl and hydroxyl groups of ligands such as CHPL. Wahed et al. (2008) observed formation of a purple complex on reaction of Cu^{2+} with CHPL in an alkaline aqueous solution (pH 13). It is actually a complex anion with metal to ligand ratio of 1:2. Fazakerley et al. (1973) found that Cu^{2+}-CHPL complex are quite stable in both aqueous and methanol solutions (Fazakerley et al., 1973). The complexion of Mn^{2+}, Co^{2+}, Ni^{2+}, Cu^{2+}, Zn^{2+}, Cd^{2+} and Hg^{2+} with CHPL occurred at around pH 7. It is prudent from the earlier studies that CHPL can act as a bidentate chelating ligand for selective coordination with Fe^{2+} in an aqueous solution. The redox reaction in the formation of iron complexes promoted by LMCT is an important source of Fe^{2+} in Fenton process (Luis et al., 2009). Hence, faster Fe^{2+} to Fe^{3+} inter-conversion has a significant role on the degradation of the contaminants (Buchanan et al., 2005). Puttaswamy et al. (2009) suggested that the improvement of degradation depends mainly on: (i) higher absorption coefficient of iron organic complexes than free iron ions, (ii) high quantum yield of Fe^{2+} generation and, (iii) generation of $CO_2^{\bullet-}$ radical.

Aqueous effluent laden with CHPL gives relatively higher COD in comparison to its BOD values i.e. its shows up lower BOD_5/COD ratio (Bel et al., 2009). The efficiency of the biological processes for the treatment of wastewater laden with CHPL is ordinarily inhibited (Csay et al., 2012).

Likewise, an investigation was performed to uncover Fe^{2+}-CHPL complex (FeCHPLCOM) formation in terms of UV-vis spectroscopy, HPLC, FTIR and LC-MS analyses. The performance of FP, PFP and UVP for the degradation of CHPL and FeCHPLCOM (in FP and PFP only) was investigated. To identify the degradation products, LC-MS spectra were acquired when CHPL decomposition was found to be almost invariant. The proposed mechanism showed the routes of CHPL decomposition with low errors (g/moL) determined from the difference between the proposed and extract masses. Furthermore, the antimicrobial activity of CHPL and its degradation products were evaluated using *E. coli*.

3.2 Results and Discussion

3.2.1 Formation of FeCHPLCOM

3.2.1.1 Evidences of FeCHPLCOM from UV-Vis spectra

The absorption spectra of CHPL and FeCHPLCOM showed three necessary maximum peaks (λ_{max}) at 213, 263 and 389 nm (Figure 3.1). The band at 213 nm may be attributed to π- π* transition. While the other two bands at 263 and 382 nm can be assigned to n- π* transitions of O-H and C=O groups of free CHPL ligand (Wahed et al., 2008). These bands slightly shifted to lower absorbance and shorter wavelength (blue shift). It signifies that O-H and C=O groups were involved in complexation with Fe^{2+} (Aresta et al., 2013). There was small shifting of both intensities and wavelength with the extent of complexation i.e. with different Fe^{2+} concentration.

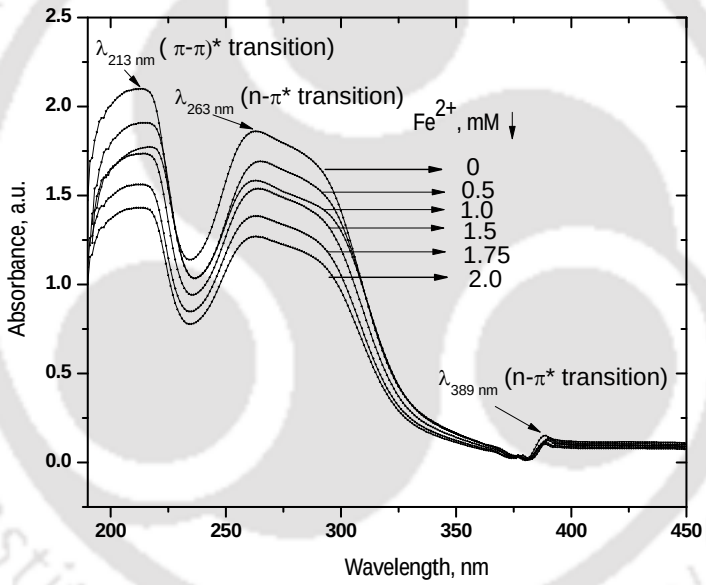

Figure 3.1. UV-Vis electronic spectra of CHPL and Fe^{2+} mixture. Experimental conditions: $[CHPL]_0$ =100 mg/L, Fe^{2+} = 0.5 to 2 mM, chelation time = 10 min, pH = 3 and temperature = 25°C.

3.2.1.2 High performance liquid chromatograph and FeCHPLCOM

Pure CHPL appeared in the chromatogram at 7.8 min (Figure 3.2). A new peak was found at 4.3 min of retention time in presence of Fe^{2+}. It evidenced for formation of a new compound i.e. FeCHPLCOM. It could easily eliminate proton (H^+) due to complexation and is more polar compared to free CHPL molecule. The chromatograph was recorded upto 45

min but no significant peak was noted. It used 6 orbitals from 4s, 4p and 4d by accepting electrons from carbonyl oxygen and -OH group attached to C_2 in complexation reaction. Both lone electron pairs and one negative ion of bidentate ligands could bond to the central Fe^{2+} ion. Fe(II) species react with H_2O_2 and $HO^{\bullet}$ is formed via Haber-Weiss reaction mechanism (Eq. 3.1) (Puma et al., 1991).

$$[Fe(II)-L_n] + H_2O_2 \rightarrow [Fe(III)-L_{n-1}]^{+} + OH^{\cdot} + OH^{-} \qquad (3.1)$$

Fe(III)-ligand complexes and $[Fe(III)\text{-}L_{n-1}]^{+}$ could be photochemically reduced to Fe(II) (Eq. 3.2).

$$[Fe(III)-L_{n-1}]^{+} + h\nu \rightarrow [Fe(II)-L_{n-2}]^{+} + L^{\cdot} \qquad (3.2)$$

It is clearly evident from the chromatograph that the peak area corresponding to CHPL gradually decreased with increase in Fe^{2+} dose at a fixed CHPL concentration (Figure 3.2). The peak area representing FeCHPLCOM increased at the same time. A linear relation between FeCHPLCOM concentration and peak area was noted at 4.3 min of retention time. Two experiments were conducted to study the possibility of Fe^{3+}-CHPL complex at pH 3 and 5. Fe^{3+} and CHPL mixture was contacted for 10 min and the mass spectra were obtained. It shows that Fe^{3+} could not form complex with CHPL (Figures 3.3 and 3.4).

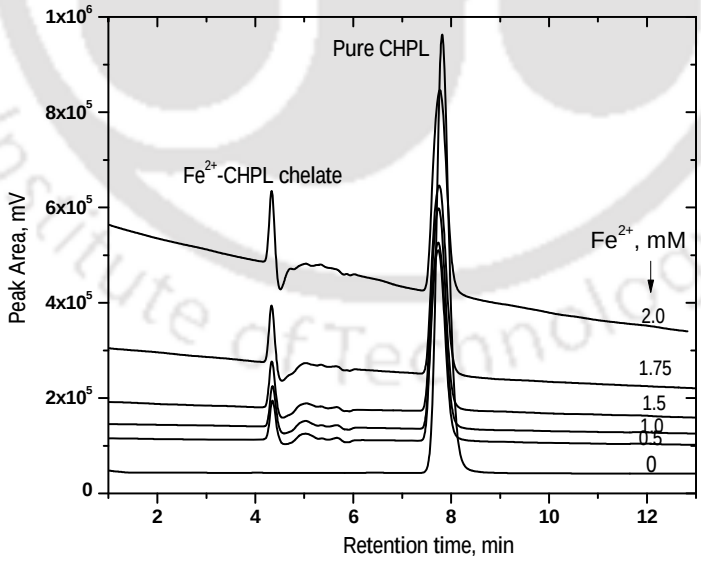

Figure 3.2. Chromatogram of pure CHPL and Fe^{2+}-CHPL mixture at different Fe^{2+} concentration. Experimental conditions: $[CHPL]_0$ =100 mg/L, Fe^{2+} = 0.5 to 2 mM, chelation time = 10 min, pH = 3 and temperature =25°C.

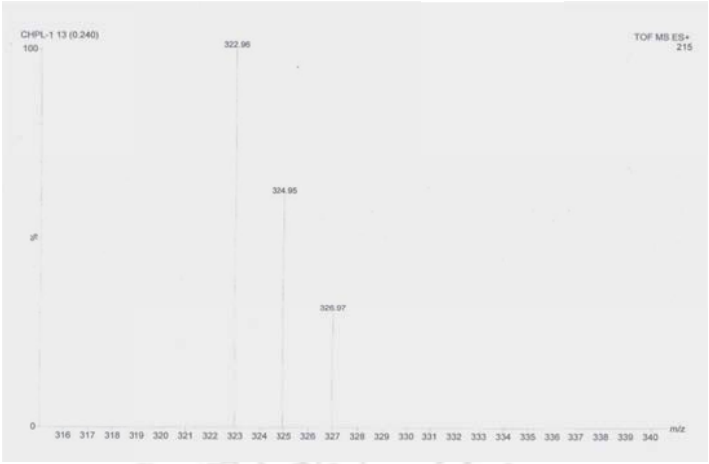

Figure 3.3. MS-spectra of CHPL-Fe^{3+} mixture after 10 min of contact time. Experimental condition: $[CHPL]_0$ =100 mg/L, Fe^{3+} = 1.75 mM, pH = 3 and temperature =25°C.

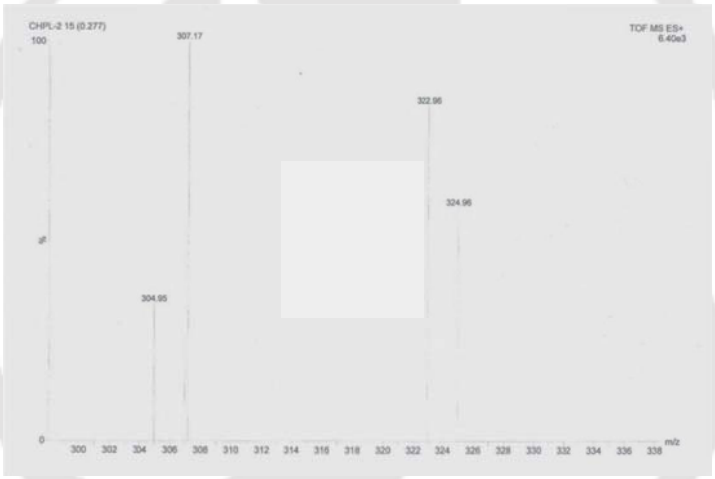

Figure 3.4. MS-spectra of CHPL-Fe^{3+} mixture after 10 min of contact time. Experimental condition: $[CHPL]_0$ =100 mg/L, Fe^{3+} = 1.75 mM, pH = 5 and temperature =25°C.

3.2.1.3 Evidences of FeCHPLCOM from IR spectra

Infrared (IR) spectra could provide important information for the formation of chelate complex of CHPL and Fe^{2+} ions by differentiating the characteristic stretching frequencies. The complexation reaction between Fe^{2+} and CHPL took place through binding of oxygen atom of carbonyl and C_1 of hydroxyl groups (Fazakerley et al., 1973). IR spectra recorded are shown in Figure 3.5. The wave numbers corresponding to different functional groups are summarized in Table 3.1 of the Supporting Information. The most interesting feature of IR

spectra of Fe^{2+}-CHPL mixture was the shifting and reduction in the frequencies of the bands. The notable differences were in the regions from 1700 to 1850 and 3200 to 3500 cm^{-1} for -C=O and –OH groups, respectively. The stretching frequencies of both O-H and C=O groups in Fe^{2+}-CHPL mixture gradually reduced with increase in Fe^{2+} concentration. The band at 1710 cm^{-1} in the free ligand can be assigned to C=O vibration and it significantly shifted to 1686 cm^{-1} in presence of Fe^{2+}. CHPL behaves as a dibasic acid having two –OH groups and they lie out of the plane. It seems that probably FeCHPLCOM was formed through attachment of one hydroxyl and one amide C=O groups. A free O-H bond increased the stretching absorption at about 3600 cm^{-1}. Fe^{2+} coordination lengthened and weakened O-H bond and so it lowered the vibrational frequency (Kemp et al., 1991). The same explanation is also valid for Fe^{2+} coordination with C=O group. Kemp et al. (1991) suggested that the presence of any hydrogen-bonding also weakens the stretching frequency of both O-H bond and –C=O group (Kemp et al., 1991). It created strain on O-H bond and made single bond character in –C=O group.

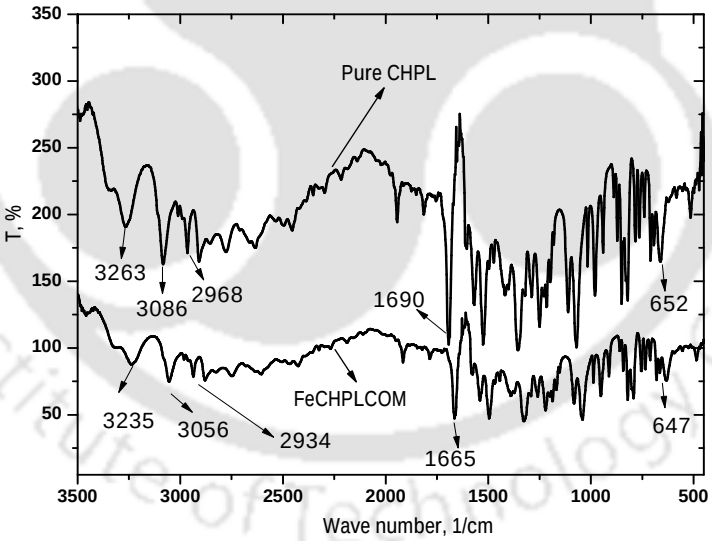

Figure 3.5. FTIR spectra of CHPL and Fe^{2+}-CHPL mixture. Experimental conditions: $[CHPL]_0$ = 100 mg/L, Fe^{2+} = 1.75 mM, pH = 3.0 and temperature = 25°C. The spectrum of FeCHPLCOM was recorded after 10 min of reaction.

Table 3.1. IR frequencies of CHPL and Fe^{2+}+CHPL mixture.

Groups	**Frequency, cm^{-1}**		
	Range of common groups	**CHPL**	**Fe^{2+}+CHPL mixture**
-OH (alcohol)	3200-3500	3263	3235
-NH (amine)	3000-3300	3086	3056
-CH (alkene)	3000-3100	3020	-
-C-H (aromatic)	3050-3100	3012	3010
-C-H (aliphatic)	2800-3000	2960	2950
$-CH_2-$	2930 (asym. stretch) 2860 (sym. stretch) 1470 (deform)	2968 2898 not assigned	2934 2874 not assigned
-C=O (ketone)	1700-1850	1690	1665
-C-Cl	700-800	652	647

3.2.1.4 Evidences of FeCHPLCOM from LC-MS spectra

LC-MS spectra of pure CHPL and CHPL-Fe^{2+} mixture are shown in Figure 3.6. Unreacted and protonated CHPL are designated with m/z of 325.26 and 326.37. It is also clear that FeCHPLCOM (m/z 381.2) was formed at 1:1 Fe^{2+} to ligand ratio. Fe(II) can form chelate complexes at Fe(II) to CHPL ratio of 1:1, 1:2 and 1:3 (Rivas et al., 2001).

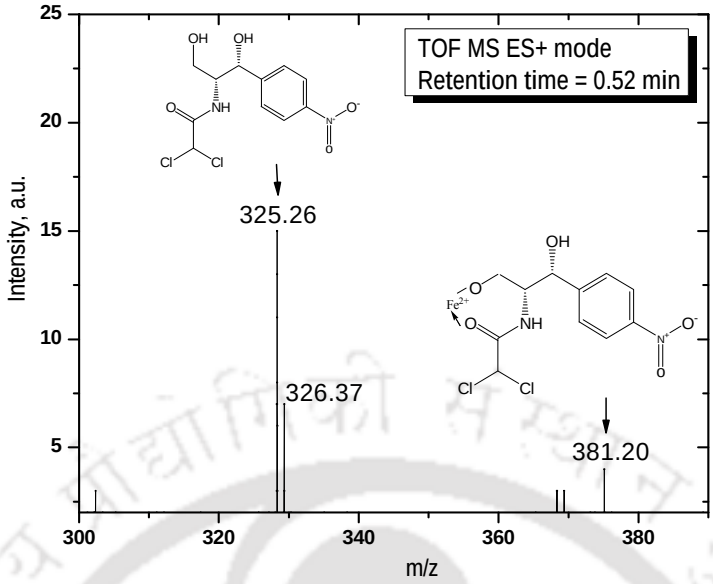

Figure 3.6. LC-MS spectrum of CHPL and Fe^{2+} mixture. Experimental conditions: $[CHPL]_0$ = 100 mg/L, Fe^{2+} = 1.75 mM, pH = 3.0 and temperature = 25°C. Photo-reaction with an UV lamp of 12 W/m^2 (9 W). The spectrum was recorded after 10 min of reaction.

3.2.2 CHPL and FeCHPLCOM degradation in FP, PFP and UVP

The use of Fe(II) as initial specie together with high initial concentrations of iron and hydrogen peroxide implies a high initial radicals generation. Consequently, the production of additional radicals is not important and that is why FP and PFP exhibited similar decomposition behaviour. The irradiation level used (12 W/m^2) was medium favouring Fenton's importance. Moreover, the role of UV was insignificant because that some intermediates of CHPL could reduce Fe^{3+} (Chen et al., 2009; Du et al., 2006). There was a slight higher removal in PFP which was confirmed from the repetition of experiments. Fe^{2+} and H_2O_2 doses were optimized in the concentration range from 1 to 2 and 5 to 25 mM (Figures 3.7 and 3.8). The optimal pH was found out by varying it in the range from 2 to 4 (Figures 3.9). The experimental optimization to maximize CHPL degradation was performed on the basis of PFP. The same condition (optimized) was in FP without UV light and UVP without Fe^{2+}.

TOC reduction of around 56-60, 62-70 and 33-55% were observed at 2.5 and 10 min of oxidation in FP, PFP and UVP, respectively. The faster initial rate of TOC removal was due to mineralization of amide chain. The second stage was related to the opening and

mineralization of substituted benzene ring. Usually, the large molecular weight intermediates are either mineralized or broken to lower molecular weight fragments like oxalic and acetic acids. Kavitha et al. (2004) indicated that carboxylic acids are eliminated quickly in PFP during the first stage of oxidation. The faster CHPL and TOC removal also can be corroborated from the residual concentration of H_2O_2 and Fe^{2+}. It was 1.3 and 45.2% for H_2O_2 and Fe^{2+}, respectively, after 45 min of Fenton reaction. The results are in well accordance with the literature (Du et al., 2007; Kavitha et al., 2004).

Iron-chelation played an important role on CHPL mineralization. PFP exhibited higher degradation ability of such complexes under UV luminesces. Oxalic acid is formed during Fenton reactions. An iron(III)-oxalate complex gets stability through conjugation with Fe(III) due to availability of a vacant 3d orbital. But it could lose its stability because of UV light absorption (Kavitha et al., 2004; Kemp et al., 1991). We didn't visualize any sludge formation in PFP. Sludge formed in FP was separated by filtration using 0.45 μm cellulose ester filter at the end of the experimental run with 1.75 mM Fe^{2+}, 20 mM H_2O_2 and pH 3. It was washed with distilled water and dissolved in conc. H_2SO_4. CHPL and TOC reduction of 3.9 and 1.8% were observed due to adsorption on iron-sludge.

The decrease in peak intensities of CHPL and FeCHPLCOM is shown Figure 3.10. About 12.9 mg/L of CHPL was found to form FeCHPLCOM with 1.75 mM Fe^{2+} at pH. It gave an initial FeCHPLCOM (MW 381.2 g/mol) of 14.9 mg/L. H_2O_2 was added after 10 min of chelation time and the variation of CHPL and FeCHPLCOM concentrations is shown in Figure 3.11. In FP, around 92.7 and 80.7% decomposition of CHPL and FeCHPLCOM was noted in 45 min. It was 95.4 and 94.1% in PFP. Around 2.7 and 13.4% more CHPL and FeCHPLCOM decomposition took place in PFP. Only 2.3% more TOC reduction was found in PFP when both the reagents (Fe^{2+} and H_2O_2) were added together in CHPL solution.

FeCHPLCOM concentration was around 14.9, 7.3 and 0.63 mg/L at pH 3, 7 and 10, respectively. It is possible that the lone electron pair could be free at acidic pH. However, at neutral or alkaline medium, hydroxyl group (-OH) attached to C_1 position gets deprotonated. Therefore, the extent of FeCHPLCOM formation should gradually decrease with increase in pH. CHPL removals were of 95.4 and 92.7% in 45 min of PFP and FP treatment, respectively. Whereas UVP showed 82.9% removal (Figure 3.12). TOC removal efficiency decreased to 65.9% in UVP against 71.9 and 69.5% in PFP and FP, respectively.

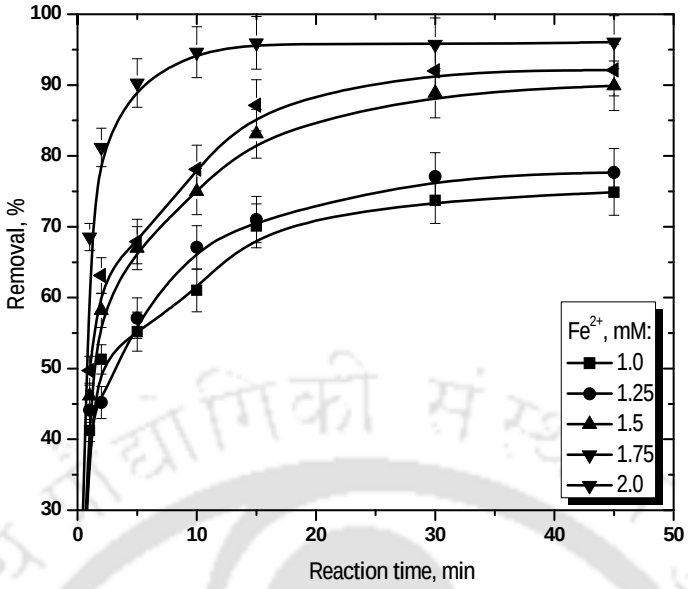

Figure 3.7. Effect of Fe^{2+} on removal of CHPL in PFP. Experimental conditions: $[CHPL]_0$ = 100 mg/L, H_2O_2= 20 mM, pH = 3.0 and temperature = 25°C. Photo-reaction with an UV lamp of 12 W/m^2 (9W).

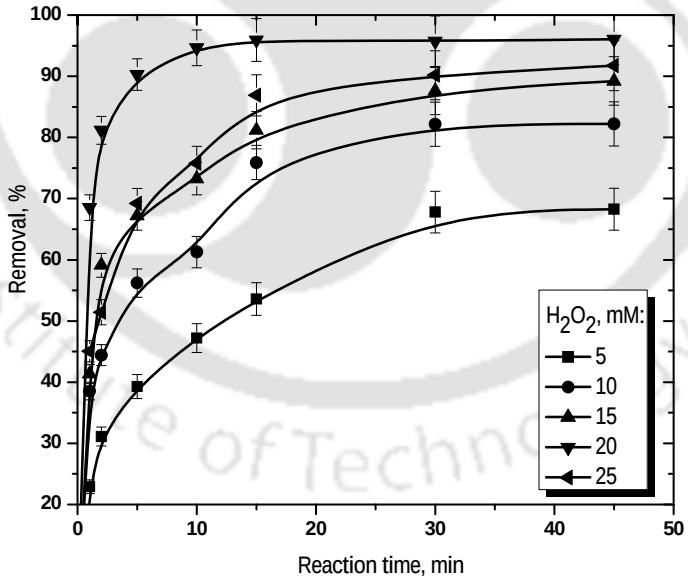

Figure 3.8. Effect of H_2O_2 on removal of CHPL in PFP. Experimental conditions: $[CHPL]_0$ = 100 mg/L, Fe^{2+} 1.75 mM, pH = 3.0 and temperature = 25°C. Photo-reaction with an UV lamp of 12 W/m^2 (9 W).

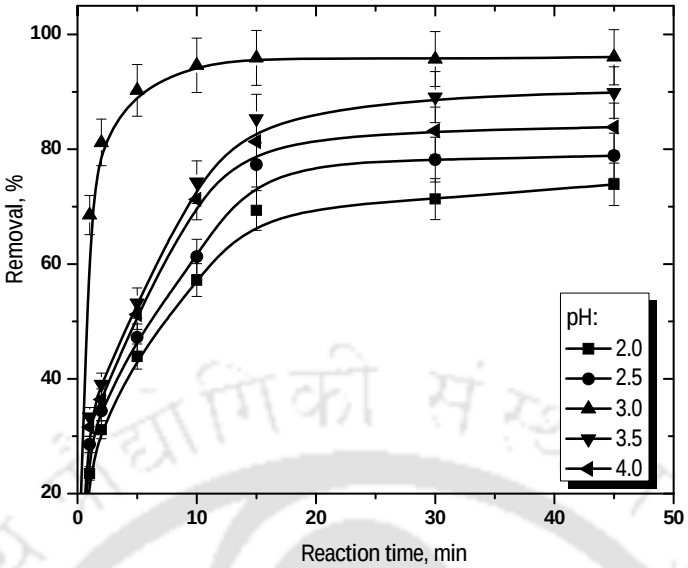

Figure 3.9. Effect of pH on removal of CHPL in PFP. Experimental conditions: $[CHPL]_0$ = 100 mg/L, Fe^{2+} 1.75 mM, H_2O_2 = 20 mM and temperature = 25°C. Photo-reaction with an UV lamp of 12 W/m^2 (9 W).

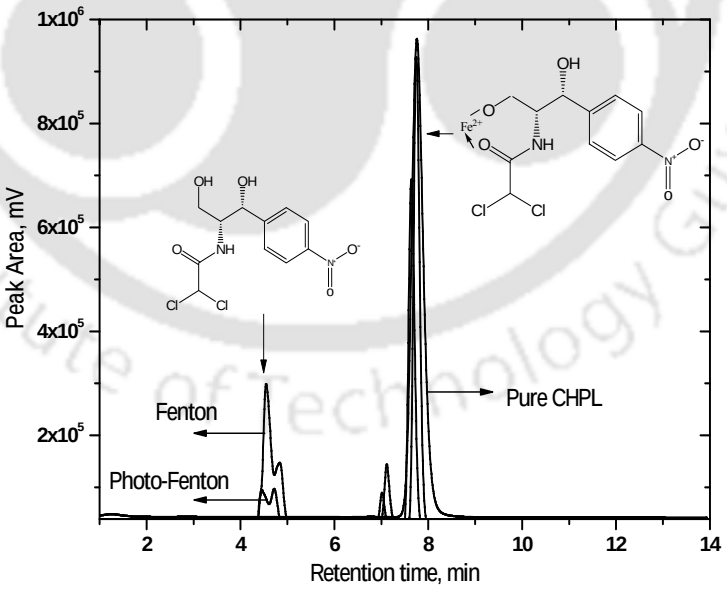

Figure 3.10. Chromatogram of residual CHPL and FeCHPLCOM found in FP and PFP at 10 min of reaction. Experimental conditions: $[CHPL]_0$ = 100 mg/L, Fe^{2+} 1.75 mM, H_2O_2 = 20 mM, pH = 3.0 and temperature = 25°C. Photo-reaction with an UV lamp of 12 W/m^2 (9 W).

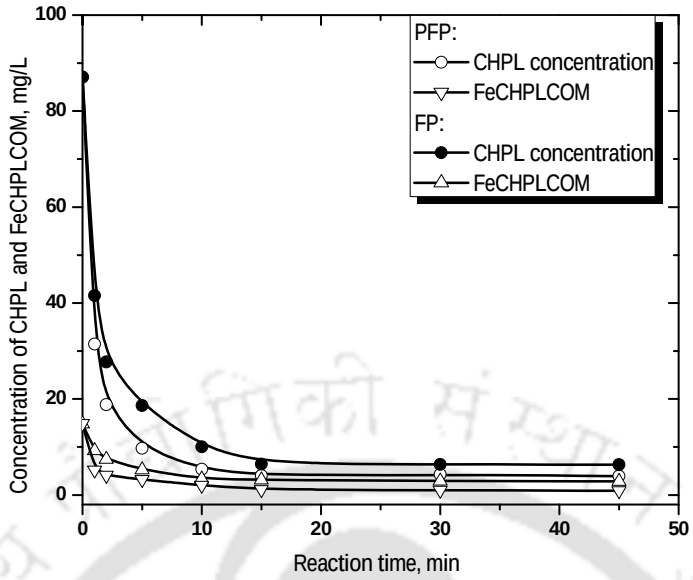

Figure 3.11. CHPL Concentration (after to form up the complex with Fe^{2+} in 10 min) and FeCHPLCOM with reaction time in FP and PFP. Experimental conditions: $[CHPL]_0$ = 100 mg/L, Fe^{2+} 1.75 mM, H_2O_2 = 20 mM, pH = 3.0 and temperature = 25°C. Photo-reaction with an UV lamp of 12 W/m^2 (9 W).

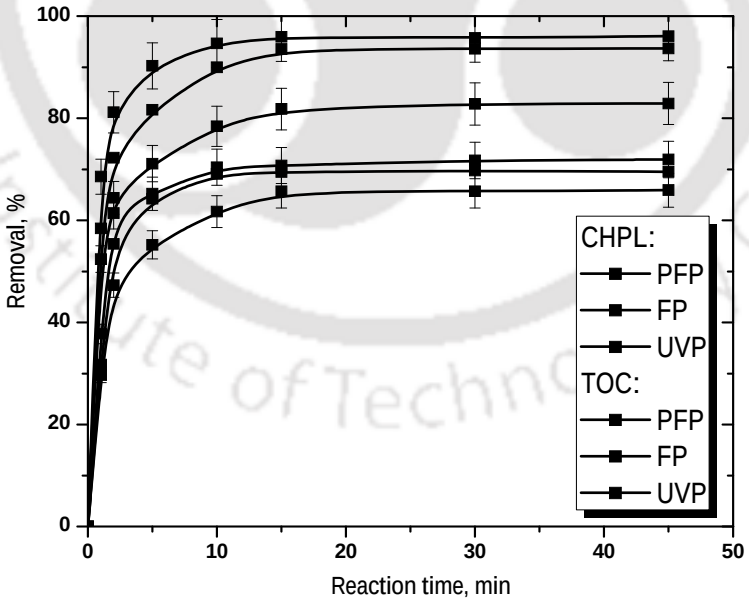

Figure 3.12. CHPL and TOC removal with reaction time. Experimental condition: $[CHPL]_0$ = 100 mg/L, pH = 3.0, Fe^{2+} = 1.75 mM (in FP and PFP), H_2O_2 = 22.5 mM (in FP, PFP and UVP) and temperature =25°C. Photo-reaction with an UV lamp of 12 W/m^2 (9 W).

3.2.3 Degradation pathways of CHPL

LC-MS spectra (Figures 3.13 to 3.15) were recorded to identify the reaction products. The mechanisms of CHPL degradation are proposed and supported from the fragments obtained in mass spectra. CHPL has two asymmetry centres i.e. C_1 and C_2 with weakly bonded hydrogen atoms. It can be easily abstracted by $HO^{\bullet}$ (Csay et al., 2012). The presence of amide group attached to C_2 centre increased neucleophilicity of both the centres (Rivas et al., 2001). All the degradation products are denoted with the symbol 'D' following the integer as subscript to count the number of fragments. The same notation used throughout this thesis indicates the intermediates formed during cleavage of different pharmaceutical compounds. There were twenty three fragments (D_1-D_{23}) in mass spectra of FP, PFP and UVP. The errors in masses were calculated from the difference of the proposed and exact structural masses of protonated ions. Reasonably low errors were obtained for most of the compounds (Table 3.2). The degradation mechanisms are presented in Figures 3.16 to 3.20. D_1 was identified in PFP formed with low error (0.06 g/mol) by direct hydroxylation of $HO^{\bullet}$ at C_2 asymmetric centre. There were two most possible pathways for the cleavage of D_1 as shown in Figure 3.16. Path #1 shows the route of formation of D_2 and D_3 with proposed mass to charge ratio (m/z) of 239.30 and 171.13. Both fragments were identified in PFP. Path #2 presents the formation route of D_4 to D_7 with m/z of 330.17, 164.97, 111.04 and 279.12, respectively.

D_2 was yielded by hydroxylation followed by decarboxylation of D_1 with formation of dichloromethane. In presence of two chlorine atoms at the geminal position of the side chain, the carbonyl carbon became slightly neucleophilic in character. There was tendency for shifting of lone electron of -Cl group towards the carbonyl carbon. The attack at C_1 asymmetric centre by $HO^{\bullet}$ yielded D_3 with m/z 171.13. The appearance of D_4 in PFP was via an unstable intermediate with m/z 333.12 from D_1 molecule. D_4 exists as a di-sodium salt in acidic medium (pH<3). p-nitrobenzoic acid (D_5) detected in PFP. It was formed from the same intermediate by an electrophilic attack of $HO^{\bullet}$ at carbonyl carbon. D_5 could form a stable iron complex (Figure 3.20) which would inhibit the reaction with peroxide (Du et al., 2007). The susceptibility of oxidation of primary alcoholic group (-CH_2OH) of the intermediate with m/z 92.08, originated D_6 (Kavitha et al., 2004). This compound also could form a chelate complex of Fe^{2+} with two coordination sites i.e. -COOH and –OH (Figure 3.20). D_6 was found both in FP and UVP (Kavitha et al., 2004). Nitrobenzene (m/z = 122.09) was originated from D_5 daughter ion on decarboxylation. D_7 was originated from the same daughter ion by intermolecular hydrogen bonding of p-nitrophenol which was yielded by direct hydroxylation at p-position with respect to –NO_2 group. Intermolecular hydrogen

bonding of p-nitrophenol is a weak bonding (Kemp et al., 1991) resulted from partial charge separation on oxygen and H-atom in -NO_2 and -OH groups. D_7 dimer was only identified in FP. Such weak H-bond could be easily broken down under UV irradiation (Gomez et al., 2007).

CHPL also could be fragmented through the routes as shown in Figure 3.16. Sodium salts of oxalic acids could be originated upon degradation of CHPL (Figure 3.16). Oxalate has tendency to form iron-complexes with both Fe(II) and Fe(III) at pH range of 2 to 3 (Wessel et al., 2006). D_8 was formed by homolytic cleavage of H-Cl bond at the geminal position with release of hypochlorous acid (path #3). The product of the cyclisation reaction at 2, 4-position of the aliphatic chain of D_8 molecule was D_9 (m/z of 221.16). Enhanced cyclisation occurred due to increase in electrophilicity of the geminal carbon atom. Path #4 shows the formation pathways of D_{10} and D_{11}. D_{10} molecule was originated by dehydrogenation from an intermediate product with m/z 119.14. It could chelate through an extensive conjugation with Fe^{2+} due to vacant 3d-orbital (Figure 3.19). The stability of such complexes could disappear in presence of UV light. D_{11} was yielded in all three processes by direct hydroxylation at less substituted double bond centre. According to the Hoffman's rule, electrophiles are added at less substituted double bond of alkene type molecules (Finar et al., 2001).

The formation route of D_{12} to D_{16} is presented through path #5. D_{12} identified in FP was originated by homolytic cleavage of CHPL along with D_{13} on further hydroxylation of an intermediate with m/z of 161.08. p-aminobenzyl alcohol (m/z 122.17) appeared on –NO_2 reduction by an aqueous electron (Paula et al., 2012; Sykes et al., 1985). It was sequentially hydroxylated to D_{14} and D_{15}. D_{14} fragment was found in all the processes. Ortho (o-) and para (p-) positions became more electron rich centres due to mesmeric effect of –NH_2 group (Sykes et al., 1985). One additional -OH was introduced at o-position with respect to –NH_2 group of D_{15}. D_{16} molecule was in equilibrium with D_{15}.

D_8 was sub-fragmented as in path #6 (Figure 3.18). An electrophilic attack at carbonyl carbon of amide group evidences the appearance of D_{17} in FP and UVP. The activity of carbonyl carbon is already discussed. Decarboxylation of –COOH group of D_{17} originated D_{18} fragment due to presence of an electron withdrawing group (–NO_2). D_{19} was formed on further dehydrogenation of D_{18}. D_{20} and D_{21} were yielded on reduction of –NO_2 and substitution of –OH groups with removal of –NH_3 (Figure 3.18). D_{22} and D_{23} both compounds (m/z of 218.06 and 258.17) were found in only UVP originated through path #6 on continuous degradation of D_8 molecule (m/z 269.13). Apart from these two products

another seven products were formed in this process (Table 3.2) by similar degradation mechanism as discussed in earlier. D_{22} was formed on hydroxylation of D_{21} which was activated in presence of –OH and $–NH_2$ groups (Finar et al., 2001). D_{23} molecule, originated upon dehydration reaction between p-hydroxy benzoic acid and p-amino benzoic acid.

Figure 3.19 shows the degradation pathway of FeCHPLCOM. D_2 and sodium oxalate were formed by hydroxylation probably during pH adjustment for the termination of Fenton reaction. Fe(III)-oxalate was mineralized to CO_2 in presence of UV-light (de Luna et al., 2013). Fe(III) to Fe(II) introversion could occurred due to redoxidation as supported by the literature (Chen et al., 2009).

Only D_{11} and D_{14} were detected in all oxidation processes even though they could not chelate with iron. The adjacent two -OH groups of these fragments are out of the plane (Wahed et al., 2008).

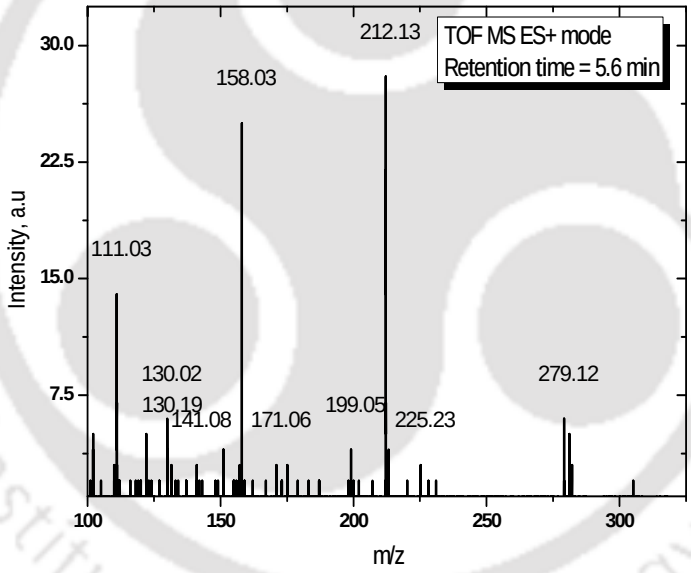

Figure 3.13. Mass spectra recorded at 10 min of FP with retention time of 5.6 min. Experimental conditions: $[CHPL]_0$ = 100 mg/L, Fe^{2+} = 1.75 mM, H_2O_2 = 20 mM, pH = 3.0 and temperature = 25°C.

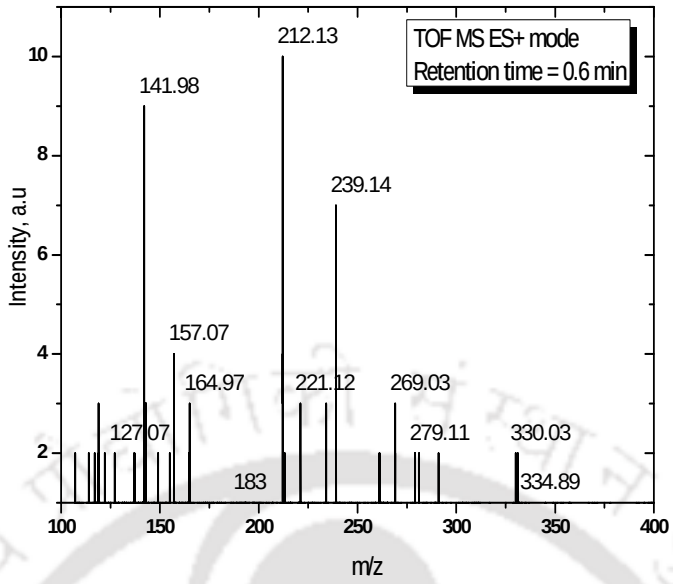

Figure 3.14. Mass spectra recorded at 10 min of PFP with retention time of 0.6 min. Experimental conditions: $[CHPL]_0$ = 100 mg/L, Fe^{2+} = 1.75 mM, H_2O_2 = 20 mM, pH = 3.0 and temperature = 25°C. Photo-reaction with an UV lamp of 12 W/m^2 (9 W).

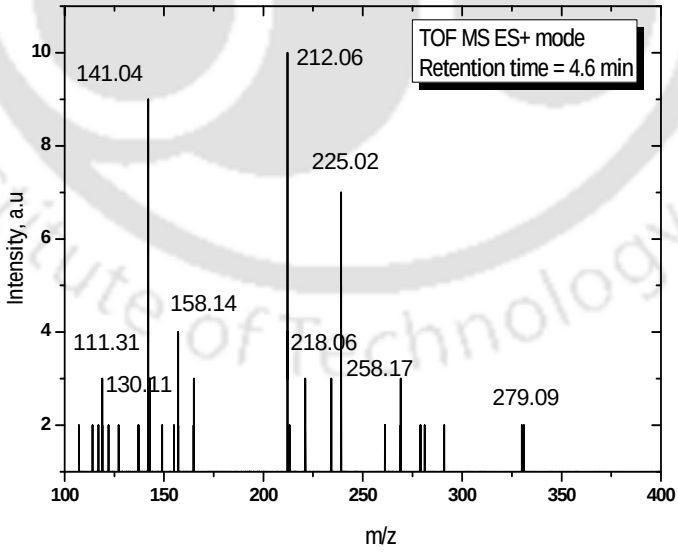

Figure 3.15. Mass spectra recorded at 10 min of UVP with retention time of 4.6 min. Experimental conditions: $[CHPL]_0$ = 100 mg/L, H_2O_2 = 20 mM, pH = 3.0 and temperature = 25°C. Photo-reaction with an UV lamp of 12 W/m^2 (9 W).

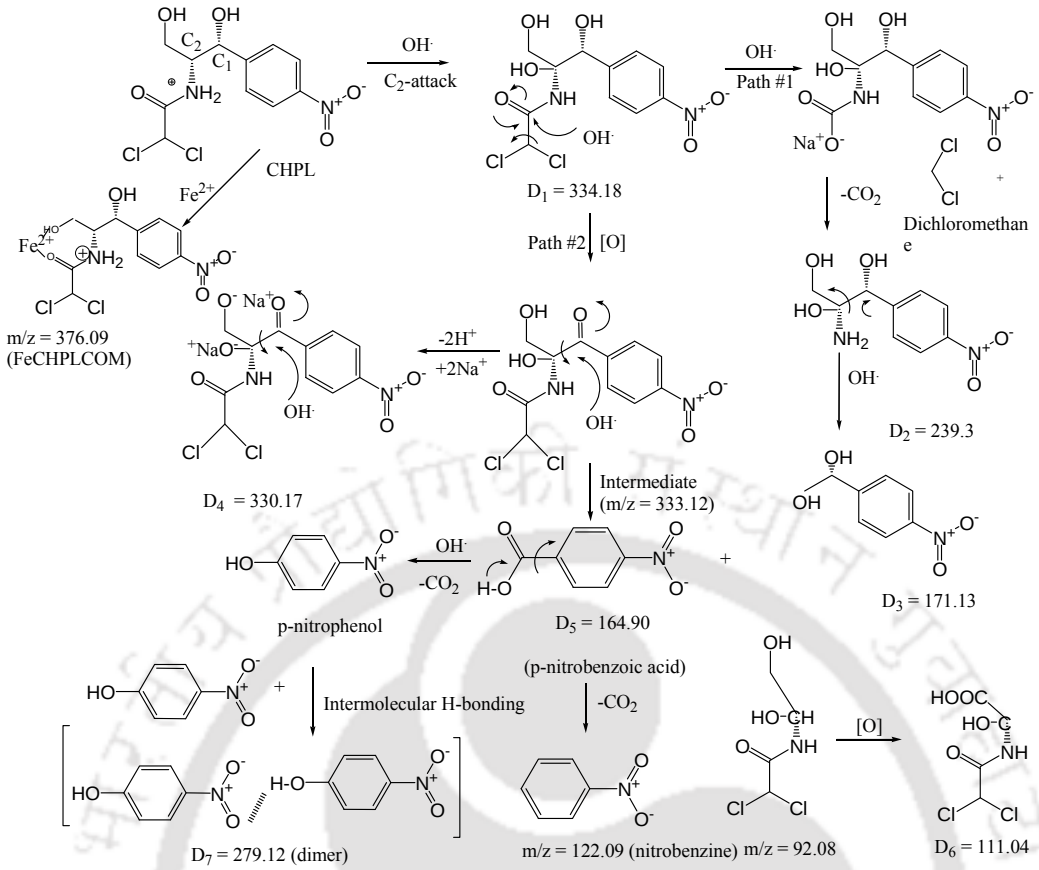

Figure 3.16. Degradation pathways of CHPL. The exact mass to charge ratio is in round parenthesis.

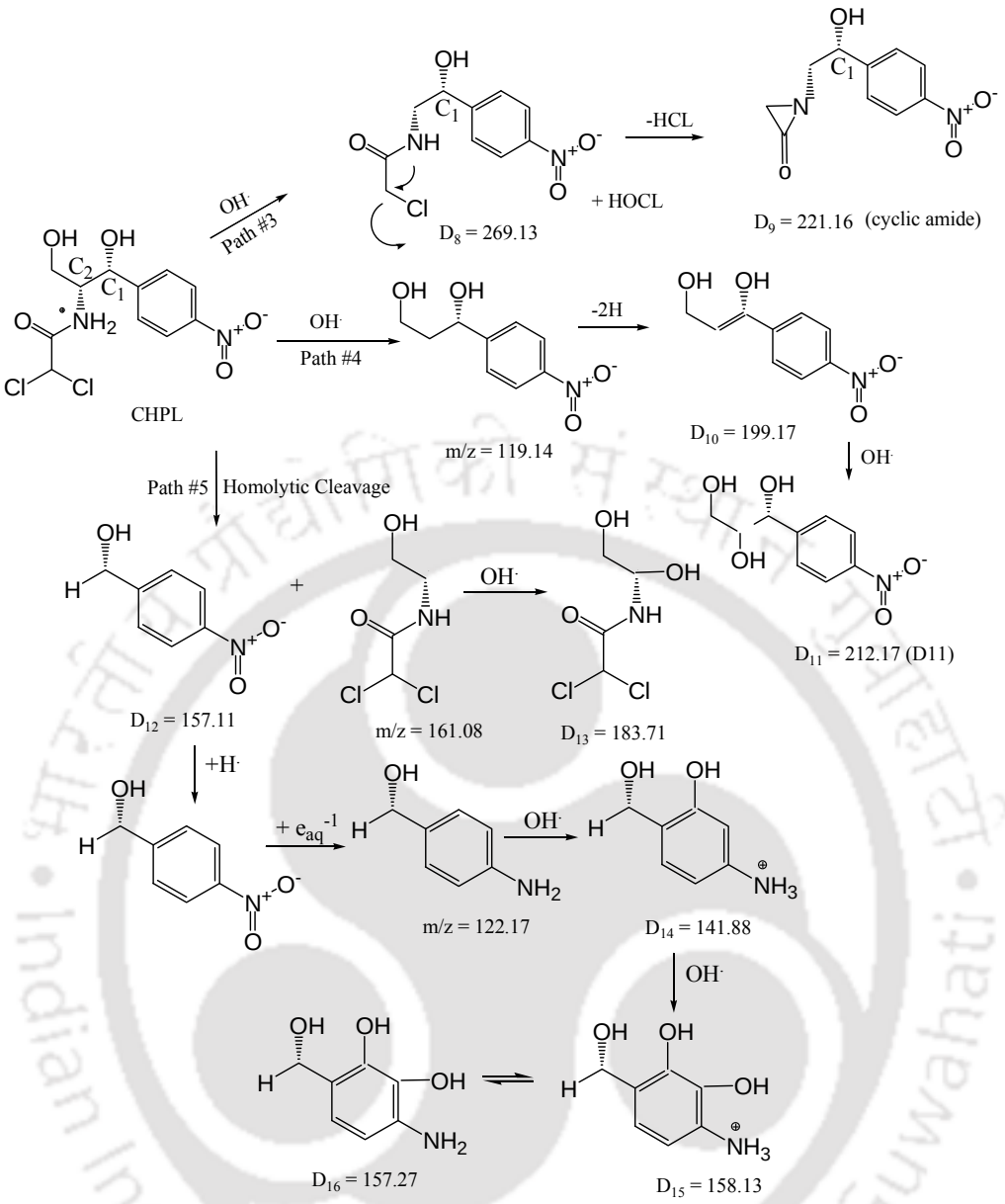

Figure 3.17. Degradation pathways of CHPL. The exact mass to charge ratio is in round parenthesis.

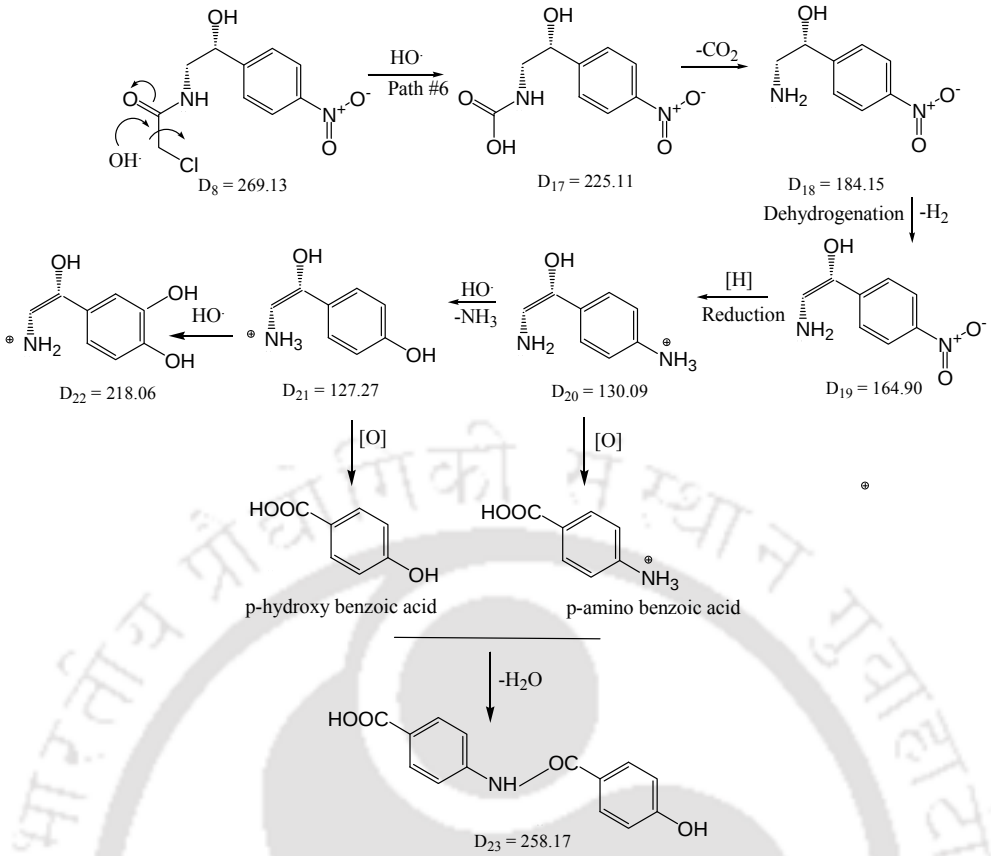

Figure 3.18. Degradation pathways of D_8 (m/z = 269.13).

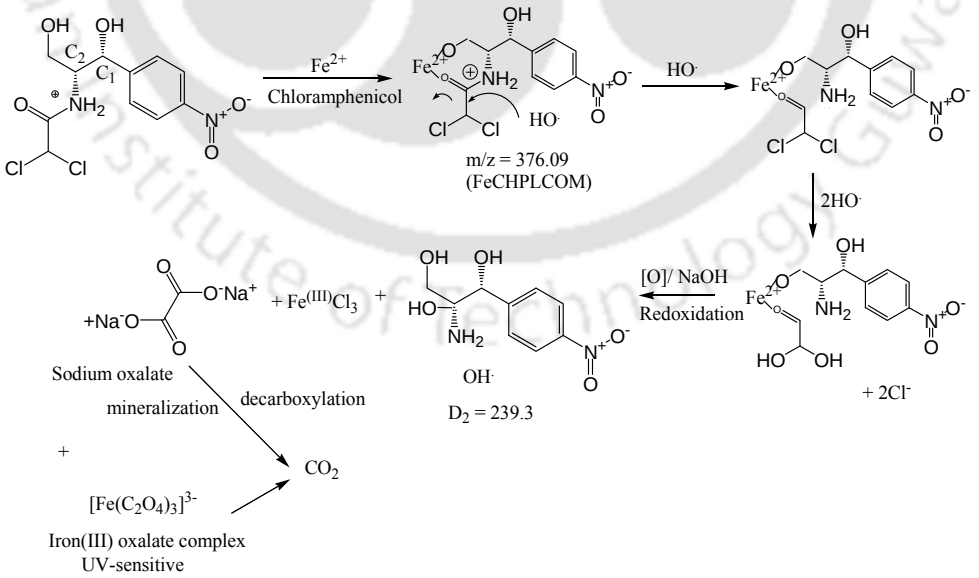

Figure 3.19. Pathways of FeCHPLCOM degradation.

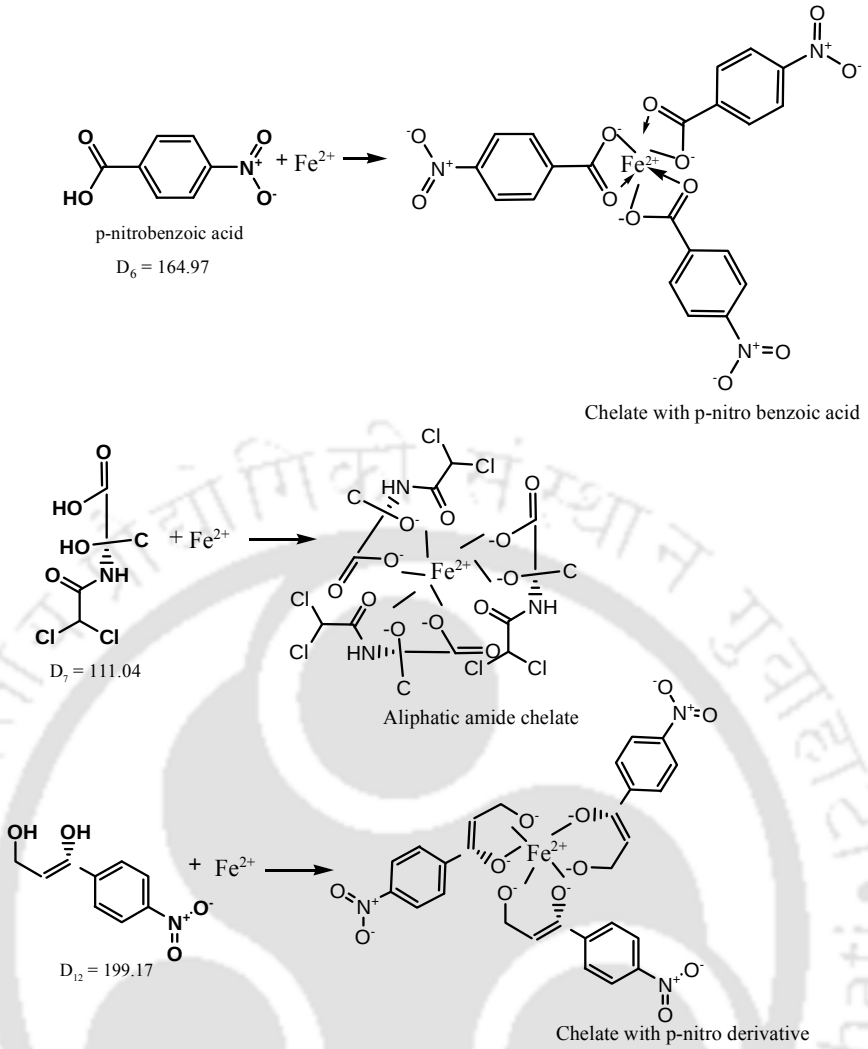

Figure 3.20. Formation of chelates.

Table 3.2. Mass to charge ratio (m/z) based on the proposed structures and mass spectra during CHPL cleavage. The symbol '+' indicates its formation in different oxidation processes.

Fragments	Formula	m/z	Mass error (g/mol)	AOPs			DBE¥
				FP	PFP	UVP	
D_1	$C_{11}H_{11}N_2O_6Cl_2$	334.18	-0.71		+		5
D_2	$C_9H_{10}N_2O_5$	239.30	0.16		+		4
D_3	$C_{11}H_9N_2O_5Cl_2$	171.13	0.07		+		4
D_4	$C_{11}H_8N_5O_2Cl_2$	330.17	0.14	+			5
D_5	$C_7H_5NO_4$	164.90	0.07		+		5
D_6	$C_3H_3O_4\ NCl_2$	111.04	0.03, -0.25	+		+	1
D_7	$C_{12}H_{10}O_6N_2$	279.12	0, 0.01, 0.03	+		+	4
D_8	$C_8H_{10}O_4\ N_2Cl$	269.13	0.1		+		6
D_9	$C_{10}H_9O_4N_2$	221.16	0.04		+		6
D_{10}	$C_9H_9O_4N$	199.17	0.12	+			5
D_{11}	$C_9H_{11}O_5N$	212.17	0.04, 0.04, 0.11	+	+	+	4
D_{12}	$C_7H_7O_3N$	157.11	0.04				4
D_{13}	$C_4H_6O_3N$	183.71	0.71		+		1
D_{14}	$C_7H_9O_2N$	141.88	0.8, -0.1, 0.84	+	+	+	4
D_{15}	$C_7H_9O_3N$	158.13	0.1	+		+	4
D_{16}	$C_9H_9O_3N$	157.27	0.04		+		4
D_{17}	$C_9H_{10}O_5N_2$	225.11	-0.12, 0.09	+		+	5
D_{18}	$C_8H_9O_3N_2$	184.15	-0.31				4
D_{19}	$C_8H_8O_3N$	164.90	0.07		+		5
D_{20}	$C_8H_{11}ON_2$	130.09	-0.1, 0.07	+		+	5
D_{21}	$C_8H_{10}O_2N$	127.27	0.2		+		5
D_{22}	$C_8H_9NO_3$	218.16	0.1			+	3
D_{23}	$C_{14}H_{11}NO_4$	258.01	0.16			+	4

¥: Double bond equivalent (DBE)

3.2.4 Antimicrobial activity of CHPL and its decomposition products

Figure 3.21 shows the toxicity of CHPL and its degradation products towards *E. coli* in LB media after 24 h of exposure. The growth of *E. coli* was inhibited almost completely in the presence of 100 mg/L CHPL (0.23×10^7 CFU/mL). The growth of *E. coli* increased to 8×10^7 CFU/mL in control toxicity assay (LB+deionized water). Liang et. al (2013) showed that the growth of *E. coli* strain more or less withdrawn in the presence of 32 mg/L CHPL after 24h of exposure (Liang et al., 2013). The toxicity in FP and UVP was comparable. The susceptibility of toxicity to *E. coli* was more in FP even though there was no significant difference between CHPL and TOC values in FP and PFP. The concentration of unreacted

CHPL was 8 mg/L (TOC 9.4 mg/L) in FP and it was 5.5 mg/L in PFP (TOC 8.8 mg/L). About 55.8, 35.2 and 63.7% cell death were observed upon 24 h exposure of *E. coli* in the reaction mixture collected after 45 min of FP, PFP and UVP, respectively in comparison to the control condition (Figure 3.21). p-nitrophenol (Sponza et al., 2001; Lipczynska-Kochany et al., 1992) and D_{15}, a benzyl alcohol derivative intermediate (Demir et al., 2010; Finar et al., 2001) are toxic in nature. p-nitrophenol was identified both in FP and PFP. Whereas D_{15} was originated only in FP.

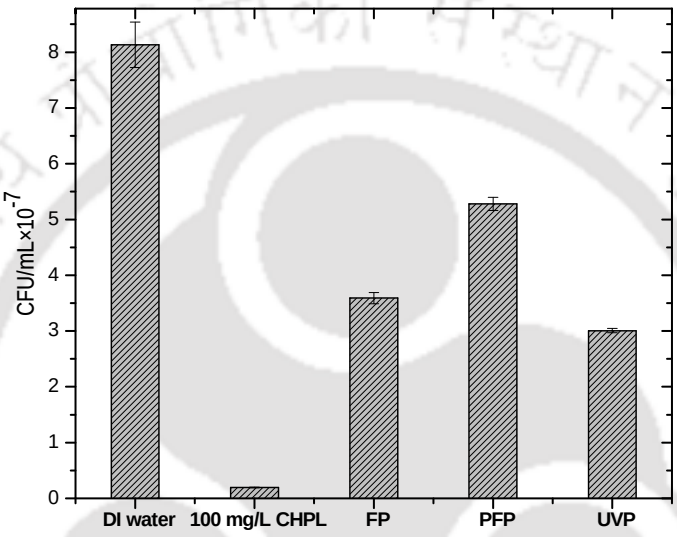

Figure 3.21. Growth of *E. coli* after 24 h of exposure. Experimental conditions: $[CHPL]_0$ = 100 mg/L, pH = 3.0, Fe^{2+} = 1.75 mM (in FP and PFP only), H_2O_2 = 20 mM (in FP, PFP and UVP only) and temperature =25°C. Photoreaction with an UV lamp of 12 W/m^2 (9 W). The reaction time is 45 min.

3.3 Major Findings

The reactivity of CHPL towards Fe^{2+} and its decomposition behaviour in Fenton and light assisted Fenton reactions were studied. FeCHPLCOM was formed at 1:1 CHPL to Fe^{2+} ratio. Chelation took place through binding of oxygen atom attached to C_2 and carbonyl oxygen of amide group. Concentration of FeCHPLCOM was calculated by high performance liquid chromatography. Oxidation and reduction of CHPL as well as its degradation products were dependent on the redox cycle of Fe^{2+} and Fe^{3+}. However enhanced FeCHPLCOM decomposition was found in PFP. Maximum CHPL removal of 92.7, 95.4 and 82.9% were noted against mineralization efficiency of 69.5, 71.9 and 65.9% in FP, PFP and UVP. Decomposition of FeCHPLCOM was more in PFP with 10.7% higher in comparison to CHPL. Total twenty three intermediates were detected in mass spectra within the mass to charge ratio of 100 to 400. The proposed mechanism implies that most of the intermediates were formed by the degradation of side chain of CHPL molecule. Aliphatic amide chain was cleaved by $HO^{\bullet}$ attack at C_2 centre. The growth of *E. coli* was completely inhibited in presence of 100 mg/L CHPL and the susceptibility of toxicity was reduced significantly in PFP compared to FP and UVP.

References

Aouiche, A., Sabaou, N., Meklat, A., Zitouni, A., Bijani, C., Mathieu, F. and Lebrihi, A., "Saccharothrix sp. PAL54, a new chloramphenicol- producing strain isolated from a Saharan soil. World", *J. Microb. Biotechnol.,* **28,** 943-951 (2012).

Aresta, A., Bianchi, D., Calvano, C. D. and Zambonin, C. G., "Solid phase microextraction-liquid chromatography (SPME-LC) determination of chloramphenicol in urine and environmental water samples", *J. Pharm. Biom. Anal.,* **53,** 440-444 (2010).

Bel, E. D., Dewulf, J., Witte, B. D., Langenhove, H. V. and Janseen, C., "Influence of pH on the sonilysis of ciprofloxacin: Biodegradability, ecotoxicity and antibiotic activity of its degradation products", *Chemosphere*, **77,** 291-295 (2009).

Buchanan, W., Roddick, F., Porter, N. and Drikas, M., "Fractionation of UV and VUV pretreated natural organic matter from drinking water", *Environ. Sci. Technol.,* **39,** 4647- 4654 (2005).

Chen, F., Li, Y., Guo, L. and Zhang, J., "Strategies comparison of eliminating the passivation of non-aromatic intermediates in degradation of orange II by Fe^{3+}/H_2O_2", *J. Hazard. Mater.,* **169,** 711-718 (2009).

Csay, T., Gergely, R., Erzsebet, T. and Wojnarovits, L., "Radiation induced degradation of pharmaceutical residues in water: Chloramphenicol", *Rad. Phy. Chem.,* **81,** 1489-1494 (2012).

Demir, E., Kocaoglu, S. and Kaya, B., "Assessment of genotoxic effects of benzyl derivatives by the comet assay", *Food Chem Toxicol.,* **48,** 1239-1242 (2010).

de Luna, M. D. G., Briones, R. M., Su, C. C. and Lu, M. C., "Kinetics of acetaminophen degradation by Fenton oxidation in a fluidized-bed reactor", *Chemosphere,* **90(4),** 1444-1448 (2013).

Du, Y. X., Zhou, M. H. and Lei, L. C., "Role of the intermediates in the degradation of phenolic compounds by Fenton-like process", *J. Hazard. Mater.,* **136(3),** 859-865 (2006).

Du, Y., Zhou, M. and Lei, L., "Kinetic model of 4-CP degradation by Fenton/O_2 system", *Water Res.*, **41,** 1121-1133 (2007).

Fazakerley, G. V., Linder, P. W. and Nassimbeni, L. R., "Complexation of copper(II) by chloramphenicol", *Inorg. Nucl. Chem. Lett.*, **9,** 1069-1072 (1973).

Finar, I. L., "*Stereochemistry and the Chemistry of Natural Products"*, 5th ed.; Longman: London, (2001).

Gomez, M. J., Martınez-Bueno, M. J. Lacorte, S., Fernandez-Alba, A. R. and Aguera, A., "Pilot survey monitoring pharmaceuticals and related compounds in a sewage treatment plant located on the Mediterranean coast", *Chemosphere,* **66,** 993-1002 (2007).

Hu, X., Zhou, Q. and Luo, Y., "Occurrence and source analysis of typical veterinary antibiotics in manure, soil, vegetables and groundwater from organic vegetable bases, northern China", *Environ. Pollut.,* **158,** 2992-2998 (2010).

Kavitha, V. and Palanivelu, K., "The role of ferrous ion in Fenton and photo-Fenton processes for the degradation of phenol", *Chemosphere,* **55,** 1235-1243 (2004).

Kemp, W., "*Organic Spectroscopy"*, 3rd ed.; Palgrave Macmillan: Edinburgh (1991).

Lai, H. T., Liu, S. M. and Chien, Y. H., "Degradation of chloramphenicol and oxytetracycline in aquaculture pond sediments", *J. Environ. Sci. Health.,* **30,** 1897-1923 (1995).

Liang, B., Cheng, H. Y., Kong, D. Y., Gao, S. H., Sun, F., Cui, D., Kong, F. Y., Zhou, A. J., Liu, W. Z., Ren, N. Q., Wu, W. M., Wang, A. J. and Lee, D. J., "Accelerated reduction of chlorinated nitroaromatic antibiotic chloramphenicol by biocathod", *Environ. Sci. Technol.,* **47,** 5353-5361 (2013).

Lin, A., Yu, T. and Lin, C., "Pharmaceutical contamination in residential, industrial, and agricultural waste streams: Risk to aqueous environments in Taiwan", *Chemosphere,* **74 (1),** 131-141 (2008).

Lipczynska-Kochany, E., "Degradation of nitrobenzene and nitrophenols by means of advanced oxidation processes in a homogeneous phase: photolysis in the presence of hydrogen peroxide versus the Fenton reaction", *Chemosphere,* **24,** 1369-1380 (1992).

Liu, H., Zhang, G., Liu, C. Q., Li, L. and Xiang, M., "The occurrence of chloramphenicol and tetracyclines in municipal sewage and the Nanming River, Guiyang City, China", *J. Environ. Monit.,* **11 (6),** 1199-1205 (2009).

Luis, A. D., Lombranda, J. I., Varona, F. and Menendez, A., "Kinetic study and hydrogen peroxide consumption of phenolic compounds oxidation by Fenton's reagent", *Korean J. Chem. Eng.,* **26(1),** 48-56 (2009).

MPEDA., "Marine ProductsExport Development Authority Notification No. MAS/12/80-2002/QC dt. 20.05.2002", Ministry of Commerce and Industry, Government of India, Chennai (2002).

Parsley, L. C., Consuegra, E. J., Kakirde, K. S., Land, A. M., Harper, W. F. and Liles, M. R., "Identification of diverse antimicrobial resistance determinants carried on bacterial, plasmid, or viral metagenomes from an activated sludge microbial assemblage", Appl. Environ. Microbiol., 76 (11), 3753-3757 (2010).

Paula, A., Batista, S., F, Raquel. and Nogueira, P., "Parameters affecting sulfonamide photo-Fenton degradation-Iron complexation and substituent group", *J. Photochem. Photobiol., A.* **232,** 8-13 (2012).

Puma, G. L. and Yue, P. L., "Photocatalytic oxidation of chlorophenols in single component and multi-component systems", *Ind. Eng. Chem. Res.,* **36,** 27-38 (1991).

Puttaswamy, S., Shubha, J. P., "Kinetics and mechanism of sodium n-halo-p toluenesulfonamides oxidation of diclofenac in alkaline medium", *J. Sci. Ind. Res.,* **49,** 13-18 (2009).

Rivas, F. J., Beltran, F. J., Frades, J. and Buxeda, P., "Oxidation of p-hydroxybenzoic acid. *Water Res.*, **35(2),** 387-96 (2001).

Sponza, D. T. and Kuscub, O. S., "Relationships between acute toxicities of para nitrophenol (p-NP) and nitrobenzene (NB) to Daphnia magna and photobacterium phosphoreum: physicochemical properties and metabolites under anaerobic/aerobic sequentials", *J. Hazard. Mater.*, **185,** 1187-1197 (2001).

Sui, Q., Huang, J., Deng, S., Chen, W. and Yu, G., "Seasonal variation in the occurrence and removal of pharmaceuticals and personal care products in different biological wastewater treatment processes", Environ. Sci. Technol., **45 (8),** 3341-3348 (2011).

Sykes, P., "*A Guidebook to Mechanism in Organic Chemistry"*, 6th ed.; Longman Scientific & Technical: New York (1985).

Trovo, A. G., Paiva, A. B. de. V., Machado, A. E. H., Carlos, A. and Santos, R. O., "Degradation of the antibiotic chloramphenicol by photo-Fenton process at lab-scale and solar pilot plant: Kinetic, toxicity and inactivation assessment", *Solar Energy*, **97,** 596-604 (2013).

Wahed, M. G., Refat, M. S. and El-Megharbel, S. M., "Spectroscopic studies on the complexation of some transition metals with chloramphenicol drug", *J. Mol. Struc.,* **892,** 402-413 (2008).

Wessel, J. C., Matyja, M., Neugebauer, M., Kiefer, H., Daldrup, T., Tarbah, F. A. and Weber, H., "Characterization of oxalic acid derivatives as new metabolites of metamizol (dipyrone) in incubated hen's egg and human", *Pharmaceut. Sci.,* **28,** 15-25 (2006).

Wongtavatchai, J., McLean, L., Ramos, F. and Arnold, D., "WHO Food Additives Series 53: chloramphenicol. JECFA (WHO: Joint FAO/WHO Expert Committee on Food Additives)", IPCS (International Programme on Chemical Safety) INCHEM, 53, 7-85 (2004).

Xu, W., Zhang, G., Li, X., Zou, S., Li, P., Hu, Z., Li, J., "Occurrence and elimination of antibiotics at four sewage treatment plants in the Pearl River Delta (PRD), South China", *Water Res.,* **41 (19),** 4526-4534 (2007).

CHAPTER 4

Ciprofloxacin Degradation: Kinetic Modelling, Reaction Pathways and Toxicity Assay

This chapter investigates on the decomposition behaviour of Ciprofloxacin (CIP) in aqueous solution using FP, PFP and UVP.

4.1 Introduction

CIP is a synthetic antibiotic drug of second-generation fluoroquinolones class. It kills bacteria by interfering with the enzymes that cause DNA to rewind, which stops synthesis of DNA and protein. According to a recent survey by Schwabe and Paffrath (2011), it was reported that CIP was globally prescribed in the order of 18.7 million defined daily doses (DDD) in the year of 2010. It corresponds to an increase of 6.2% compared to 2009 reflecting a total amount of 9.5 tons. CIP could exist in the target organisms even up to 72% of the nonmetabolized form (Ternes et al., 2003).

The concentration of CIP in disposed water from a production unit of 90 bulk drugs in Patancheru, near Hyderabad (India) was around 1000 times above the toxicity level to some bacteria (Larsson et al., 2007). In continuation of the earlier work, it was reported that even 0.2% (v/v) of this effluent could notably reduce the growth rate of tadpoles and the underlying toxicity is still unknown (Gunnarsson et al., 2009). CIP residues have been widely found in hospital wastewater, sewage treatment plant effluent and surface water; (Li et al., 2011; Christian et al., 2003; Golet et al., 2002). Furthermore, CIP strongly adsorbs on sewage sludge with as high as 6.3 mg/kg dry of matter (Golet et al., 2002). Limited insight has been provided to understand the degradation mechanism of CIP.

Several in vitro experiments confirm that Fe^{2+} has the capacity to reduce molecular oxygen to superoxide radical for the production of hydroxyl radical ($HO^{\bullet}$) (Eq. 4.1) (Stepfan et al., 2004).

$$Fe^{2+} + O_2 \rightarrow Fe^{3+} + O^{\bullet}_2{}^{-} \quad (4.1)$$

The overall reaction of the combined steps (Eqs. 1.1 and 4.1) is called Haber-Weiss reaction (Eq. 1.8). In general, $HO^{\bullet}$ react with the organic pollutants (RH) by the abstraction of H atom from C-H, N-H, or O-H bonds and by the addition of C-C bonds to the conjugate aromatic rings. The general rate equation of the key organic molecule can be written as Eq. (4.2).

$$-\frac{dC_{RH}}{dt} = \sum_i k_{OH^{\bullet}} . C_{OH^{\bullet}} . C_{RH_i} + \sum_i k_{OX_i} C_{OX_i} C_{RH_i} \quad (4.2)$$

OX_i represent other oxidants than $HO^{\bullet}$ such as ferryl $[Fe(IV)O]^{2+}$ or $\cdot OOH$. Most of the studies assume that $HO^{\bullet}$ formation and disappearance rate are instantaneous (Mantzavinos et al., 1996). However, it is prudent to consider $[HO^{\bullet}]$ at higher pollutant concentration (Martins et al., 2010). Investigations on $[HO^{\bullet}]$ determination and its inclusion to the kinetics of FP, PFP and UVP for the degradation of pharmaceutical compounds still lack in literature.

Determination of $HO^{\bullet}$ includes electron spin resonance spectroscopy in which the electron paramagnetic resonance spectrum of a spin adduct derivative is measured after trapping (Doll et al., 2004). This method is less sensitive and difficult to employ readily to acquire quantitative estimation of $HO^{\bullet}$ as unstable $HO^{\bullet}$-adduct is formed. $HO^{\bullet}$ can be measured from the concentration of hydroxylated products formed with aromatic compounds such as phenol, benzoic acid and salicylic acid (Gulkaya et al., 2006). The problems associated in $HO^{\bullet}$ determination in AOPs include: (i) multiple reactions, (ii) secondary generation of superoxide, (iii) limited solubility adduct and, (iv) formation of iron (+2, +3)-salicylic acid complex that hinders $HO^{\bullet}$ formation in Fenton and Fenton-like reactions (Kang et al., 2002).

To overcome these limitations, dimethyl sulphoxide (DMSO) as the chemical probe can be used for $HO^{\bullet}$ determination. It is based on the reaction between $HO^{\bullet}$ with DMSO to produce formaldehyde (HCHO). DMSO is highly water soluble and could trap most hydroxyl radicals ($HO^{\bullet}$) generated in AOP's. It does not form complexes with iron or other metals ions in FP and PFP (Ternes et al., 2003; Lindsey et al., 2000).

The influence of pH, reaction time, Fe^{2+} to H_2O_2 molar ratio on TOC, COD decay and mean oxidation number of carbon (MONC) variation have been studied in this chapter. A mechanism of CIP oxidation is proposed and supported by the results obtained in LC-MS spectra. An oxidative kinetic equation involving $HO^{\bullet}$ for [CIP] as well as for degradation products [DP_s] was developed. The concentration of $HO^{\bullet}$ was determined using DMSO as a chemical probe. The studies on the antimicrobial activity of CIP and its decomposition products were also carried out.

4.2 Determination of Mean Oxidation Number of Carbon (MONC)

The mean oxidation number of carbon (MONC) reveals the experimental errors incurred in COD and TOC measurements. Chemically, the MONC must lie in the range from - 4 to 4 with respect to the simplest organic compound, CH_4 and CO_2. The MONC for a single organic molecule containing '*n*' number of carbon atoms can be represented as in Eq. 4.3. ON_i indicates the oxidation number of i^{th} carbon atom (Vogel et al., 2000). The oxidation number of the individual carbon atom is provided in Figure 4.1 in round parenthesis for the CIP molecule. An oxidation number of 0, +1, +0.5, +2 were considered for the C-C σ- and π-bonds; C=C σ- and π-bonds and; C=O σ- and π-bonds, respectively (Hesse et al., 2008). It gave net 'zero' oxidation number of carbons in both piperazine ring and cyclopropyl group.

$$\text{MONC} = \frac{\sum_{i=1}^{n} \text{ON}_i}{n} \tag{4.3}$$

COD and TOC values also can be combined together to compute the MONC irrespective to the number of organic molecule present in the sample as in Eq. 4.4 (Vogel et al., 2000). COD and TOC are expressed in mg/L.

$$\text{MONC} = 4 - 1.5\frac{\text{COD}}{\text{TOC}} \tag{4.4}$$

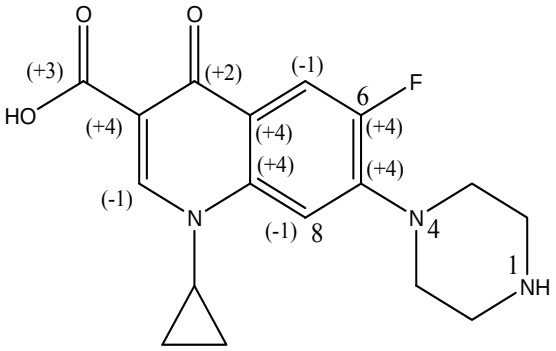

Figure 4.1. Chemical structure of CIP drug [1-cyclopropyl-6-fluoro-4-oxo-7-(piperazin-1-yl)-Quinoline-3-carboxylic acid].

4.3 Kinetic Model Development

CIP molecules are targeted by $HO^{\bullet}$ immediately upon its generation and a number of products are formed (Eq. 4.5). The solution in the batch reactor was completely mixed and the reaction temperature was controlled in a narrow range (23 to 25°C). The pH variation was insignificant during degradation experiment. It was assumed that active $HO^{\bullet}$ was the main oxidant to cleavage the organic substances in the solution.

$HO^{\bullet}$ radical was utilized for the oxidation of CIP (Eq. 4.6) and degradation products (DP_s) (Eq. 4.7). The initial CIP concentration was quite high and $HO^{\bullet}$ showed exponential decay with oxidation time at the optimal Fe^{2+}/H_2O_2 and pH. It implies that the rate of CIP oxidation was dependent on $[HO^{\bullet}]$. So the rate equation is expressed in terms of concentration of CIP (Eqs. 4.6 and 4.7). k_1 and k_2 (1/M·s) are the second order rate constants. CIP, DP_s and $HO^{\bullet}$ in square parenthesis indicate their concentration.

$$CIP + HO^{\bullet} \rightarrow CIP_{oxidixed} \tag{4.5}$$

$$-\frac{d[CIP]}{dt} = k_1\,[CIP][HO^{\bullet}] \tag{4.6}$$

$$-\frac{d[DP_s]}{dt} = k_2\,[DP_s][HO^{\bullet}] \tag{4.7}$$

Eqs. 4.6 and Eq. 4.7 can be combined as in Eq. 4.8:

$$-\frac{d[HO^{\bullet}]}{dt} = -\left(\frac{d[CIP]}{dt} + \frac{d[DP_s]}{dt}\right) = k_1[CIP][HO^{\bullet}] + k_2[DP_s][HO^{\bullet}] \tag{4.8}$$

4.4 Results and Discussion

4.4.1 Optimal Fe^{2+}/H_2O_2 molar ratio

The dose of Fe^{2+} and H_2O_2 determine the operational cost as well as the efficiency of degradation of contaminant. The concentration of Fe^{2+} drops quickly with the progress of reaction (Eq. 4.5). It is consequently balanced by the formation of Fe^{2+} through reduction of Fe^{3+} (Eq. 4.9) and Fe^{2+} concentration reaches at the steady state.

$$Fe^{3+} + H_2O_2 \rightarrow Fe^{2+} + HOO^{\bullet} + H^{+} \quad (4.9)$$

The optimal Fe^{2+}/H_2O_2 molar ratio was found out by varying it in the range from 0.025 to 0.18 with a fixed H_2O_2 dose of 10 mM. The experimental optimization to maximize CIP degradation was performed in FP. The setting obtained in FP was adopted in PFP and UVP (without Fe^{2+}) with UV light. The change in [$HO^{\bullet}$] can be divided into two phases. At the initial phase, $HO^{\bullet}$ radicals production is faster. It was resulted in higher CIP degradation (Figure 4.2). In the second phase, [$HO^{\bullet}$] decreased even though CIP oxidation mostly occurred within the 1st stage (Bautista et al., 2007). It was primarily due to progressive depletion of H_2O_2.

CIP removal increased with increase in Fe^{2+}/H_2O_2 molar ratio and maximum removal of 74.4% was obtained at 0.125. It decreased with further rise of Fe^{2+}/H_2O_2 ratio. Generally, the rate of $HO^{\bullet}$ formation increases with rise of Fe^{2+}/H_2O_2. However, excess H_2O_2 with respect to Fe^{2+} can directly oxidize Fe^{2+} to Fe^{3+}. It reduces the production rate of $HO^{\bullet}$ and CIP removal fell down (Kugelmann et al., 2011; Saadatjou et al., 2010). CIP removal per unit Fe^{2+}/H_2O_2 molar ratio dropped almost linearly (Figure 4.2). It suggests that FP was more proficient in consumption of Fe^{2+} and H_2O_2 for drug degradation at lower dose. At $Fe^{2+}/H_2O_2 > 0.125$, CIP removal dropped a bit. It implies that the optimal Fe^{2+}/H_2O_2 ratio was around 0.125 in terms of percentage CIP removal.

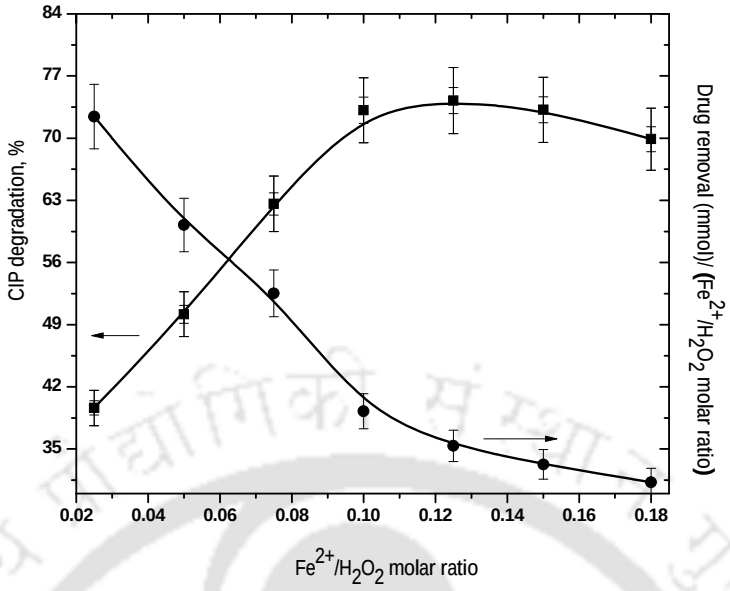

Figure 4.2. Effect of Fe^{2+}/H_2O_2 molar ratio on CIP degradation in FP. Experimental conditions: $[CIP]_0$ =15 mg/L, reaction time = 45 min, pH = 3.5 and temperature = 25°C.

4.4.2 Optimal pH in FP

pH controls the production rate of $HO^{\bullet}$ and the nature of iron species. pH was varied in the range from 2 to 4.5 (Figure 4.3). The dynamics of drug removal followed similar trend at different pH. Removal efficiency gradually increased with rise of pH and it reached a maximum value of 74.4% at pH 3.5 (Figure 4.3). Further pH elevation decreased drug removal. $HO^{\bullet}$ could be consumed by the scavenging effects of H^+ (Eq. 4.10) at pH<3.5 which would limit the degradation rate (Shrivastaval et al., 2010). It might also be possible that H_2O_2 was stable by acquiring a proton to form an oxonium ion (Eq. 4.11) at lower pH (Stumm et al., 1981).

$$HO^{\bullet} + H^+ + e^- \rightarrow H_2O \quad (4.10)$$

$$H_2O_2 + H^+ \rightarrow H_3O_2^+ \quad (4.11)$$

The concentration of iron used in Fenton experiment was lower than the theoretical solubility of Fe(II) and Fe(III) (Ghosh et al., 2012; Kolpin et al., 2002). $[Fe^{2+}]$ was more than 99.9% at pH<4 (Tekin et al., 2006). However, brownish appearance of the solution was visually noted with addition of CIP into Fenton reagent and it transformed into steady particle form in about 10 min. It implies that probably iron-organo complexes of lower solubility

were formed. It reduced the total available iron, primarily Fe^{2+}, and CIP in solution. Sludge may be converted to more stable solid modifications such as α-FeOOH(s) and α-Fe_2O_3(s) with progress of the reaction. Indeed, highly heterogeneous nature of iron sludge could be formed (Klavarioti et al., 2009; Qiang et al., 2003). The results obtained at different pH indicate that the optimal pH of CIP removal was around 3.5.

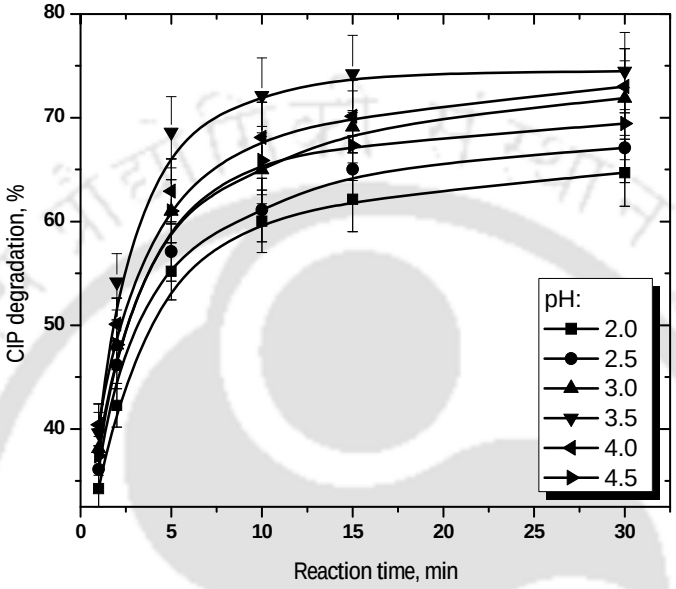

Figure 4.3. Effect of pH on % CIP degradation. Experimental conditions: $[CIP]_0$ = 15 mg/L, Fe^{2+} = 1.25 mM, H_2O_2 = 10 mM and temperature= 25°C.

4.4.3 Comparative CIP, COD and TOC removal at optimal condition with the variation HO• concentration in FP, PFP and UVP

Removal of CIP, COD and TOC per unit HO• consumption is shown in Figures 4.4 to 4.6. HO• consumption was calculated by the difference of its initial and concentration at different time intervals. The initial [HO•] calculation procedure is elaborated in section 4.4.6. It was found out that one unit HO• could reduce 2.49 mmol CIP at 1 min in FP and it increased to 3.11 mmol in 45 min. The same was 2.68 and 0.47 mmol CIP at 1 and 45 min in PFP. It reduced to 5.16 and 1.03 in UVP. It varied between 46.5 to 73.7 and 42.6 to 87.2 mmol for the reduction of COD and TOC, (Figures 4.4 to 4.6). It clearly implies that HO• was predominantly consumed for the fragmentation of daughter ions in comparison to CIP cleavage. COD removal includes oxidation of carbon and non-carbon atoms. Therefore, the fraction of HO• consumed for TOC

removal was less than of for COD reduction. On the other way it indicates that TOC removal per unit $HO^{\bullet}$ radical consumption for the expulsion of carbon atom was higher.

The elevated initial rate of $HO^{\bullet}$ formation was resulted in higher initial rate of CIP (till 5 min), COD (till 15 min) and TOC (till 15 min) removal. Maximum COD reduction was found as 47.1, 54.8 and 32.9% at 15 min in FP, PFP and UVP, respectively. The corresponding TOC removal was 37.9, 45.1 and 27.3% against CIP cleavage of 74.4, 78.4 and 52.7%. After that, there was no notable effect of treatment time on the removal efficiencies.

There was no sludge formation in PFP. Sludge formed in FP was separated by filtration using 0.45 μm cellulose ester filter. It was then washed in distilled water and dissolved in conc. H_2SO_4 solution. Amount of CIP adsorbed on sludge was determined after 45 min of FP under the optimal condition (Fe^{2+}/H_2O_2 molar ratio 0.125 and pH 3.5). About 3, 4 and 6% CIP, COD and TOC reduction was observed due to sludge appearance. It implies that CIP adsorption on iron sludge would not affect the kinetics of CIP oxidation. Stable CIP (or intermediates)-iron complex formed was resistant to FP.

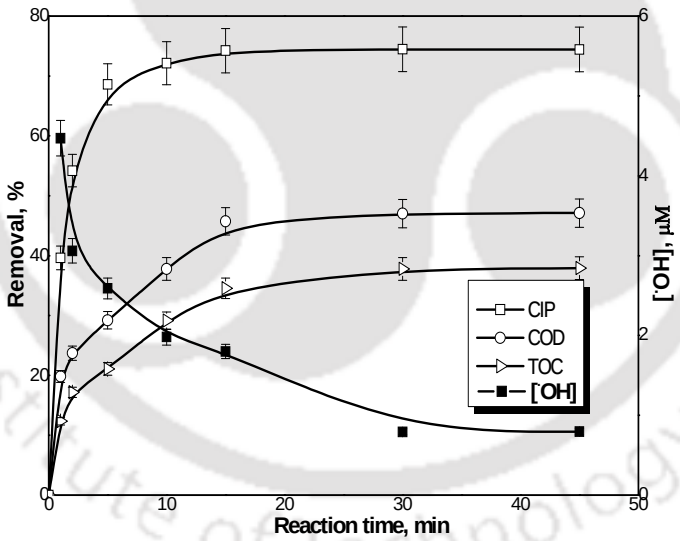

Figure 4.4. Removal of CIP, COD and TOC along with the variation of hydroxyl radical concentration with the progress of reaction time in FP. Experimental conditions: $[CIP]_0$ =15 mg/L, Fe^{2+} = 1.25 mM, H_2O_2 = 10 mM, pH = 3.5 and temperature =25°C.

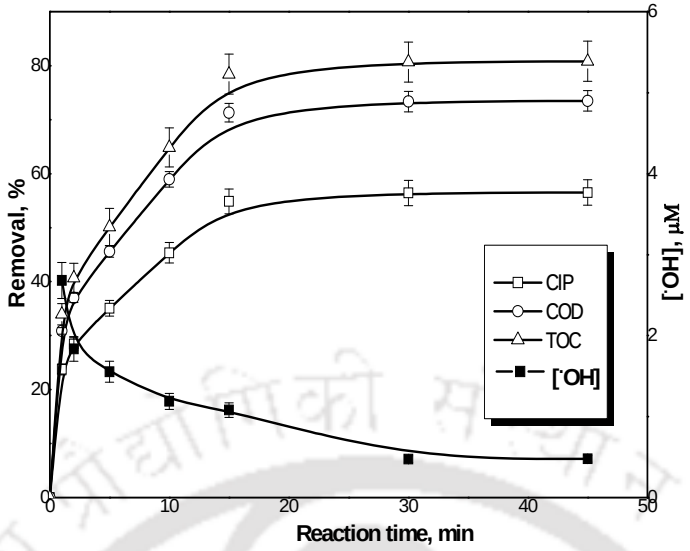

Figure 4.5. Removal of CIP, COD and TOC along with the variation of hydroxyl radical concentration with the progress of reaction time in PFP. Experimental conditions: $[CIP]_0$ =15 mg/L, Fe^{2+} = 1.25 mM, H_2O_2 = 10 mM, pH = 3.5, UV irradiation 12 W/m^2 (9 W) and temperature =25°C.

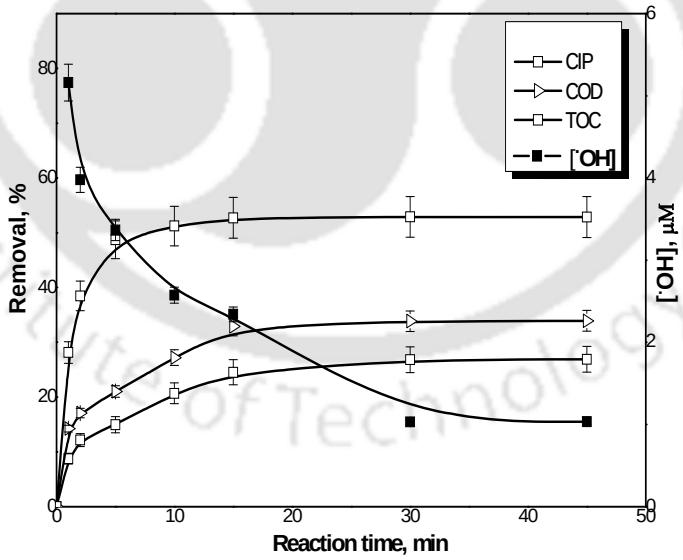

Figure 4.6. Removal of CIP, COD and TOC along with the variation of hydroxyl radical concentration with the progress of reaction time in UVP. Experimental conditions: $[CIP]_0$ =15 mg/L, H_2O_2 = 10 mM, pH = 3.5, UV irradiation 12 W/m^2 (9 W) and temperature =25°C.

4.4.4 Variation of MONC with reaction time

Iron sludge formed during FP was removed preceded by Fe^{2+} oxidation at high pH and; residual $HO^{\bullet}$ and H_2O_2 were destroyed by heating the samples to avoid the interference. The experimentally determined COD value was therefore readily employed for the estimation of MONC. The results are shown in Figure 4.7. MONC values estimated using Eqs. (4.3) and (4.4), were of 1.17 and 1.28. It implies that COD and TOC were determined with reasonable accuracy. The MONC increase was faster at <2.5 min and then it increased gradually. MONC increased to 1.68, 2.1, 1.42 from the initial value of 1.28 in FP, PFP and UVP, respectively. The result can be corroborated by the refractory nature of the quinolone moiety and oxidation of greater numbers of products in PFP.

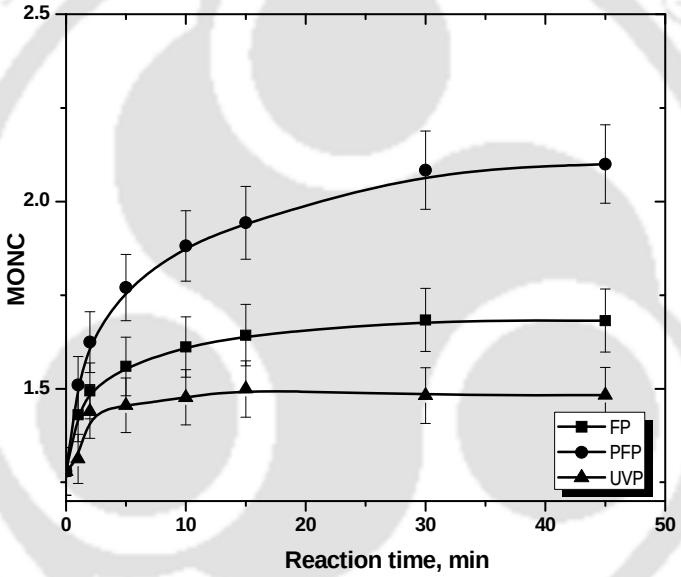

Figure 4.7. Variation of MONC with progress of reaction: Experimental conditions: $[CIP]_0$ =15 mg/L, Fe^{2+} = 1.25 mM (in FP and PFP only), H_2O_2 = 10 mM, pH = 3.5 and temperature =25°C. Photo-reaction with an UV lamp of 12 W/m^2.

4.4.5 Proposed mechanisms of CIP degradation

N_4 in piperazine ring of fluoroquinolone compounds is typically the specific site of $HO^{\bullet}$ attack. N_1 is likely less reactive than N_4 because of its weaker basicity (Zhang et al., 2005). Two strong electron-withdrawing nitrogen substituents i.e. fluorine and -COOH groups are there in the aromatic ring (Figure 2.1). On the other way it indicates that fluoroquinolone ring is less electron-donating because of highly electron-withdrawing fluorine substituent (Klavarioti et al., 2009). In general, the loss of carboxyl moiety ([M+H-

44]$^+$) and fluoride ([M+H-22]$^+$), are the typical fragmentation pathways of fluoroquinolone (Klauson et al., 2010). The appearance of such fragmentations in the MS^n spectra gives some hints for the subtraction of different moieties based on their mass losses such as 44 for -COOH group.

The mass spectra are depicted in Figures 4.8 to 4.10 for CIP cleavage in FP. The mass spectra obtained in PFP are shown in Figures 4.11 and 4.12. In case of UVP, only seven intermediates appeared in the mass spectra (Figure 4.13). The formation of daughter ions could follow two pathways for the degradation of CIP i.e. piperazine moiety degradation and decarboxylation. The possible routes of oxidation of CIP molecule are illustrated in Figures 4.14 to 4.16 in FP. The peaks in the mass spectra with m/z of 305, 186, 198, 217, 242 and 261 were for the retention time of 5.36 min (Figure 4.8). D_1 with m/z 305 has the same specific mass of 7-[2-amino-ethyl) amino]-6-fluoroquinoline formed by the loss of the piperazine ring (Figure 4.14) under acidic condition. It appeared with the cleavage of piperazine ring via an unstable intermediate product in FP, PFP and UVP as shown in Figures 4.11, 4.16 and 4.20, respectively. The nitrogen atom of piperazine ring with a lone pair electron, abstracted the proton from the solvent at acidic pH and the C-C bond was broken. The fragmentations with m/z of 186, 198, 239, 261, 304, 354 and 386 at 5.76 min of retention are presented in Figure 4.9. The daughter ion with m/z ratio of 304 (D_2) was formed due to piperazine ring breaking along with defluorination followed by hydroxylation of D_1 in FP (Figure 4.14). D_3 (m/z of 239) appeared in FP with the loss of fluorine atom at position 6 and expulsion of ethylenediamine molecule (Figure 4.14). Decarboxylation of CIP led to formation of D_4 having the same m/z of D_2 and formed only in FP. MS spectra of the compound with m/z = 301 (D_5) originated in FP theoretically represents a fragment of CIP which might be formed by the loss of fluorine atom (Figure 4.15). The steric effect between carbonyl and carboxylic (-COOH) groups and the presence of fluoride group could trigger such decarboxylation. The peaks with m/z of 205, 239, 279 and 301 in the mass spectra corresponding to retention time of 6.50 min are shown in Figure 4.10. –OH group was expelled out from the quinolone moiety in presence of electron withdrawing N atom and carbonyl group. Therefore, D_1 was further broken into D_6 (m/z of 287) by dehydroxylation in FP. Piperazine ring suffers an angle stress in presence of high electronegative fluorine atom.

It led to formation of a three-membered cyclic amine ring (D_7) (Figure 4.16) originated in FP, PFP and UVP (Table 4.1). Amine group makes the quinolone moiety more electron rich compound and it is easily targeted by $HO^{\bullet}$ because of electrophile nature of the free radical. As a result, D_8 was formed by hydroxylation in FP. D_9 (m/z 198) and D_{10} (m/z

217) both were formed in FP, PFP and UVP and yielded due to cleavage of N-C bond of cyclic amine ring (Figure 4.16). D_1 broken into D_{11} (m/z 242) on defluorination and partial piperazine moiety oxidation because of steric hindrance (Figure 4.16) and obtained in all three processes. A similar explanation for D_{12} is also applicable which was formed in FP, PFP and UVP. The possible route for the formation of D_{13} with m/z 279 is shown in Figure 4.16. D_{13} molecule was originated in FP and UVP. The pathways for the formation of daughter ions are summarized in Table 4.1. Lower TOC removal is in accordance with the proposed mechanism of CIP degradation as carbon atoms mainly remained to the quinolone moiety. The variation of MONC also gives the hint for the successive oxidation of CIP molecule. MONC for the individual daughter ions were varied in the range of 0.8 (D_{11}) to 1.72 (D_8) at 10 min of Fenton reaction with 28% unreacted CIP (in FP) against the same of 1.18 for CIP.

Nineteen numbers of intermediates were identified in PFP. The primary pathways for photolytic degradation of CIP include (i) photooxidation (in presence of UV illumination), (ii) defluorination and, (iii) cleavage of piperazine ring (Figures 4.17 to 4.19). A close look reveals that the mechanistic pathways for degradation of CIP in PFP (Figures 4.17 to 4.19) were mostly similar to FP (Figures 4.14 to 4.16). D_{14} to D_{26} were formed only in PFP and also their routes of formation are summarized in Table 4.1. Paul et al. (2010) identified D_8 (m/z 344) during CIP cleavage in PFP. They showed that D_8 was formed through decarboxylation followed by partial piperazine ring cleavage and hydroxylation reaction of CIP molecule. Most distinctly, tris-ethylenediamine-Fe(III) complex (D_{19}) with mass number of 237.5 (Figure 4.19) could form in PFP. The low molecular weight compound, ethylenediamine ($C_2H_8N_2$) could act as a chelating agent.

D_1 (m/z 305) was first formed on hydrolysis followed by partial cleavage of piperazine ring of CIP molecule (Figure 4.20). D_1 was further broken as sketched and outlined in Figure 4.20 (Lester et al., 2011).

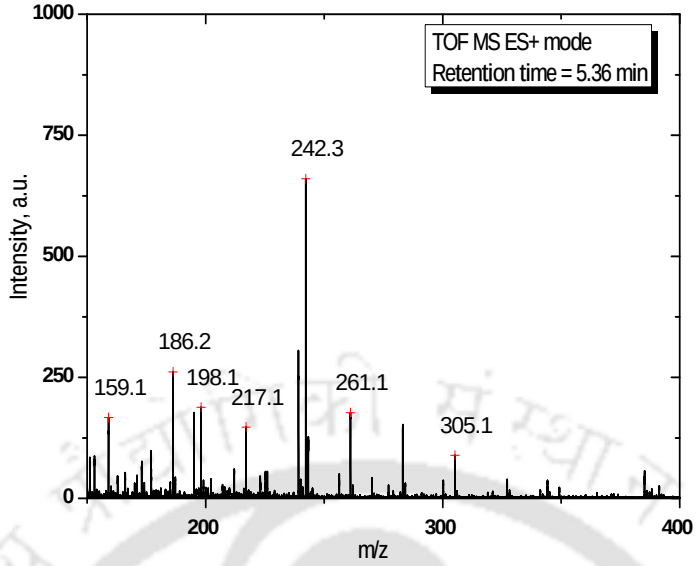

Figure 4.8. Mass spectra recorded at 10 min of reaction in FP with reaction time of 5.36 min. Experimental conditions: $[CIP]_0$ = 15 mg/L, Fe^{2+} = 1.25 mM, H_2O_2 = 10 mM, pH = 3.5 and temperature = 25°C.

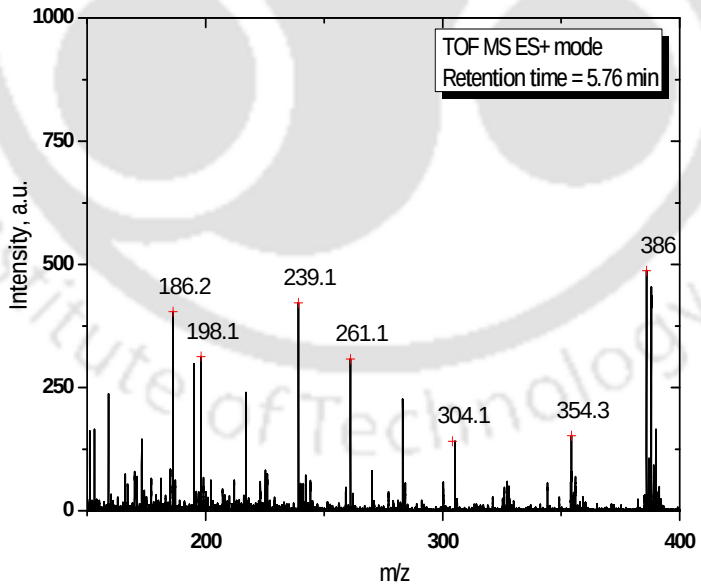

Figure 4.9. Mass spectra recorded at 10 min of reaction in FP with reaction time of 5.76 min. Experimental conditions: $[CIP]_0$ = 15 mg/L, Fe^{2+} = 1.25 mM, H_2O_2 = 10 mM, pH = 3.5 and temperature = 25°C.

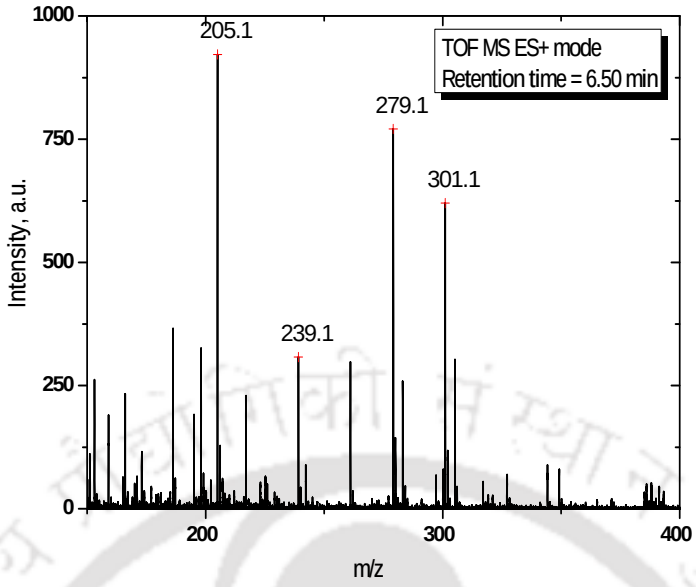

Figure 4.10. Mass spectra recorded at 10 min of reaction in FP with reaction time of 6.50 min. Experimental conditions: $[CIP]_0$ = 15 mg/L, Fe^{2+} = 1.25 mM, H_2O_2 = 10 mM, pH = 3.5 and temperature = 25°C.

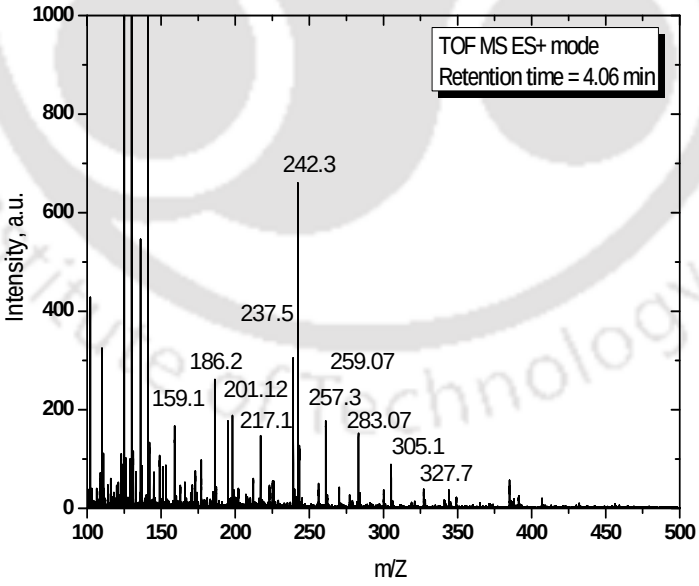

Figure 4.11. Daughter-ion spectrum obtained at 10 min of PFP with retention time of 4.06 min. Photo reaction with an UV lamp of 12 W/m^2 (9 W). Experimental conditions: $[CIP]_0$ = 15 mg/L, Fe^{2+} = 1.25 mM, H_2O_2 = 10 mM, pH = 3.5 and temperature = 25°C.

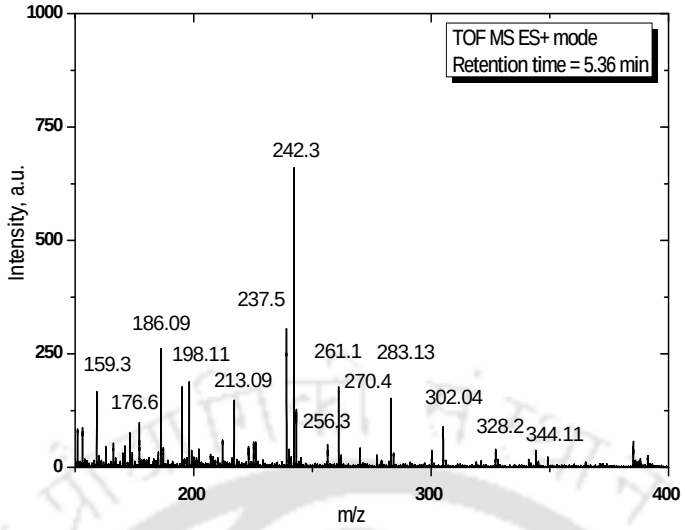

Figure 4.12. Daughter-ion spectrum of at 10 min of PFP with retention time of 5.36 min. Photo reaction with an UV lamp of 12W/m^2 (9 W). Experimental conditions: $[CIP]_0$ = 15 mg/L, Fe^{2+} = 1.25 mM, H_2O_2 = 10 mM, pH = 3.5 and temperature = 25°C.

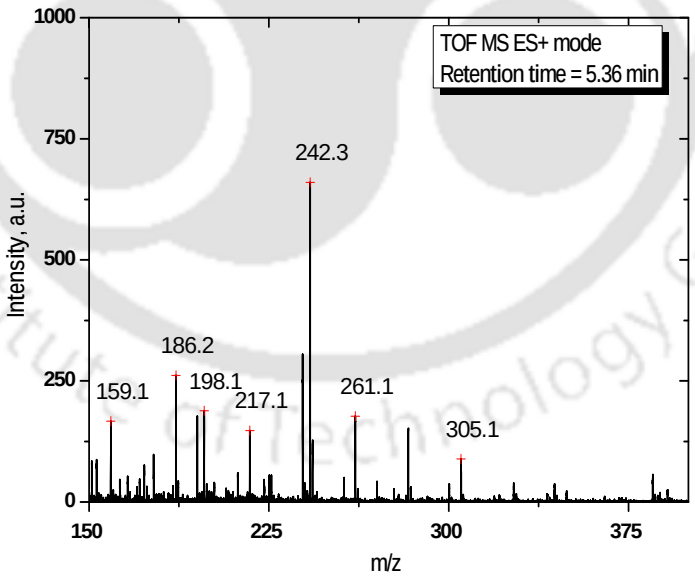

Figure 4.13. Mass spectra recorded at 10 min of UVP with retention time of 5.36 min. Experimental conditions: $[CIP]_0$ =0.149 mM, $[H_2O_2]_0$ = 10 mM, pH = 3.5 and temperature =25°C. Photo-reaction with an UV lamp of 12 W/m^2 (9 W).

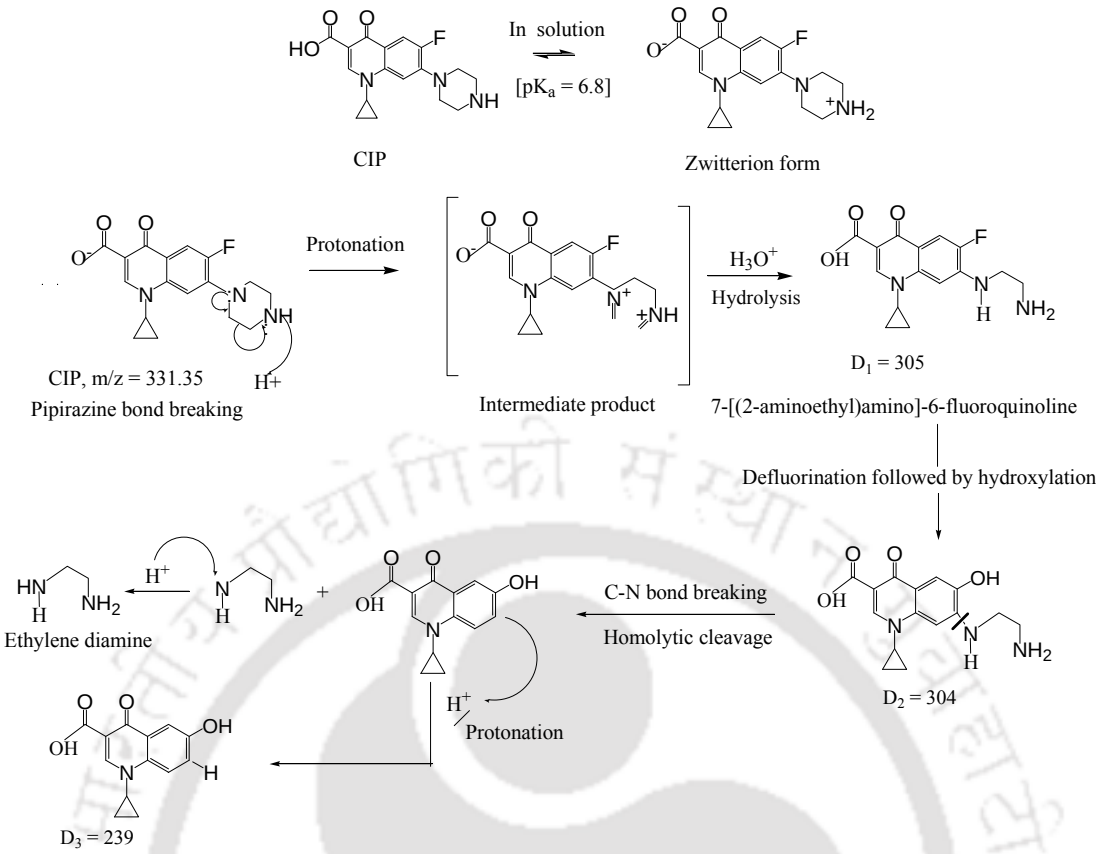

Figure 4.14. Mechanisms for the formation of daughter ions in FP: Piperazinyl moiety degradation.

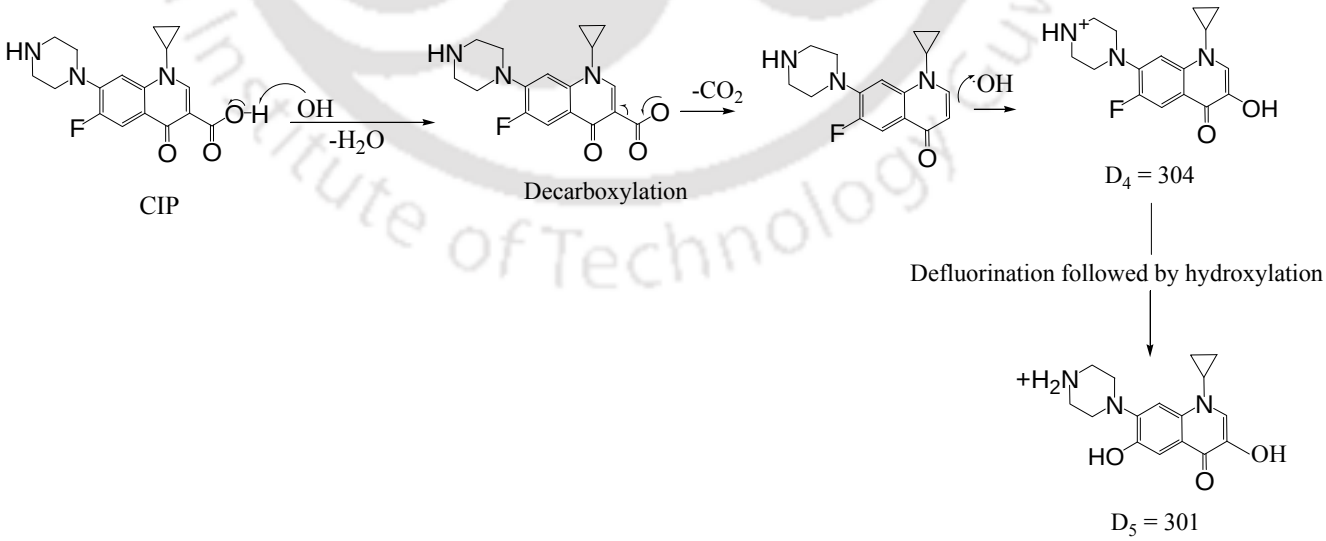

Figure 4.15. Mechanisms for the formation of daughter ions in FP: Decarboxylation.

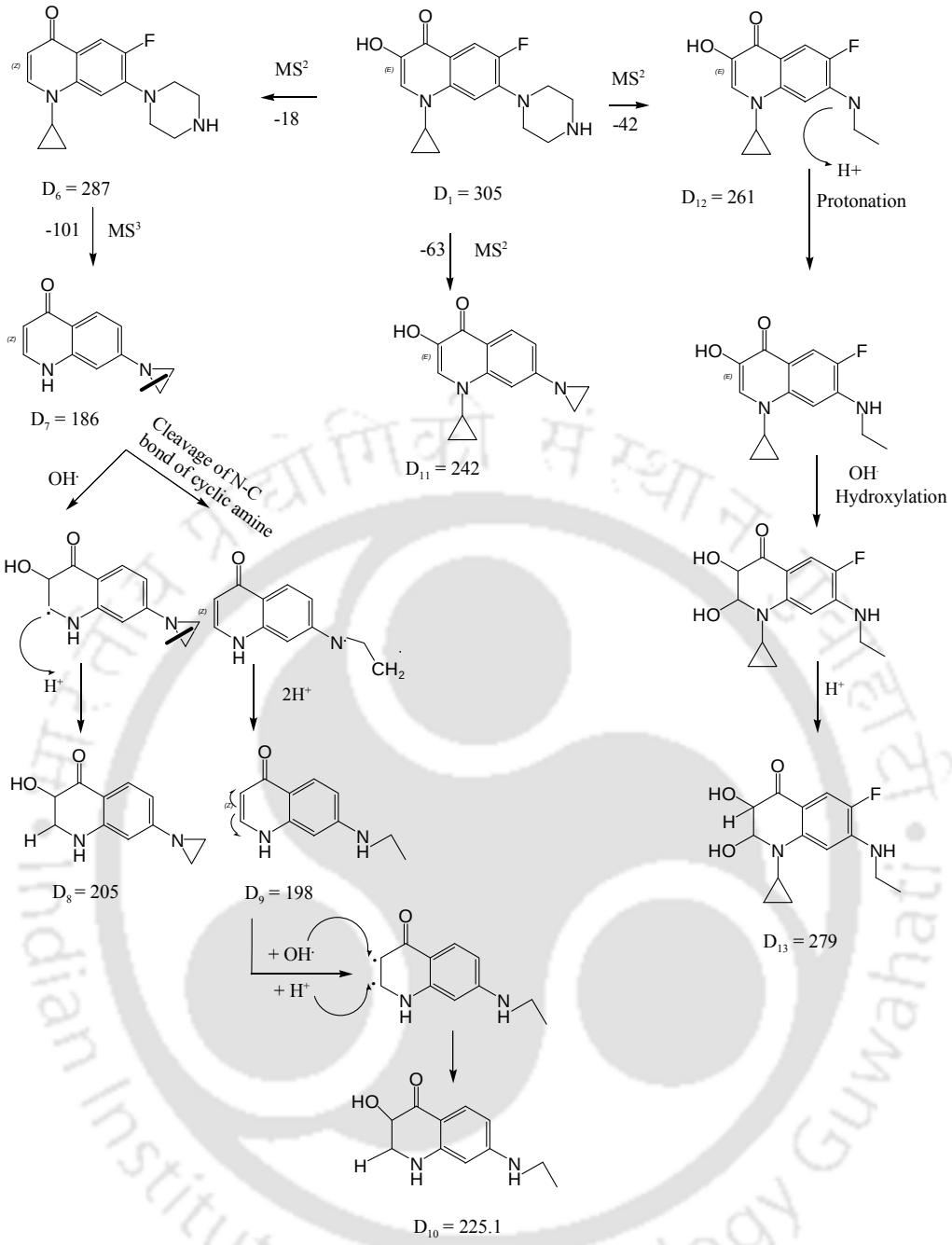

Figure 4.16. Further fragmentation of D_1 with m/z 305.

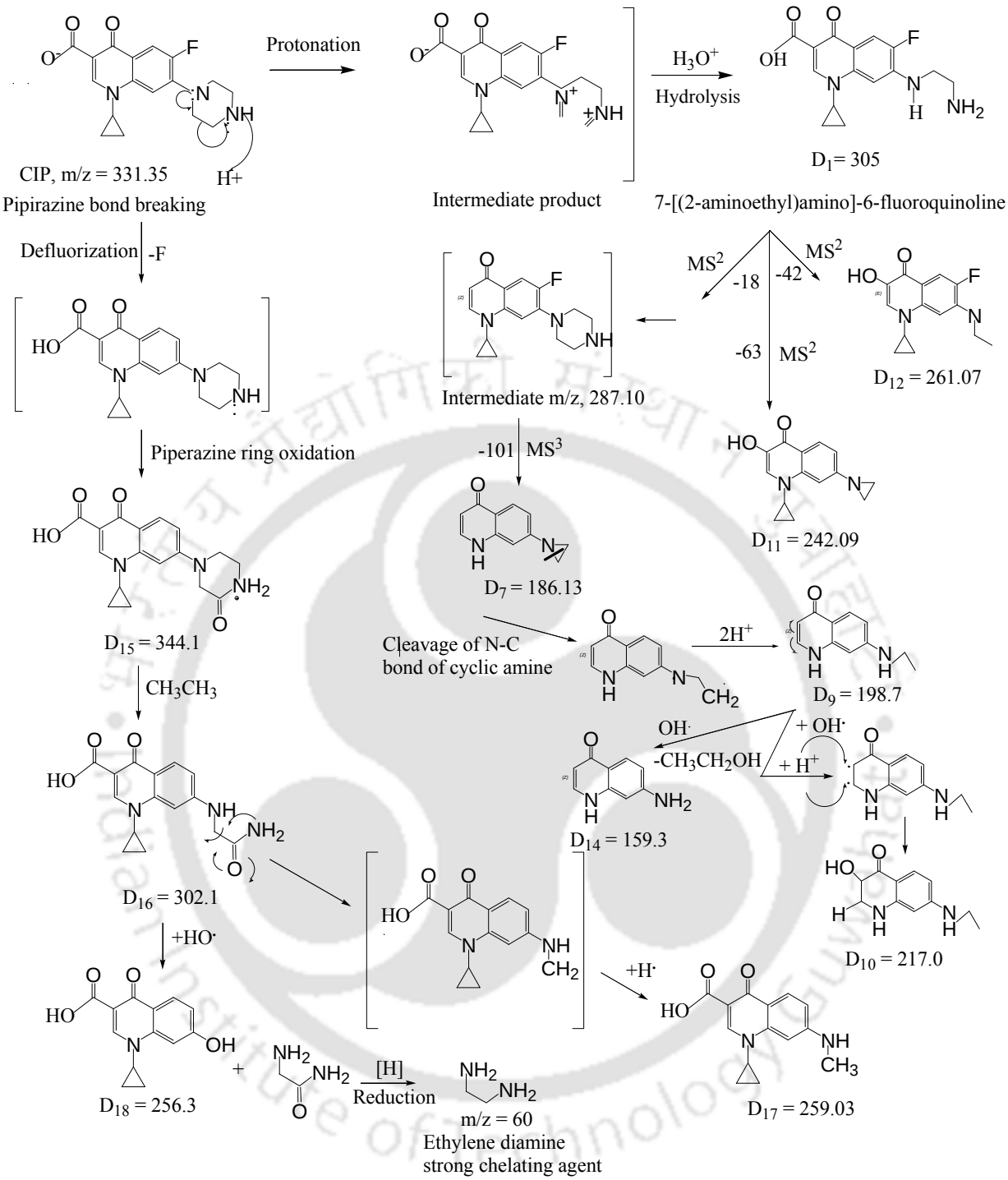

Figure 4.17. Mechanisms for the formation of daughter ions in PFP. Decomposition pathways of CIP molecule with m/z 331.35.

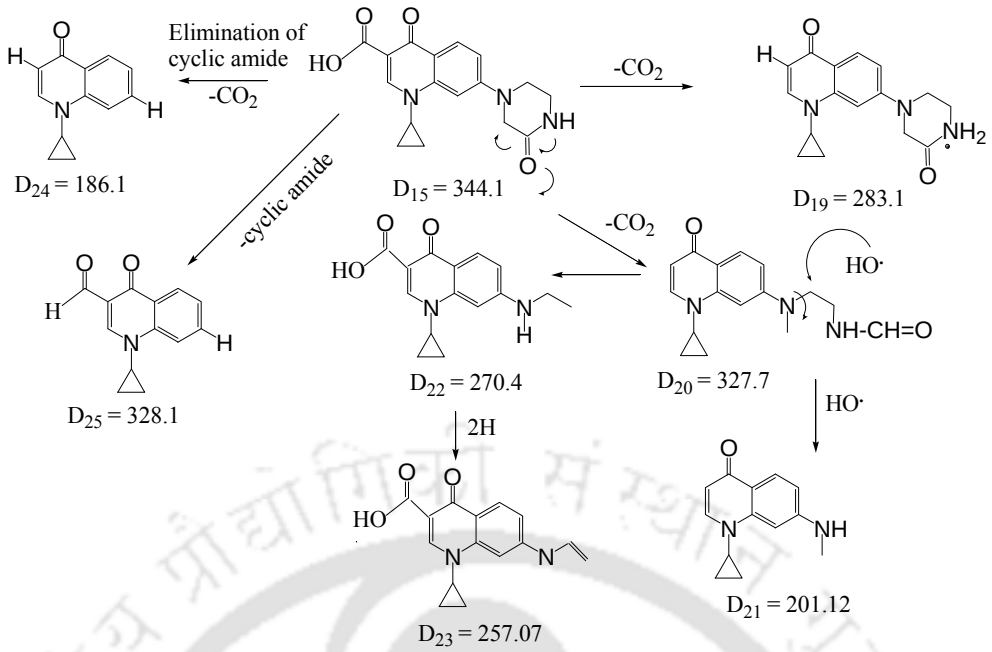

Figure 4.18. Mechanisms for the formation of daughter ions in PFP. Continuation of pathways of D_{17} cleavage.

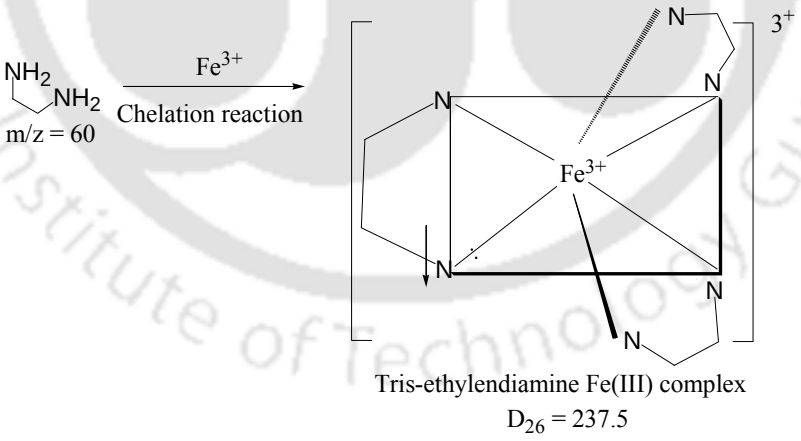

Figure 4.19. Formation of $[Fe(III)\text{-}en]^{3+}$ chelate compound.

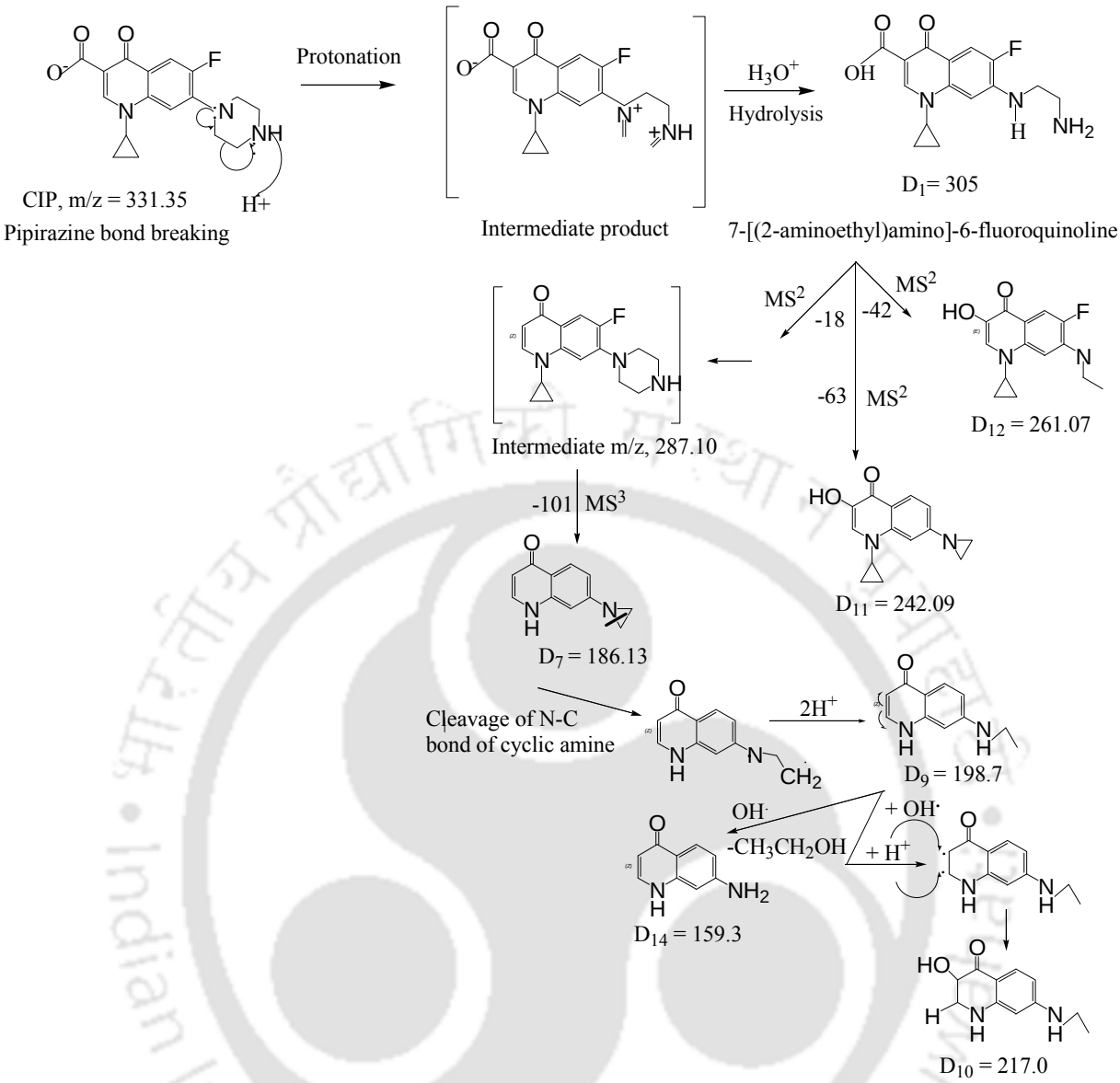

Figure 4.20. Mechanisms for the formation of daughter ions in UVP.

Table 4.1. Mass to charge ratio (m/z) based on the proposed structures and their appearance in the mass spectra during CIP cleavage. The symbol '+' indicates the appearance of intermediates in oxidation processes.

Daughter ions	Formula	m/z	AOPs			Degradation route
			FP	PFP	UVP	
D_1	$C_{15}H_{16}O_3N_3F$	218.11	+	+	+	Partial piperazine ring cleavage
D_2	$C_{15}H_{17}O_4N_3$	279.11	+			Defluorination followed by hydroxylation of D_1
D_3	$C_{13}H_{11}O_4N$	250.07	+			Complete piperazine ring cleavage of D_2
D_4	$C_{13}H_{15}O_2N_3F$	136.04	+			Decarboxylation of CIP
D_5	$C_{13}H_{16}O_3N_3$	176.07	+			Defluorination followed by hydroxylation of D_4
D_6	$C_{16}H_{16}ON_3F$	198.11	+			Dehydroxylation of D_1
D_7	$C_{11}H_{10}ON_2$	199.11	+	+	+	Partial piperazine ring breaking followed by defluorination of D_6
D_8	$C_{11}H_{12}O_2N_2$	205.11	+			Hydroxylation of D_7
D_9	$C_{11}H_{12}ON_2$	189.06	+	+	+	Cleavage of cyclic amine of D_7
D_{10}	$C_{11}H_{10}O_2N_2$	225.11	+	+	+	Hydroxylation of D_9
D_{11}	$C_{14}H_{14}O_2N_2$	186.11	+	+	+	Partial piperazine ring breaking followed by defluorination of D_1
D_{12}	$C_{14}H_{14}O_2N_2F$	171.21	+	+	+	Partially piperazine ring cleavage of D_1
D_{13}	$C_{14}H_{16}O_3N_2F$	187.19	+		+	Hydroxylation followed by protonation of D_{12}
D_{14}	$C_{14}H_{12}ON_3$	159.3		+		Reduction of partial piperazine ring of D_9
D_{15}	$C_{17}H_{18}O_4N_3$	344.1		+		Oxidation of piperazine ring of CIP
D_{16}	$C_{15}H_{15}O_4N_4$	302.1		+		Partial piperazine ring breaking of CIP
D_{17}	$C_{13}H_{14}O_3N_2$	259.03		+		Partial piperazine ring breaking of D_{16}

D_{18}	$C_{12}H_{11}O_3N$	256.3		+		Piperazine ring breaking followed by hydroxylation of D_{16}
D_{19}	$C_{16}H_{18}O_2N_3$	283.1		+		Decarboxylation of D_{15}
D_{20}	$C_{15}H_{19}O_2N_3$	327.7		+		Partial piperazine ring breaking of D_{15}
D_{21}	$C_{13}H_{14}ON_2$	201.12		+		Reduction of piperazine ring of D_{20}
D_{22}	$C_{15}H_{15}O_2N_2$	270.4		+		Oxidation of D_{20}
D_{23}	$C_{15}H_{13}O_3N_2$	257.07		+		Dehydrogenation of D_{22}
D_{24}	$C_{11}H_9ON$	186.1		+		Cleavage of cyclic amide of D_{15}
D_{25}	$C_{13}H_{11}O_2N$	328.1		+		Decarboxylation of D_{24}
D_{26}	$[Fe(C_2N_2H_8)_3]$	237.5		+		Chelation of ethylene diamine with of Fe^{2+}

4.4.6 Kinetic model for the oxidation of CIP and degradation products

The contribution of TOC due to unreacted CIP was determined at the same concentration of CIP. TOC of DP_s was calculated by subtracting the share for unreacted CIP. An atomic number average molecule was proposed from the structure of intermediates (Table 4.1) as in the mechanisms. The molecular weights were 218, 250 and 206 g/mol in FP, PFP and UVP, respectively. Hence, the concentration of DP_s was calculated from their TOC values. Therefore, a better estimation of initial $HO^{\bullet}$ radical concentration ($C^0_{OH^{\bullet}}$) and the second order rate constant of CIP oxidation can be done. However, the uncertainly may arise from the calculation of average molecular weight of DP_s.

The least square technique was used to estimate the kinetic constants and $C^0_{OH^{\bullet}}$. The best fit graphics are shown in Figure 4.21 to 4.23. The results imply that both CIP and DP_s fairly followed the 2nd order kinetics. In FP, the fitted $C^0_{OH^{\bullet}}$, k_1 and k_2 were found as 11.67 µM, 3.13×10^3 and 4.89×10^3 M^{-1} s^{-1}, respectively. Higher k_2 value implies that the overall reactivity of DP_s towards $HO^{\bullet}$ was more than CIP. On similar way the kinetic constants and $C^0_{OH^{\bullet}}$ were calculated for PFP and UVP. The estimated values of $C^0_{OH^{\bullet}}$, k_1 and k_2 were 11.91 µM, 4.37×10^3 1/M.s and 5.09×10^3 1/M.s in PFP. The same were 11.08 µM, 3.53×10^3 1/M.s

and 3.91×10^{3} 1/M.s in UVP (Table 4.2). $C^{0}_{OH^{\bullet}}$ exhibited good accordance to the earlier reports. Hayashi et al. (2007) showed that [HO$^{\bullet}$] in FP typically varies in the range from 1 to 0.01 μM. The average HO$^{\bullet}$ generation and CIP degradation rates were found as 3.83×10^{-8} and 2.97×10^{-8} M/s in FP. These were 4.03×10^{-8} and 3.17×10^{-8} M s^{-1} in PFP and; 2.11×10^{-8} and 2.09×10^{-8} M/s in UVP. Maezono et al. (2011) reported a close value of the average HO$^{\bullet}$ formation rate as 9.3×10^{-10} M s^{-1} for the oxidation of Orange II with 60 mg/L at pH 3 and Fe^{2+}/H_2O_2 molar ratio of 0.01 in photo-assisted Fenton process. The TOC values of unreacted CIP and DP_s were experimentally found out at different time intervals.

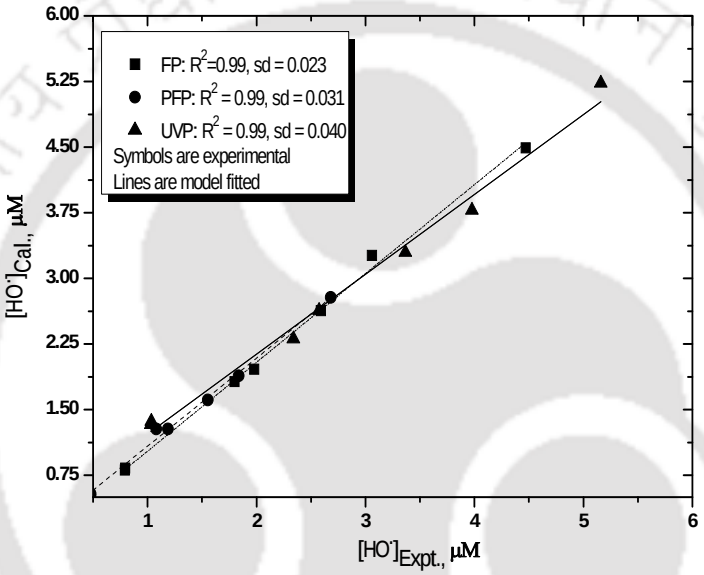

Figure 4.21. Experimental vs. model (Eq. 4.8) predicted concentration of HO$^{\bullet}$ in FP, PFP and UVP. Experimental conditions: $[CIP]_0$=15 mg/L, Fe^{2+} = 1.25 mM (in FP and PFP only), H_2O_2 = 10 mM, pH = 3.5 and temperature = 25°C. Photo-reaction with an UV lamp of 12 W/m^2.

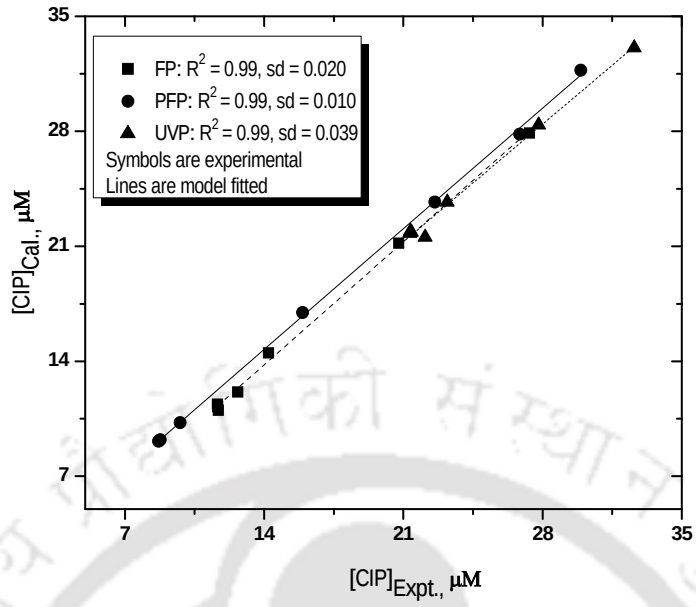

Figure 4.22. Experimental vs. model (Eq. 4.8) predicted CIP concentration in FP, PFP and UVP. Experimental conditions: $[CIP]_0$=15 mg/L, Fe^{2+} = 1.25 mM mM (in FP and PFP only), H_2O_2 = 10 mM, pH = 3.5 and temperature = 25°C. Photo-reaction with an UV lamp of 12 W/m^2.

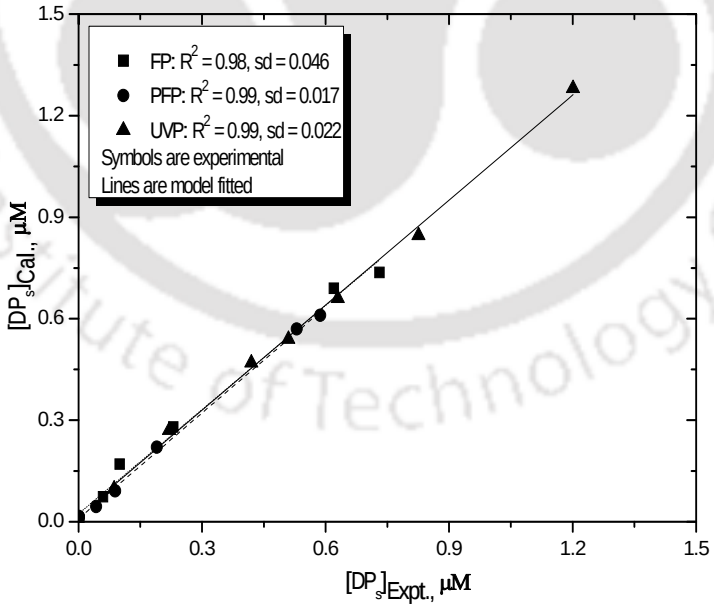

Figure 4.23. Experimental vs. model (Eq. 4.8) predicted degradation products (DPs) in FP, PFP and UVP. Experimental conditions:$[CIP]_0$ =15 mg/L, Fe^{2+} = 1.25 mM (in FP and PFP only), H_2O_2 = 10 mM, pH = 3.5 and temperature = 25°C. Photo-reaction with an UV lamp of 12 W/m^2.

Table 4.2. Fitted model parameters.

Process	k_1 , 1/M.s	k_2 , 1/M.s	$C^0_{OH^\bullet}$, µM	R^2
FP	3.13×10^3	4.89×10^3	11.67	0.98
PFP	4.37×10^3	5.09×10^3	11.91	0.98
UVP	3.53×10^3	3.91×10^3	11.08	0.97

4.4.7 Antimicrobial activity of CIP and its decomposition products

Figure 4.24 shows the antimicrobial activity of CIP and its degradation products towards *E. coli* bacteria in LB media. The exposure of *E. coli* in 15 mg/L CIP caused about 98.4% cell death with respect to the control media. It reduced to 75, 71.2 and 90% upon decomposition of CIP in FP, PFP and UVP, respectively. The growth of *E. coli* inhibited significantly even after 45 min of reaction is probably due to formation of nitrogenous intermediates. Liang et. al (2013) reported that the antimicrobial activity could reduce on reduction of –nito ($–NO_2$) to amine ($-NH_2$) compounds.

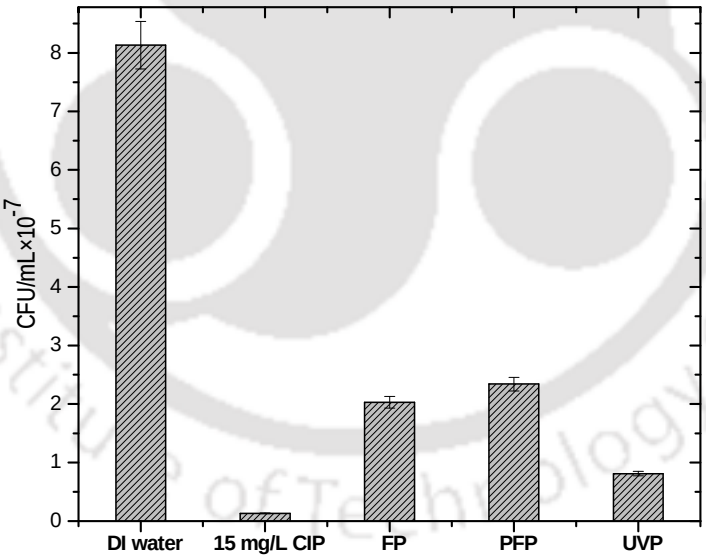

Figure 4.24. Growth of *E. coli* after 24 h of exposure. Experimental conditions: $[CIP]_0$ =15 mg/L, Fe^{2+} = 1.25 mM (in FP and PFP only), H_2O_2 = 10 mM, pH = 3.5 and temperature = 25°C. Photo-reaction with an UV lamp of 12 W/m^2 (9 W). The oxidation time is 45 min.

4.5 Major Findings

Maximum CIP removal of 75.4, 78.4 and 52.7% were found at the optimal condition in FP, PFP and UVP, respectively. The corresponding TOC reduction was 37.9, 45.1 and 27.3%. Only 3, 4 and 6% CIP, COD and TOC reduction took place due to sludge formation in FP. Sludge didn't form in PFP. Residual hydroxyl radical ($HO^{\bullet}$) concentrations of 11.67, 11.74 and 11.30 μM were determined using DMSO probe after 30 min of FP, PFP and UVP. MONC increased to 1.68, 2.1 and 1.42 from the initial value of 1.28 in FP, PFP and UVP. Thirteen, nineteen and seven numbers of daughter ions were originated upon degradation of CIP in FP, PFP and UVP through piperazine moiety degradation. A 2^{nd} order kinetic model for the cleavage of both CIP and degradation products (DP_s) exhibited excellent agreement to the experimental data. Rate constant of CIP and DP_s oxidation varied between (2.19 to 5.07)$\times 10^3$ and (3.57 to 6.91)$\times 10^3$ 1/M.s with the highest value in PFP. The growth of *E. coli* was almost completely withdrawn in CIP solution (15 mg/L). The cell death was reduced by 23, 27 and 8% after 45 min of treatment in FP, PFP and UVP.

References

Bautista, P., Mohedano, A. F., Gilarranz, M. A., Casas, J. A. and Rodriguez, J. J., "Application of Fenton oxidation to cosmetic wastewaters treatment", *J. Hazard. Mater.,* **143(1-2),** 128-134 (2007).

Christian, T., Schneider, R. J., Farber, H. A., Skutlarek, D., Meyer, M. T. and Goldbach, H. E., "Determination of antibiotic residues in manure, soil, and surface waters", *Acta Hydroch. Hydrob.,* **31,** 36-44 (2003).

Doll, T. E. and Frimmel, F. H., "Kinetic study of photo catalytic degradation of carbamazepine, clofibric acid, iomeprol and iopromide assisted by different TiO_2 materials determination of intermediates and reaction pathways", *Water Res.,* **38,** 955-964 (2004).

Vogel, F., Harf, J., Hug, J. and Rohar, P. R. V., "The mean oxidation number of carbon (MOC) - a useful concept for describing oxidation processes", *Water. Res.,* **34(10),** 2689-2702 (2000).

Ghosh, P., Kelapure, P., Samanta, A. N. and Ray, S., "Determination of reaction rate constant for p-Chlorophenol and nitrobenzene reacting with $HO^{\cdot}$ during oxidation by Fe(II)/H_2O_2 system", *Intern. J. Chem. Tech. Res.,* **4(1),** 116-123 (2012).

Golet, E. M., Strehler, A., Alder, A. C. and Giger, W., "Determination of fluoroquinolone antibacterial agents in sewage sludge and sludge-treated soil using accelerated solvent extraction followed by solid-phase extraction", *Anal. Chem.,* **74,** 5455-5462 (2002).

Gulkaya, G. A. and Dilek, F. B., "Importance of H_2O_2/Fe^{+2} ratio in Fenton's treatment of a carpet dyeing waste water", *J. Hazard. Mater.,* **136(3),** 763-769 (2006).

Gunnarsson, L., Kristiansson, E., Rutgersson, C., Sturve, J., Fick, J., Forlin, L. and Larsso, D. G. J., "Pharmaceutical metabolites in the environment: Analytical challenges and ecological risks", *Environ. Toxicol. Chem.,* **28(12),** 2639-2647 (2009).

Hesse, M., Meier, H. and Zeeh, B., "Spectroscopic methods in organic chemistry", second ed., Thieme, New York (2008).

Kang, S. F., Liao, C. H. and Chen, M. C., "Pre-oxidation and coagulation of textile wastewater by the Fenton process", *Chemosphere,* **46,** 923-928 (2002).

Klauson, D., Babkina, J., Stepanova, K., Krichevskaya, M. and Preis, S., "Aqueous photocatalytic oxidation of amoxiline", *Catal. Today,* **151,** 39-45 (2010).

Klavarioti, M., Mantzavinos, D. and Kassinos, D., "Removal of residual pharmaceuticals from aqueous systems by advanced oxidation processes", *Environ. Int.,* **35,** 402-417 (2009).

Kolpin, D. W., Furlong, E. T., Meyer, M. T., Thurman, E. M. and Buxton, H. T., "Pharmaceuticals, hormones, and other organic wastewater contaminants in U.S. streams, 1999-2000: A national reconnaissance", *Environ. Sci. Technol.,* **36,** 1202-1211 (2002).

Kugelmann, E., Albert, R. C., Bringmann, G. and Holzgrabe, U., "Fenton's oxidation: A tool for the investigation of potential drug metabolites", *J. Pharm. Biomed. Anal.,* **54,** 1047-1058 (2011).

Larsson, D. G. J., Pedro, C. de. And Paxeus, N., "Effluent from drug manufactures contains extremely high levels of pharmaceuticals", *J. Hazard. Mater.,* **148,** 751-755 (2007).

Lester, Y., Avisar, D., Gozlan, I. and Mamane, H., "Removal of pharmaceuticals using combination of UV/H_2O_2/O_3 advanced oxidation process", *Water Sci. Technol.,* **64,** 2230-2238 (2011).

Li, X., Zhou, Q., Wei, S., Ren, W. and Sun, X., "Adsorption and desorption of carbendazim and cadmium in typical soils in northeastern China as affected by temperature", *Geoderma,* **160,** 347-354 (2011).

Liang, B., Cheng, H. Y., Kong, D. Y., Gao, S. H., Sun, F., Cui, D., Kong, F. Y., Zhou, A. J., Liu, W. Z., Ren, N. Q., Wu, W. M., Wang, A. J. and Lee, D. J. "Accelerated reduction of chlorinated nitroaromatic antibiotic chloramphenicol by biocathod", *Environ. Sci. Technol.*, **47**, 5353-5361 (2013).

Lindsey, E. M. and Tarr, A. M., "Quantitation of hydroxyl radical during Fenton oxidation following a single addition of iron and peroxide", *Chemosphere,* **41,** 409-417 (2000).

Maezono, T., Tokumura, M., Sekine, M. and Kawase, Y., "Hydroxyl radical concentration profile in photo-Fenton oxidation process: Generation and consumption of hydroxyl radicals during the discoloration of azo-dye Orange II", *Chemosphere,* **82,** 1422-1430 (2011).

Mantzavinos, D., Livingstong, A. G. and Hellenbrand, R., "Wet air oxidation of polyethylene glycol; mechanisms, intermediates and implications for integrated chemical-biological waste water treatment", *Chem. Eng. Sci.,* **51(18),** 4219-4235 (1996).

Martins, R. C., Rossi, A. F. and Quinta-Ferreira, R. M., "Fenton's oxidation process for phenolic wastewater remediation and biodegradability enhancement. *J. Hazard. Mater.,* **180,** 716-712 (2010).

Qiang, J., Chang, C. H. and Huang, C. P., "Electrochemical regeneration of Fe^{2+} in Fenton oxidation processes", *Water Res.,* **37,** 1308-1319 (2003).

Paul, T., Dodd, M.C. and Strathmann, T. J., "Photolytic and photocatalytic decomposition of aqueous ciprofloxacin: transformation products and residual antibacterial activity", *Water Res.,* **44,** 3121-3132 (2010).

Saadatjou, M., Taghdiri, R. and Farrokhi, I., "Municipal solid waste landfill leachate treatment by fenton, photo-Fenton and Fenton-like processes: Effect of some variables", *J. Environ. Health Sci. Eng.,* **7(4),** 345-352 (2010).

Schwabe, U. and Paffrath, D., "Arzneiverordnungs-report 2011", Springer-Verlag, Berlin, Heidelberg, New York (2011).

Shrivastaval, K. S., Rathore1, N. S. and Solanki1, A. K., "Pharmaceutical science and technology today: evolving to reflect the modern industrial life-science environment", *J. Pharm. Sci. Tech.,* **2(3)** 163-170 (2010).

Stepfan, M. I. and Williamson, C. T., "Advanced Oxidation Processes for Water and Wastewater Treatment, second ed., IWA Publishing, London (2004).

Stumm, W. and Morgan, J. J., "Aquatic chemistry, second ed., John Wiley, New York (1981).

Tekin, H., Bilkay, O., Selale, S. and Tolga, H., "Use of Fenton oxidation to improve the biodegradability of a pharmaceutical wastewater", *J. Hazard. Mater.,* **136,** 258-265 (2006).

Ternes, A. T., Stuber, J., Herrmann, N., McDowell, D., Ried, A., Kampmann, M. and Teiser, B., "Ozonation: a tool for removal of pharmaceuticals, contrast media and musk fragrances from wastewater", *Water Res.,* **37,** 1976-1982 (2003).

Vogel, F., Harf, J., Hug, A. and Von Rohr, P. R., "The mean oxidation number of carbon (MOC)-A useful concept for describing oxidation processes", *Water Res.,* **34,** 2689-2702 (2000).

Zhang, H. and Huang, C.H., "Oxidative transformation of fluoroquinolone antibacterial agents and structurally related amines by manganese oxide", *Environ. Sci. Technol.,* **39,** 4474-4483 (2005).

CHAPTER 5

Dipyrone Degradation: Mineralization, Reaction Pathways, Biodegradability and Toxicity Assay

In this chapter, the hydrolytic and decomposition behaviour of Dipyrone (DIPY) were investigated in aqueous solution using FP, PFP, UVP and UVPC. It also includes the studies on the antimicrobial activity test.

5.1 Introduction

Dipyrone (DIPY) is one of the most popular analgesic and antipyretic drugs. It is also known as Metamizole and Novalgin. DIPY is rapidly hydrolyzed into its main metabolite, 4-methylaminoantipyrine (4-MAA). 4-MAA is absorbed and bio-transformed by enzymatic reactions (Oliveira et al., 2006). The metabolites of DIPY can be subdivided into two groups; (i) decarboxylated metabolites and, (ii) metabolites with a degraded pyrazolinone moiety. The metabolic route is shown in Figure 5.1. 4-MAA is metabolized to 4-aminoantipyrine (4-AA) in human liver via demethylation and further acetylated to acetylaminoantipyrine (4-AAA) (Figure 5.1). 4- formylaminoantipyrine (4-FAA) is generated by an uncharacterized oxidation of n-methyl group of 4-MAA (Figure 5.1).

The use of DIPY has been banned in USA and UK, because of its association with the diseases like agranulocytosis, a type of acute and severe and leukopenia (Banchero and Giachetto, 2002). DIPY is still one of the most consumed drugs in the countries like India, Germany, Italy and Spain. About one-third of its remains unchanged and be found in urinary

excretion. More than 500 tons of DIPY and their metabolites were consumed in Germany in 1997 (Sanderson et al., 2003). A recent paper shows the predicted and measured loads of DIPY metabolites in different sewage effluents and sewage-prone surface water in Berlin, Germany (Feldmann et al., 2007). The average annual estimated discharges were 10.5 and 3.2 kg of 4-AA/4-AAA and 4-FAA, respectively, for the military hospital. It was 333 and 133 kg for sewage treatment plant (STP). There was only 26% decrease in 4-AA/4-AAA loads in STP and 4-FAA load was almost invariant. DIPY was detected even upto 4.9 µg/L in a wastewater treatment station in the southern Spain. The metabolites of DIPY, namely, 4-AA and 4-FAA, had been found in public water treatment plants in Germany and Czech Republic in concentrations ranging from 20 to 939 ng/L (Wiegel et al., 2004). Although untreated wastewater containing DIPY can permeate aquatic environments, however the information concerning the toxicity of the drug towards aquatic organisms is somewhat rare. A 6.25% solution of DIPY could exhibit acute toxicity towards a range of test organisms, causing significant nuclear structural damage and resulting almost 100% mortality within 24 h of observation (Arkhipchuk et al., 2005).

The metabolites of DIPY enter into the environment from several anthropogenic sources such as pharmaceutical industry and infirmary effluent, water disinfection and waste incineration facilities. It is not completely eliminated by biological treatment and thus their presence has been referenced in STP effluents and surface water at high concentrations. The evaluation of the photochemical behaviour of 4-AAA, 4-FAA and 4-MAA under simulated solar irradiation revealed that 4-MAA was the most degradable DIPY metabolite with half-life times ($t_{1/2}$) ranging from 0.12 to 0.58 h, depending on the irradiation conditions and salt composition of waters (Gyenge-Szabo et al., 2014).

In this study, four AOPs namely, FP, PFP, UVP and UVPC, are compared based on their performance for the: (i) oxidation and mineralization of 4-MAA (primary metabolite and hydrolysed form of DIPY), (ii) formation of degradation products and, (iii) variation of biodegradability (BOD_5/COD) and antimicrobial activity. A unified mechanism of 4-MAA oxidation is presented. It would help to elucidate the effect of unreacted drug and degradation products on the variation of biodegradability and antimicrobial activity in different oxidation processes.

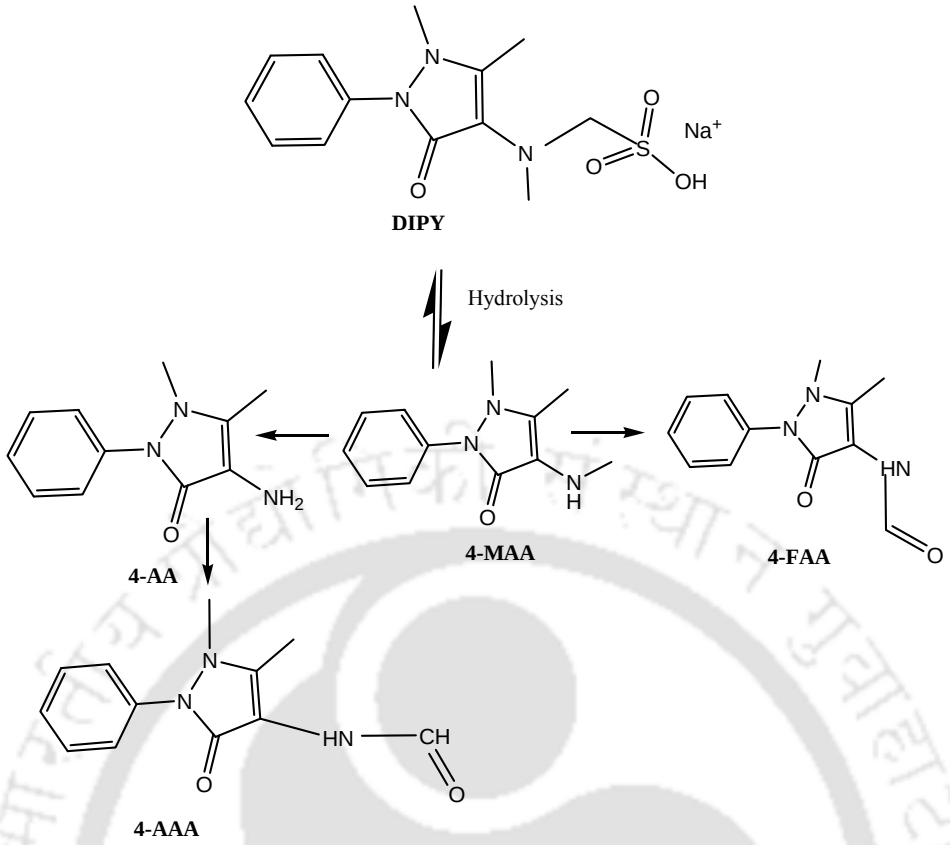

Figure 5.1. Chemical structure of dipyrone drug (sodium [(2, 3-dihydro- 1, 5-dimethyl- 3-oxo- 2-phenyl- 1- pyrazol- 4-yl) methylamino] methanesulfonate) and its metabolic pathways.

5.2 Results and Discussion

5.2.1 Optimal Fe^{2+} concentration for 4-MAA degradation in FP

The experiment first was performed in FP to maximize 4-MAA degradation. The same experimental conditions were used in PFP and UVP with UV light. Fe^{2+} was not added in UVP. 4-MAA cleavage reached to 94.1% with 2.25 mM Fe^{2+} in 45 min (Figure 5.2). With further increase in Fe^{2+} concentration, 4-MAA removal fell down. Generally, the rate of $HO^{\bullet}$ formation increases with rise of Fe^{2+} due to increase in the catalytic activity. However, direct conversion of Fe^{2+} to Fe^{3+} is predominant at higher concentration (Saadatjou et al., 2010; Kugelmann et al., 2011).

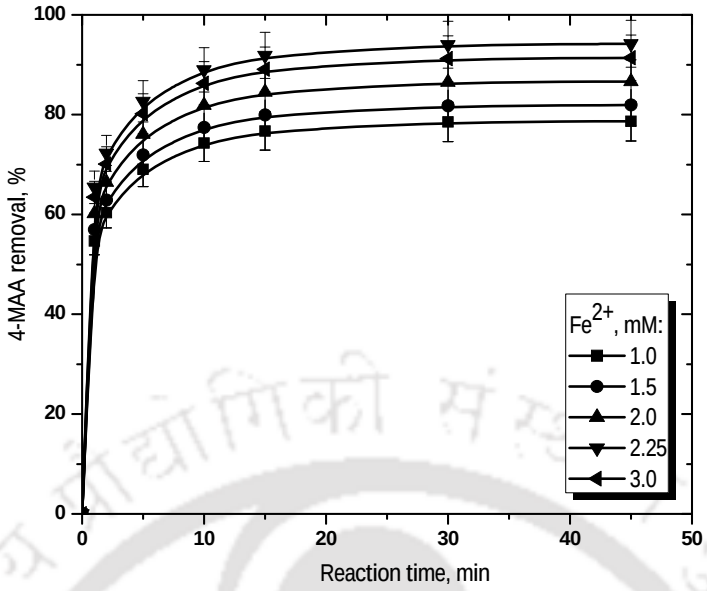

Figure 5.2. Effect of Fe^{2+} concentration on removal of 4-MAA in FP. Experimental conditions: $[4\text{-MAA}]_0$ = 50 mg/L, H_2O_2 = 20 mM, pH = 3.5 and temperature 25°C.

5.2.2 Effect of H_2O_2 concentration in FP

The optimal H_2O_2 doses were found out by varying it in the range from 5.0 to 25 mM. 4-MAA removal increased with increase in H_2O_2 doses with the maximum of about 94% using 22.5 mM (Figure 5.3). However, 4-MAA degradation rates were somewhat decreased at> 22.5 mM. A similar explanation as outlined before is also valid here (Section 4.4.1, Chapter #4).

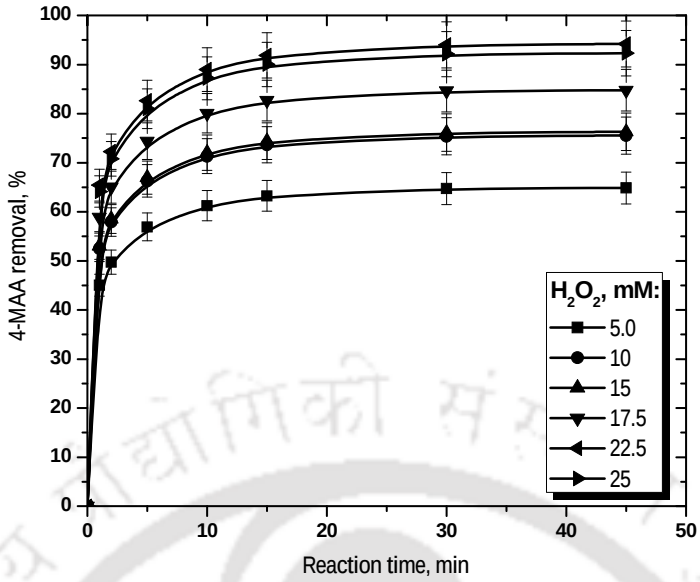

Figure 5.3. Effect of H_2O_2 concentration on removal of 4-MAA in FP. Experimental conditions: $[4\text{-MAA}]_0$ = 50 mg/L, Fe^{2+} = 2.25 mM, pH = 3.5 and temperature 25°C.

5.2.3 pH dependent 4-MAA cleavage

The efficiency for removal of 4-MAA as a function of pH in the range of 2-4 is shown in Figure 5.4. The test was done using the dose of Fe^{2+} and H_2O_2 of 2.25 and 22.5 mM, respectively, as from the earliest results (Figures 5.2 and 5.3). pH showed a gradual positive influence on 4-MAA degradation and a maximum 4-MAA removal of 94.1% at pH 3.5 was achieved (Figure 5.4). pH imparted a negative effect with further increase from 3.5 and removal efficiency dropped to 93.2% at pH 4. It implies that the optimal pH was 3.5 in decomposition of 4-MAA. Similar results of pH variation on CIP removal was also observed as in Section 4.4.1 (Chapter #4).

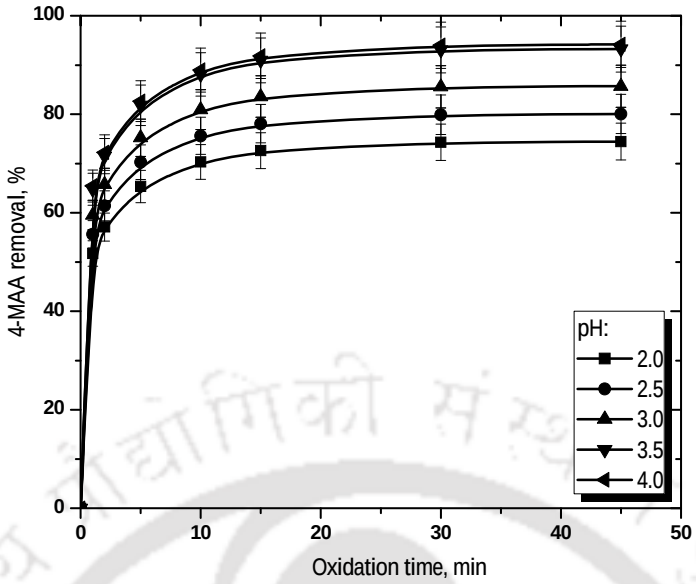

Figure 5.4. Effect of pH on removal of 4-MAA in FP. Experimental conditions: [4-MAA]$_0$ = 50 mg/L, Fe^{2+} = 2.25 mM, H_2O_2 = 22.5 mM and temperature 25°C.

5.2.4 Influence of TiO_2 on 4-MAA decomposition in UVPC

The concentration of TiO_2 was varied from 0.5 to 1.0 g/L at a fixed pH of 2.5. pH was selected based on the earlier studies (Sohrabi et al., 2008). The results are shown in Figure 5.5. There was a sharp increase in 4-MAA degradation when TiO_2 dose of 1 g/L used in comparison to 0.5 g/L. Maximum removal of 88.6% was noted with 1 g/L TiO_2 in 45 min. Higher TiO_2 dose (>1 g/L) supressed the removal efficiency. It is due to the combined effect of the working conditions of the reactor, particle morphological behaviour and UV exposure (Sohrabi et al., 2008; Bahnemann et al., 2007; Klavarioti et al., 2006). Higher TiO_2 concentration enhances the formation efficiency of surface $HO^{\bullet}$ radicals (Bahnemann et al., 2007; Klavarioti et al., 2006). However, too higher concentration could promote particles aggregate and it hinders the penetration of light in the reactor inside (Sohrabi and Ghavami, 2008).

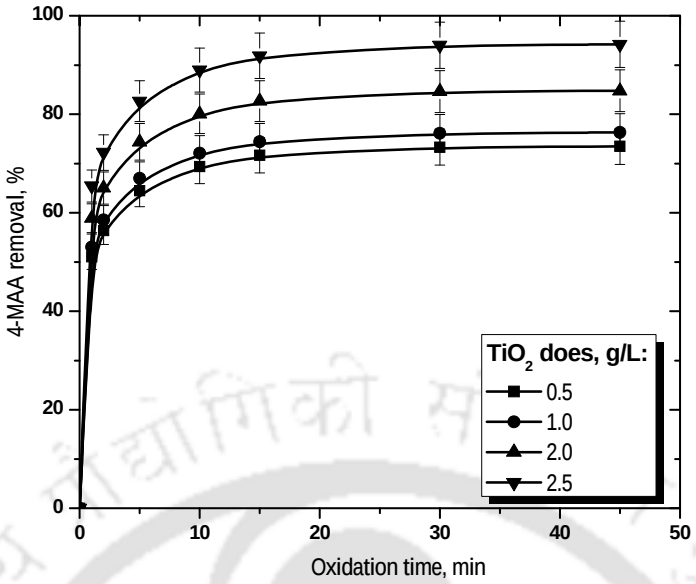

Figure 5.5. Effect of TiO_2 concentration on removal of 4-MAA in UVPC. Experimental conditions: $[4\text{-MAA}]_0$ = 50 mg/L, pH = 2.5 and temperature 25°C. Photo-reaction with an lamp of 12 W/m^2 (9 W).

5.2.5 4-MAA removal versus mineralization

Removal efficiency of 4-MAA increased with rise of one of these parameters i.e. pH, Fe^{2+} and H_2O_2 doses (Figures 5.2 to 5.4). It reached a maximum value and then fell down. The best performance of FP, PFP, UVP and UVPC in terms of 4-MAA and TOC removal are illustrated in Figures 5.6 and 5.7. Temperature, solution volume, reaction time and extent of mixing were same for all the processes in order to compare their efficiencies for degradation of 4-MAA. The order of percentage removal of 4-MAA at any time of the reactor was found to be: PFP>FP>>UVP>UVPC. Percentage removal of 4-MAA rose to 96.4, 94.1, 74.4 and 71.1%, respectively, in 45 min.

4-MAA removal showed two distinct rate periods (Figure 5.6), i.e. an initial faster drug removal followed by a virtually constant rate even though there was notable amount of unreacted 4-MAA present in solution in case of UVP and UVPC. The transition for these two processes lasted for a long period (2.5 to 15 min) compared to Fenton reaction with and without UV light (2.5 to 10 min). It implies that $HO^{\bullet}$ generation is predominant at < 2.5 min irrespective to the oxidation process. The rate of formation of $HO^{\bullet}$ falls because of H^+ scavenging (Eq. 4.10) and H_2O_2 auto decomposition (Eq. 4.11) with progress of reaction

(>2.5 min). In case of FP and PFP, 4-MAA removal of 73.5 and 83.2 % in 2.5 min of oxidation rose to 94.1 and 96.4 %, respectively, in 45 min.

Application of UV light during Fenton reaction generates excess $HO^{\bullet}$ radicals and ferric ions are reduced into ferrous leading to further generation of $HO^{\bullet}$ (Eqs. 1.1 and 1.5). Increase in gross $HO^{\bullet}$ concentration gave a bit higher degradation of 4-MAA in PFP. It is evident from Figure 5.6 that UVP and UVPC are less effective compared to other two processes. UVP showed higher removal efficiency than UVPC. The first process exhibits a rate constant of nearly 25 times higher than UVPC (Jayson et al., 1972). Drug removal achieved was 56.4 and 44.5 % within first 2.5 min in UVP and UVPC, respectively. It increased to 74.4 and 71.1% in 45 min. $HO^{\bullet}$ radicals are generated by photolysis of the peroxide bond on the surface of TiO_2 (Eqs. 5.1 and 5.2) and adsorbed 4-MAA on the surface is oxidized. Hence, the reaction occurs at diffusion-controled regime in case of UVPC (Petrovic et al., 2011).

$$TiO_2\left(h^+_{vb}\right) + H_2O_{ad} = TiO_2 + HO^{\bullet}_{ad} + H^+ \quad (5.1)$$

$$TiO_2\left(h^+_{vb}\right) + OH^-_{ad} = TiO_2 + HO^{\bullet}_{ad} \quad (5.2)$$

The trend of mineralization was similar to that of 4-MAA removal. The highest TOC removal took place in PFP. It was very close in case of FP and UVP (Figure 5.7). The initial rapid mineralization was up to 2.5 and 5 min for FP and PFP. However, it was not such distinct for other two processes. TOC removal of 28.4 and 42.78% was obtained in 2.5 and 5 min with FP against 53.6 and 56.0% in PFP. The first stage of TOC removal was very fast due to mineralization of three-methyl moieties. The slow second stage is related to the opening and mineralization of pyrazolinone ring (Gomez et al., 2007). Usually, large molecular weight intermediates were either mineralized or broken to lower molecular weight products like oxalic and acetic acids (Leonidas et al., 2007). Kavitha et al. (2004) indicated that carboxylic acids are eliminated in PFP very quickly during the first stage of oxidation. Bauer et al. (1999) reported continuous formation and as well as degradation of light weight carboxylic acids during UVPC. There was a difference of about 20% in drug removal between FP and UVP. However TOC reduction was almost same. It is necessary to mention

that H_2O_2 (22.5 mM) alone gave around 12.8% 4-MAA decomposition. However, only UV irradiation didn't show notable effect on 4-MAA removal.

There is a significant role of iron-chelation on drug mineralization. Fe(III)-chelate complexes are more stable in FP because of less possibility of further degradation (Knight et al., 1975). PFP would have higher ability to degrade such complexes under UV luminesce. Knight et al. (1975) suggested that Fe(III)-humate complexes are easily reduced to Fe(II) by H_2O_2 in PFP. In addition, humic acids themselves are photo-degraded through formation Fe(III) complexes (Fukushima et al., 2001). Klamerth et al. (2013) pointed out that PFP could breakdown metal complexes of molecular acids and iron through separation between heavy metal and its complexing agent. TOC removed in PFP mostly corresponds to oxidation of hydrophobic components which predominate in natural organic compounds present in raw water (Buchanan et al., 2005). It can be explained by greater aromaticity of hydrophobic fraction giving higher reactivity towards oxidizing agents. The refractory hydrophilic fraction is consisting of as short-chain aliphatic amines, alcohols, aldehydes, esters, ketones, aliphatic amides ($<C_5$), polyfunctional alcohols, carbohydrates, cyclic amides and polysaccharides (Buchanan et al., 2005). In the present work, acidic digestion of sludge formed in FP showed 2.74% 4-MAA appearance on sludge phase.

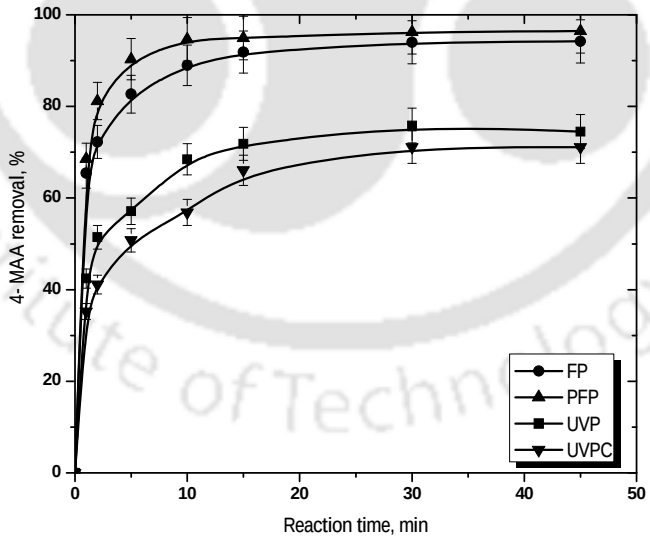

Figure 5.6. Removal of 4-MAA in different AOPs with reaction time. Experimental condition: $[4\text{-MAA}]_0$ = 50 mg/L, pH = 3.5, Fe^{2+} = 2.25 mM (in FP and PFP), H_2O_2 = 22.5 mM (in FP, PFP and UVP), TiO_2 = 1.0 g/L (in UVPC) and temperature = 25°C. Photo-reaction with an UV lamp of 12 W/m^2 (9 W).

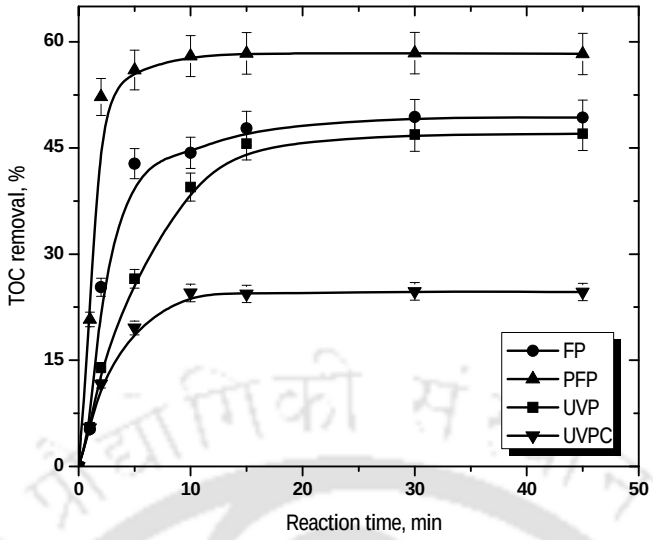

Figure 5.7. Removal of TOC in different AOPs with reaction time. Experimental condition: $[4\text{-MAA}]_0$ = 50 mg/L, pH = 3.5, Fe^{2+} = 2.25 mM (in FP and PFP), H_2O_2 = 22.5 mM (in FP, PFP and UVP), TiO_2 = 1.0 g/L (in UVPC) and temperature =25°C. Photo-reaction with an UV lamp of 12 W/m^2 (9 W).

5.2.6 Mechanisms of 4-MAA degradation

Fenton, TiO_2-photo-catalysis and their allied processes are characterized by the formation of a common oxidizing agent i.e. $HO^{\bullet}$ radical mostly responsible for the decomposition of organic compounds. However, the extent of the degradation of parent compounds and the formation of the intermediates are largely depends on process parameters such as pH, dose of Fe^{2+}/H_2O_2 and TiO_2 etc. A unified mechanism is developed to elucidate the possible routes of 4-MAA degradation by $HO^{\bullet}$ generated both in homogeneous and heterogeneous catalytic processes. 4-MAA (m/z = 218.11) is formed quickly due to presence of more water soluble sulphonate group (-SO_3H). 4-MAA (D_1) contains a pyrazolinone structure. It was first separated on a reverse phase HPLC column using an isocratic mobile phase. Then the mass to charge (m/z) ratio recorded in MS spectra was verified using 4-isopropylantipyrine (m/z 231.3) as an internal standard (Ojha et al., 2009). The nitrogen atom instead of carbon in pyrazolinone moiety is the most preferred site of $HO^{\bullet}$ attack releasing aniline (Pignatello et al., 2006). It was formed via hydroxylation of aromatic ring by addition of $HO^{\bullet}$ as in Figure

5.12. N-atom is mainly released in the form of N_2 and ammonia from –NH-NH- moiety at around 70 and 7% of the stoichiometric amount (Calza et al., 2005).

The mass spectra acquired in different oxidation processes are shown in Figures 5.8 to 5.11. Total twenty seven (D_1-D_{27}) intermediate products were detected in four oxidation processes on the basis of m/z. The error in mass was calculated from the difference between the exact and proposed structural mass of protonated ions. Fairly low errors values were obtained for the most of the proposed compounds (Table 5.1). There are two most possible pathways for the cleavage of 4-MAA as shown in Figure 5.12. Path #1 shows the route of formation of D_2 to D_7 corresponding to proposed m/z of 279.11, 250.07, 136.04, 176.07, 198.11 and 199.11, respectively. Path #2 presents the formation route of D_8 to D_{10} with m/z of 205.11, 189.06 and 225.11, respectively. D_2 was formed by hydroxylation of double bond in pyrazolinone ring of D_1 due to nucleophilic character of π-electron. D_2 formed a chelate compound (m/z= 346.07) with Fe^{3+} due to availability of lone electron pair on N-atom (Figure 5.12).

The opening of pyrazolinone ring was confirmed by the detection of 1-acetyl-1-methyl-2-aminomethyl-oxamoyl-2-phenylhydrazide (D_3). This compound was yielded by addition of two $HO^{\bullet}$ radicals to double bond of pyrazolinone ring of D_1 followed by C-C bond breaking. D_3 is found as a derivative in the biotransformation of DIPY in humans (Wessel et al., 2006). The formation of D_4 was via an unstable intermediate with m/z 220.03 because of presence of a di-keto group more susceptible towards oxidation in acidic medium (Ojha et al., 2009). The cleavage of N–N bond in the hydrazine group led to formation of N-phenylacetamide (D_4) with m/z = 136.04 and as well as an acetamide (Figure 5.12). D_5 was originated in PFP (Figure 5.9) with low error (0.031 g/mol) by hydroxylation of carbonyl group followed by C-N bond breaking along with formation of acetic acid. Attack of $HO^{\bullet}$ radical to carbonyl group due to its electrophilic nature (i.e. electron deficient centre) caused aniline formation with complete elimination of pyrazolinone ring. D_6 was detected in FP, PFP and UVP with very low error (-0.86-0.46 g/mol). It was originated by addition reaction between D_4 and aniline on dehydration. Successive hydroxylation of aniline at –ortho and –para positions originated a compound with m/z of 130.27 (Figure 5.12). $–NH_2$ group activates benzene nucleus for the electrophilic substitution reaction due to +R effect (mesmeric). D_7 was identified in PFP and UVP (Figures 5.10 and 5.11). The lone electron pair on N-atom of D_6 compound acts as a Lewis base that appeal protons. Therefore, D_6 and D_7 are in equilibrium as shown in Figure 5.12.

4-aminoantipyrine (D_8, 4-AA) was formed with methanol in FP on hydrolysis of D_1. D_9 (m/z = 189.06) was detected in MS spectra of FP. The loss of NH_3 from pyrazolinone ring of the previous compound yielded D_9 (error -0.06 mg/L) because of a shifting of lone pair electron on N_1. D_{10} was found both in UVP and UVPC (Figures 5.12 and 5.13). A similar explanation outlined for the formation of D_2 is also valid here. D_2 was traced in mass spectra of UVP and UVPC (Figures 5.10 and 5.11). D_{12}, D_{14}-D_{16} and D_{19} formed in PFP were originated from D_2 (Figure 5.9). Whereas, only D_{16} was formed in FP (Figure 5.8). It indicates formation of iron-chelate complex which is unstable under UV luminance (Zepp et al., 1992). Carboxylic (Figure 5.12) and dicarboxylic acids (Figure 5.14) are also known to form stable iron complexes which inhibit the reaction with peroxide (Leonidas et al., 2007). Carboxylic acids mainly exist as acetate and oxalate (Kavitha et al., 2004). Oxalic acid could form a Fe(III)-oxalate complex as shown in Figure 5.12. Such complex got stability through an extensive conjugation with Fe(III) due to availability of vacant 3d-orbital. Its stability could lose because of UV light absorption (Zhou et al., 2011). The ability of light absorption depends on electron distribution of a molecule. Generally, the light absorption capacity of sigma (σ) bonds (C−H, C−C, C−O, and O-H) are very less above 200 nm. Whereas pi (π) bonds (carboxylic, carbonyl group) and especially conjugated pi systems boost up the ability of a compound to absorb UV light at 254 nm by lowering energy barrier between ground and excited states (Hesse et al., 2008). Double bond equivalent (DBE) was calculated by the summations of total number of pi bonds and the residual ring(s). It is also referred as degree of unsaturation (Finar et al., 2001). PFP generated more number of compounds having higher DBE (Table 5.1). Indeed, it can be seen from Table 5.1 that compounds formed in UVPC were consisting of lower DBE. The highest DBE of 9 was calculated for both D_6 and D_7.

There are also possibilities for cleavage of D_2 following path #3 and path #4 as shown in Figure 5.13. Path #3 shows the route of formation of D_{11} and D_{12} corresponding to m/z of 186.11 and 171.21, respectively. D_{11} and D_{12} both were formed from the same intermediate (m/z = 164.11) via oxidation of D_4 originated by hydrolysis of D_3 compound (Path #1) as presented before. This compound seems to be more stable in FP. Further attack of $HO^{\bullet}$ at α-carbon of D_4 caused formation of D_{11} in case of PFP. Carbonyl group is very susceptible to be oxidized at lower pH (<3.5) (Fabre et al., 1982). The valency of carbon atom in D_{12} is saturated by two additional hydroxyl group (-OH) due to availability of partially vacant p-orbital in N_1-atom. Path #4 represents the formation route of D_{13} to D_{19} with m/z of 187.19,

152.19, 152.09, 166.09, 155.06, 183.11 and 212.02, respectively. The structures of these compounds are proposed with low errors (2.11 to -0.22 g/mol) (Figure 5.13). D_{13} was formed by hydroxylation of α-carbon of an intermediate with respect to N_2 atom. Both D_{14} and D_{15} compounds have almost the same mass (m/z = 152.19 and 152.09). Structures of these compounds are different and were appeared from the same intermediate with m/z of 194.08. The first compound was originated in PFP by decarboxylation ($-CO_2$). The second was the hydroxylation product with formation of NH_3 and CO_2. Identification of D_{14} (Figure 5.9) evidences the opening of pyrazolinone ring by an alternative route (Figure 5.13). The proposed structure suggests oxidative cleavage of N–N bond to a multiple hydroxylated derivative. $HO^{\bullet}$ radical can easily attack at N_1 position of the pyrazolinone ring in presence of a partially vacant p-orbital of N-atom (Sykes et al., 2005). D_{16} and D_{17} were originated by hydroxylation. Oxidation of α-carbon in D_{17} with loss of hydroxyl amine evidences formation of D_{16}. The α-carbon in D_{17} behaves like a nucleophilic center because of lone pair electron on N_1 position shifted towards the terminal carbon atom through conjugation. D_{18} was formed from D_{17} (Figure 5.13). A possible explanation similar to D_{15} is applicable. Primary alcohol group of pyrazolinone moiety was oxidized to D_{19} found in PFP. Waki et al. (2000) suggested that primary alcohol in acidic solution gives acid products on oxidation. D_{20} was detected in UVPC with a low error (-0.42 g/mol). Direct hydroxylation of D_5 at N_1 position with the loss methyl amine justifies its formation. D_{20} was broken in three different routes (path# 5 to path# 7) (Figure 5.14). Path# 5 represents formation of D_{21} molecule with loss of proton from D_{21}. It is stable as a salt form because of slightly acidic in nature of -OH group.

D_{22} compound was seen both in PFP and UVP yielded from N-hydroxyl aniline derivative with formation of oxalic acid (path# 6). It was ultimately transformed to CO_2 giving effective TOC reduction. The aniline derivative by its p-position attack with acetanilide, formed D_{22} compound. Electrons are more localized at 4-position with respect to N-substituted amine group due to shifting of lone pair electron and $HO^{\bullet}$ attack at more electrophilic centre of carbonyl group. D_{23} and D_{24} were identified in PFP. N_1 atom has a vacant p-orbital to accept electron of $HO^{\bullet}$ radicals (Figure 5.14) (path# 7). This compound exists as a salt of sodium ion in alkaline medium (pH >8). It might have formed during pH adjustment at >12 for the termination of oxidation reaction. Further oxidation of D_{23} compound yielded the corresponding quinone-imine intermediate (D_{24}) which is generally unstable but it appeared in the MS spectra (Figure 5.9). Hydroxylation probably occurred at p-position due to availability of more electron density. Enol form of D_{24} compound is less

stable due to positive charge on N_1-atom. It has greater tendency to be transformed into quinone form (Leonidas et al., 2007) i.e., the formation of D_{25} compound obtained both in FP and UVP having positive characteristics of benzene nucleus.

D_{26} and D_{27} also appeared from D_{25} by its successive hydroxylation (Figure 5.14). First molecule was detected in FP and UVP. Whereas, the second one was found in UVPC. D_{27} is alicyclic in nature and was resulted by hydroxylation. This compound lost its aromaticity by substituting two -OH groups at 2 and 6 positions with respect to N, N-hydroxyl amine group.

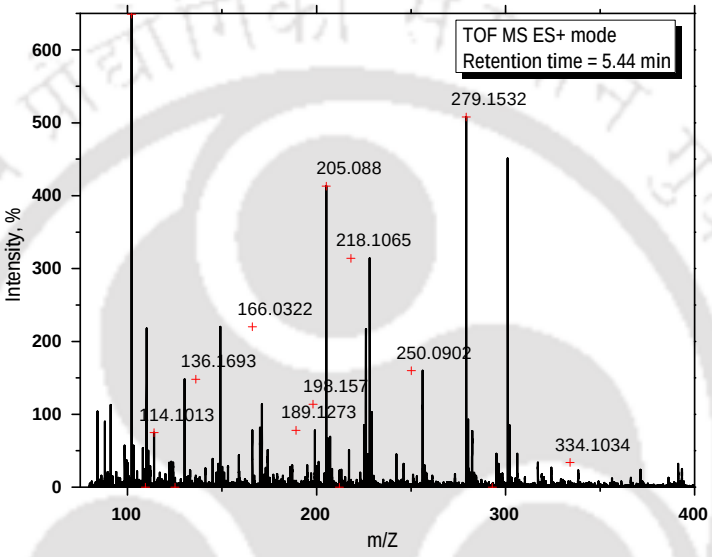

Figure 5.8. Mass spectra recorded at 10 min of FP with retention time of 5.44 min. Experimental conditions: $[4\text{-MAA}]_0$ = 50 mg/L, Fe^{2+} = 2.25 mM, H_2O_2 = 22.5 mM, pH = 3.5 and temperature = 25°C.

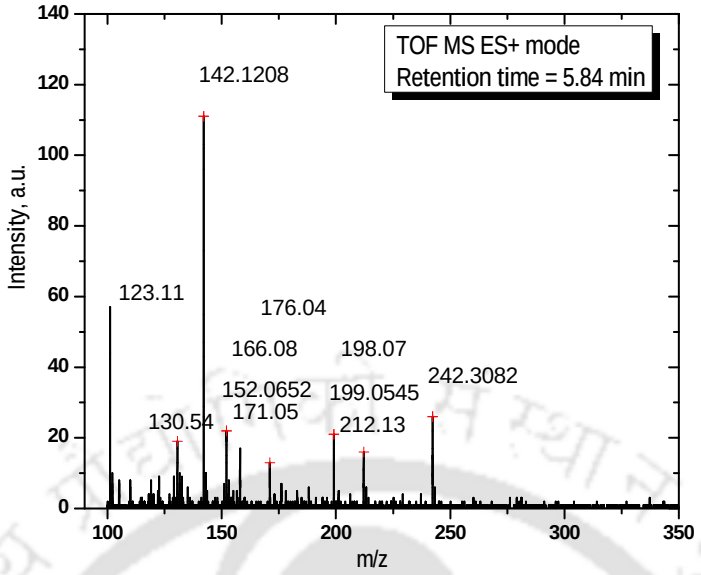

Figure 5.9. Mass spectra recorded at 10 min of PFP with retention time of 5.84 min. Experimental conditions: $[4\text{-MAA}]_0$ = 50 mg/L, Fe^{2+} = 2.25 mM, H_2O_2 = 22.5 mM, pH = 3.5 and temperature = 25°C. Photo-reaction with an UV lamp of 12 W/m^2 (9 W).

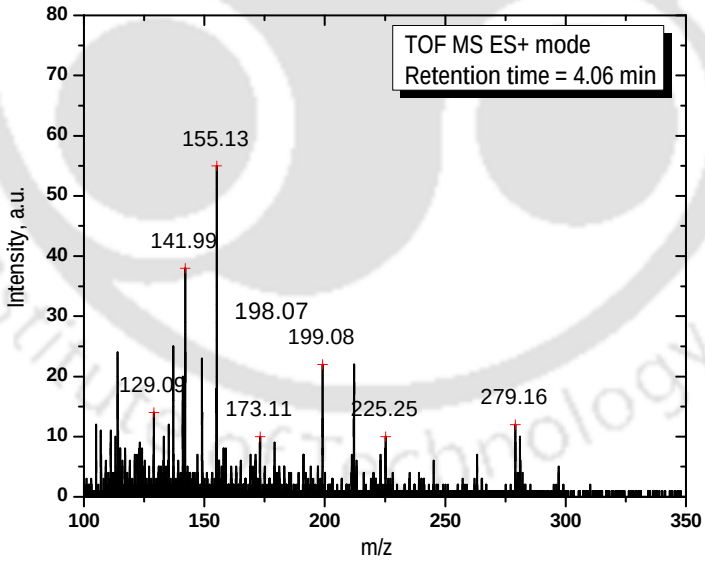

Figure 5.10. Mass spectra recorded at 10 min of UVP with retention time of 4.06 min. Experimental conditions: $[4\text{-MAA}]_0$ = 50 mg/L, H_2O_2 = 22.5 mM, pH = 3.5and temperature = 25°C. Photo-reaction with an UV lamp of 12 W/m^2 (9 W).

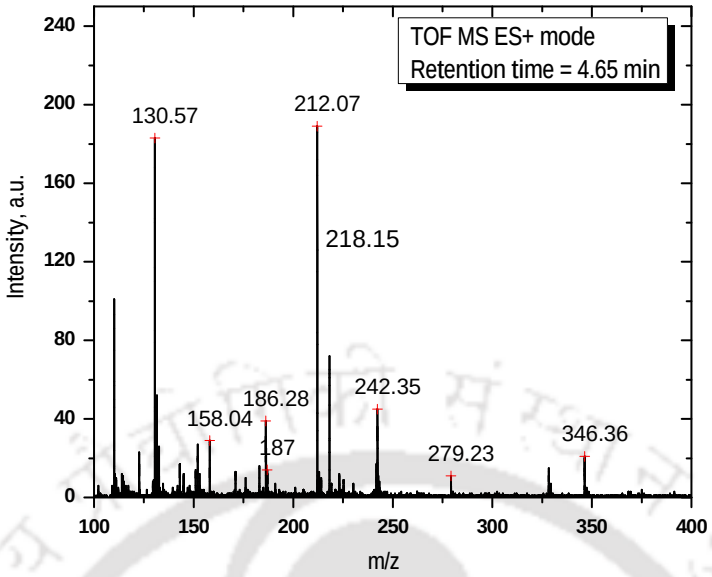

Figure 5.11. Mass spectra recorded at 10 min of UVPC with retention time of 4.65 min. Experimental conditions: $[4\text{-MAA}]_0$ = 50 mg/L, TiO_2 = 1.0 g/L, pH = 2.5 and temperature = 25°C. Photo-reaction with an UV lamp of 12 W/m^2 (9 W).

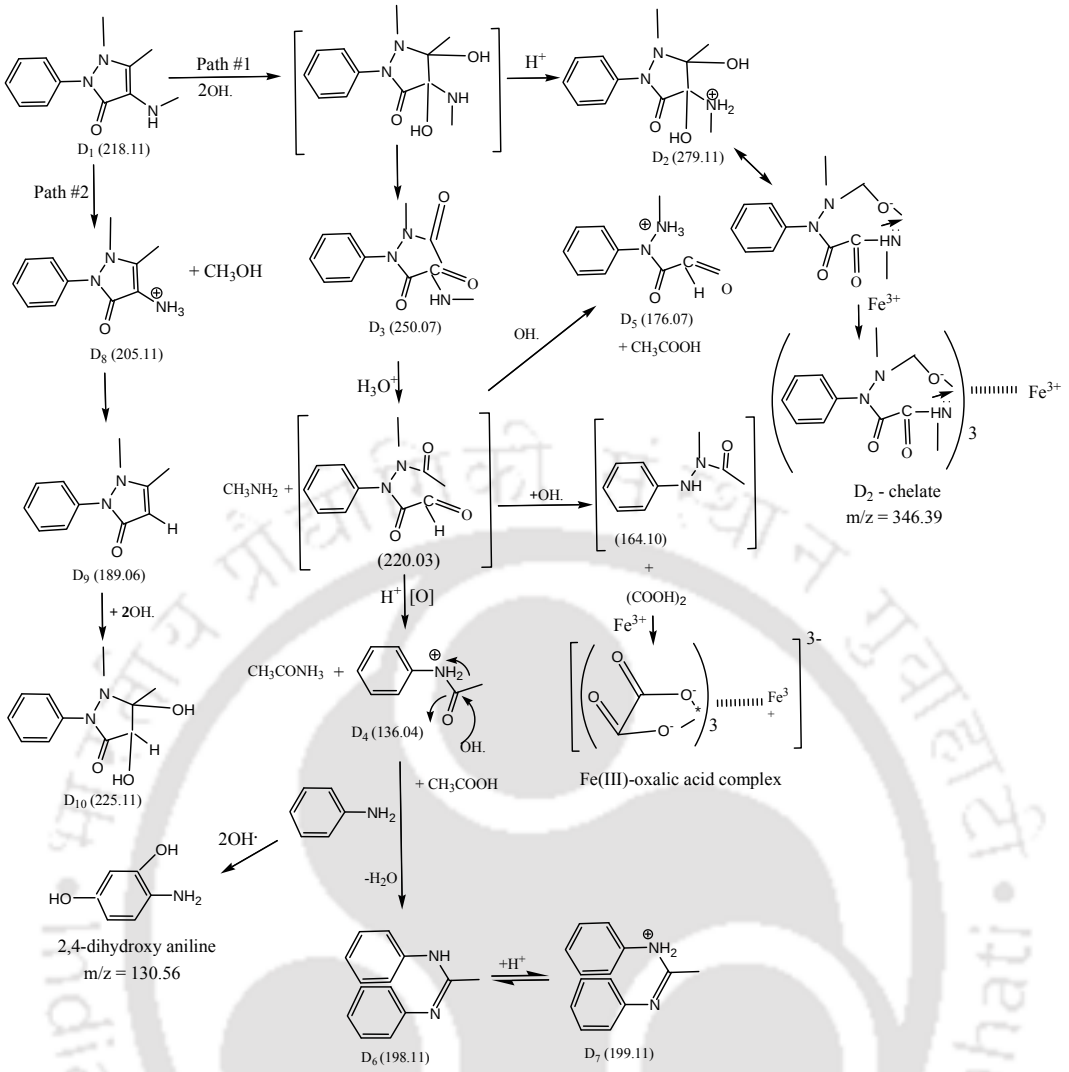

Figure 5.12. Degradation pathways of 4-MAA. The exact mass to charge ratio is in the round parenthesis.

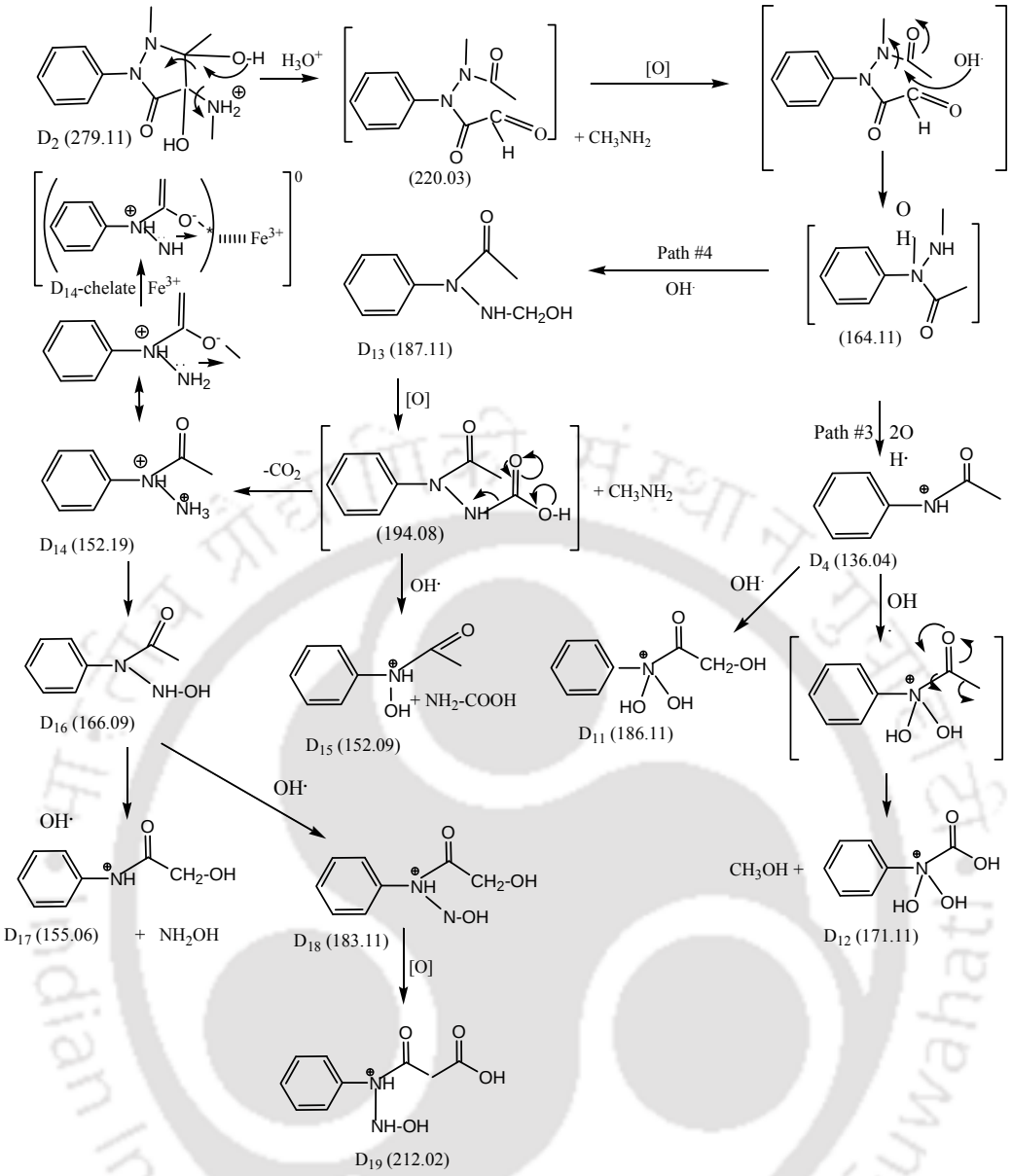

Figure 5.13. Degradation pathways of D_2 (m/z = 279.11) continued from Figure 5.12.

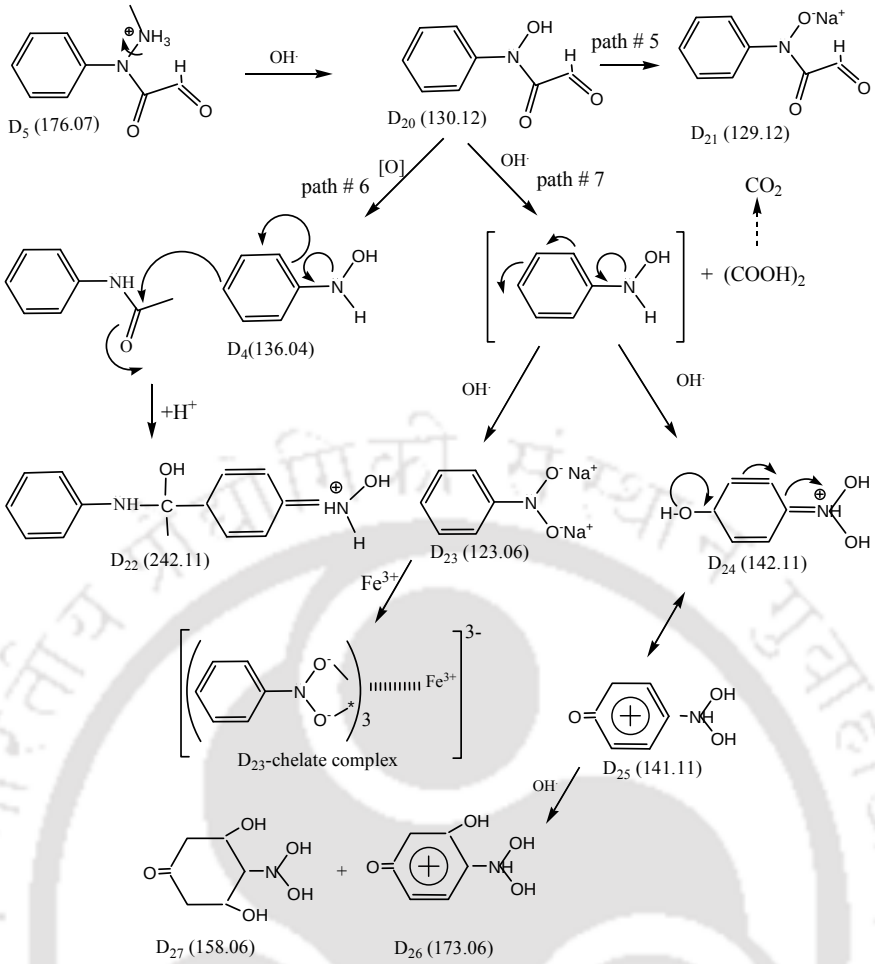

Figure 5.14. Further fragmentation of D_5 (m/z = 176.07) continued from Figure 5.12.

Table 5.1. Mass to charge ratio (m/z) based on the proposed structures and their appearance in the mass spectra during 4-MAA cleavage. The symbol '+' indicates the appearance of intermediates in oxidation processes.

Fragments	Formula	m/z	Mass error (g/mol)	Oxidation process				DBE[¥]	BOD_5/COD
				FP	PFP	UVP	UVPC		
D_1	$C_{12}H_{16}N_3O$	218.11	0.04	+			+	6	0.09 (Present work)
D_2	$C_{12}H_{19}N_3O_3$	279.11	-0.07			+	+	5	
D_3	$C_{12}H_{16}N_3O_3$	250.07	0.02	+				7	0.57[†] (Wessel et al., 2004)
D_4	$C_8H_{10}NO$	136.04	-0.12	+				5	0.53 (Marciniec et al., 1985)
D_5	$C_9H_{12}N_2O$	176.07	0.03		+			6	
D_6	$C_{14}H_{14}N_2$	198.11	-0.86-0.46	+	+	+		9	
D_7	$C_8H_{15}N_2$	199.11	-0.06		+	+		9	
D_8	$C_{11}H_{13}N_2O_2$	205.11	0.02	+				6	0.47[†] (Teng et al., 2011)
D_9	$C_{11}H_{13}N_2O$	189.06	0.32	+				6	
D_{10}	$C_{10}H_{11}N_2O$	225.11	0.35			+	+	5	
D_{11}	$C_8H_{10}NO_4$	186.11	-0.17				+	5	
D_{12}	$C_7H_{10}NO_4$	171.21	-1.49		+			5	
D_{13}	$C_8H_{12}N_2O_2$	187.19	0.81				+	5	
D_{14}	$C_8H_{10}NO_2$	152.19	0.13		+			5	0.4 (Weber et al., 1996)
D_{15}	$C_8H_{12}N_2O$	166.09	0.06		+			5	
D_{16}	$C_8H_{10}N_2O$	155.06	0.51	+	+			5	
D_{17}	$C_8H_{10}NO_2$	152.09	2.11			+		5	
D_{18}	$C_8H_{11}N_2O_3$	183.11	0.43			+		5	
D_{19}	$C_9H_{11}N_2O_4$	212.02	-0.22		+		+	6	
D_{20}	$C_8H_7NO_3$	130.12	-0.42				+	6	
D_{21}	$C_8H_{10}NO$	129.12	0.95			+		6	
D_{22}	$C_{14}H_{16}N_2O_2$	242.11	0.66		+	+		8	
D_{23}	$C_6H_5NO_2$	123.06	0.01		+			4	

D_{24}	$C_6H_7NO_3$	142.11	0.01		+			4	
D_{25}	$C_6H_6NO_3$	141.11	1.01	+		+		4	
D_{26}	$C_6H_7NO_4$	173.06	-0.06	+		+		3	
D_{27}	$C_6H_8NO_5$	158.06	0.02				+	2	

†: With respect to theoretical COD calculation
¥: Double bond equivalent

5.2.7 Biodegradability and antimicrobial activity of 4-MAA and its degradation products

The ratio of biochemical oxygen demand to chemical oxygen demand (BOD/COD) is an important indicator to study the nature of biodegradability of organic contaminants (Tekin et al., 2008). It is termed as biodegradability index. Generally, wastewater containing pharmaceutical and personal care products are considered to be reasonably biodegradable with $BOD_5/COD > 0.4$ (Tang et al., 1997). The initial BOD_5 and COD were 3.75 and 41.3 mg/L for an aqueous solution with 50 mg/L DIPY. It implies non-biodegradable nature of DIPY ($BOD_5/COD \approx 0.1$).

From Figure 5.15, it is evident that the extent of 4-MAA decomposition was around 5% higher in PFP than FP. Nevertheless, PFP resulted notably higher biodegradability (Figure 5.15). BOD_5/COD of 1.51 was achieved in PFP in comparison to 0.62 in FP. It signifies that the 1st process generated more (by gross) biodegradable intermediates. UVPC exhibited about 20% higher BOD_5/COD improvement than UVP (Figure 5.15). It was about 11% higher than the corresponding drug decomposition. Comparatively lower BOD_5/COD in UVP and UVPC than FP and PFP was largely due to unreacted 4-MAA and intermediate products. Beltran et al. (1999) reported that higher extent of conjugation due to formation of chelates of three different heavy metals i.e., Cd(II), Hg(II) and Pb(II) and (dicarboxyethoxy) ethyl]aspartic acid (BCA6), improves biodegradability. Kummerer et al. (2000) pointed out that newly formed intermediates act as chelating agents that significantly reduces their biodegradability.

It can be seen from Figures 5.12 to 5.14 that D_2, D_3, D_{14} and D_{23} could form chelate with Fe^{3+}. D_1, D_2, D_6 and D_{25} traced in FP could exhibit more biodegradability because of extended conjugation. Therefore, the net effect of chelation and its stability under UV irradiance and, formation of intermediate products and their different extent of conjugation were resulted higher biodegradability in PFP. The biodegradable nature of a number of

intermediates as in the proposed structure is found out from the earlier reports. It is summarized in Table 5.1.

Biodegradability index provides an indirect measurement of easiness or difficulty for biological treatment of organic effluent under aerobic condition using mixed micro-organism. The organic compounds serve as food for the micro-organisms. Whereas the antimicrobial activity test gives the information on the easiness or difficulty for the growth of a specific bacteria (*E. coli* most commonly used) in presence of organic compounds in comparison to the control media. The results of antimicrobial activity test of DIPY/4-MAA and degradation intermediates towards *E. coli* bacteria in LB media are shown in Figure 5.15. The exposure of *E. coli* exhibited about 56.1, 35.8, 61.7 and 79.0% cell death with respect to the control media in FP, PFP, UVP and UVPC, respectively.

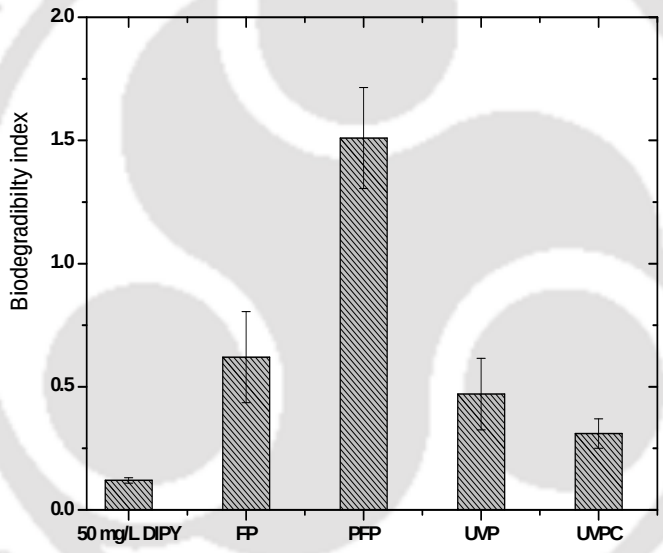

Figure 5.15. Variation of biodegradability index (BOD_5/COD). Experimental conditions: [4-MAA]$_0$ = 50 mg/L, pH = 3.5, Fe^{2+} = 2.25 mM (in FP and PFP), H_2O_2 = 22.5 mM (in FP, PFP and UVP), TiO_2 = 1.0 g/L (pH = 2.5 in UVPC) and temperature =25°C. Photo-reaction with an UV lamp of 12 W/m^2 (9 W). The reaction time is 45 min.

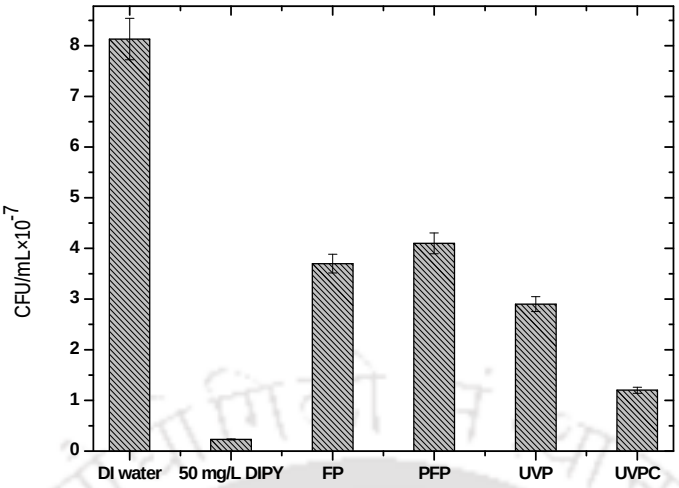

Figure 5.16. Growth of *E. coli* after 24 h of exposure. Experimental conditions: $[4\text{-MAA}]_0$ = 50 mg/L, pH = 3.5, Fe^{2+} = 2.25 mM (in FP and PFP), H_2O_2 = 22.5 mM (in FP, PFP and UVP only), TiO_2 = 1.0 g/L (pH = 2.5 in UVPC) and temperature =25°C. Photo-reaction with an UV lamp of 12 W/m^2 (9 W). The reaction time is 45 min.

5.3 Major Findings

DIPY at lower concentration (50 mg/L) was completely hydrolyzed to 4-MAA within 30 min at pH 3.5 and temperature 25°C. Maximum 4-MAA removal of 94.1, 96.4, 74.4 and 71.2% were noted against mineralization efficiency of 49.3, 58.2, 47 and 24.6% in FP, PFP, UVP and UVPC, respectively. TiO_2 photocatalysis showed more hydroxylated products resulted from attack of $HO^{\bullet}$ formed on the catalyst surface. Total twenty seven intermediate products appeared in mass spectra within the mass to charge ratio of 100 to 400 in four oxidation processes from the same parent molecule. Proposed mechanism implies that most of the intermediates formed by pyrazolinone ring degradation preceded by cleavage of methyl moieties. The trend of biodegradability was found to be as, PFP>>FP>UVP>UVPC. The growth of *E. coli* was almost completely suppressed in 4-MAA solution of 50 mg/L. About 20.3, 25.8 and 43.9 % more cell death was observed in FP, UVP and UVPC in comparison to PFP.

References

Arkhipchuk, V., Goncharuk, V. V., Chernykh, V. P., Maloshtan, L. N., Gritsenko, I. S., "Using the nucleolar biomarker and the micronucleus test on in vivo fishfin cells", J. Appl. Toxicol., **24,** 401-407 (2005).

Bahnemann, W., Muneer, M., Haque. M. M., "Titanium dioxide-mediated photocatalysed degradation of few selected organic pollutants in aqueous suspensions", *Catal. Today,* **124(3-4),** 133-148 (2007).

Banchero, P. and Giachetto, G., "Agranulocitosis inducida pormedicamentos", *Arch. Prediatr. Urug.,* **73 (2),** 76-79 (2002).

Bauer, R., Waldner, G., Fallmann, H., Hager, S., Klare, M., Krutzler, T., Malato, S. and Maletzky, P., "The photo-Fenton reaction and the TiO_2/UV process for wastewater treatment – novel developments," *Catal. Today,* **53,** 131-144 (1999).

Bautista, P., Mohedano, A. F., Gilarranz, M. A., Casas, J. A. and Rodriguez, J. J., "Application of Fenton oxidation to cosmetic wastewaters treatment", *J. Hazard. Mater.,* **143(1-2),** 128-134 (2007).

Beltran, J., Rivas, J., Alvarez, P. M., Alonso, M. A. and Acedo, B. A., "Kinetic model for advanced oxidation processes of aromatic hydrocarbons in water: Application to phenanthrene and nitrobenzene", *Ind. Eng. Chem. Res.,* **38,** 41-49 (1999).

Buchanan, W., Roddick, F., Porter, N. and Drikas, M., "Fractionation of UV and VUV pretreated natural organic matter from drinking water," *Environ. Sci. Technol.*, **39,** 4647-4654 (2005).

Calza, P., Sakkas, V. A., Medana, C., Baiocchi, C., Dimou, A., Pelizzetti, E. and Albanis, T., "Photocatalytic degradation study of diclofenac over aqueous TiO_2 suspensions", *Appl. Catal. B: Environ.,* **67,** 197–205 (2005).

Fabre, H., Eddine, N. H., Bressolle, F. and Mandrou, B., "Stability indicating assay for dipyrone - Part I", *Analyst,* **107,** 61–66 (1982).

Feldmann, D. F., Zuehlke, S. and Heberer, T., "Occurrence, fate and assessment of polar metamizole (dipyrone) residues in hospital and municipal wastewater", *Chemosphere,* **71,** 1754-1764 (2008).

Finar, I. L., "Stereochemistry and the Chemistry of Natural Products", Volume 2, 5th ed., London: Holloway, 8-9 (2001).

Fukushima, M., Tatsumi, K. and Nagao, S., "Degradation Pathways of Pentachlorophenol by Photo-Fenton Systems in the Presence of Iron(III), Humic Acid, and Hydrogen Peroxide", *Environ. Sci. Technol.,* **35,** 3683-3690 (2001).

Gyenge-Szab, Z., Szoboszlai, N., Frigyes, D., Zaray, G. and Mihucz, V. G., "Monitoring of four dipyrone metabolites in communal wastewater bysolid phase extraction liquid chromatography electrospray ionizationquadrupole time-of-flight mass spectrometry", *J. Pharmaceut. Biomed. Anal.,* **90,** 58-63 (2014).

Gomez, M. J., Martınez-Bueno, M. J. Lacorte, S., Fernandez-Alba, A. R. and Aguera, A., "Pilot survey monitoring pharmaceuticals and related compounds in a sewage treatment plant located on the Mediterranean coast," *Chemosphere*, ***66,*** 993-1002 (2007).

Hesse, M., Meier, H. and Zeeh, B., "Spectroscopic Methods in Organic Chemistry", 2nd ed., Thieme: New York, 15-17 (2008).

Jayson, G. G. and Parsons, B. J., "Oxidation of ferrous ions by perhydroxyl radicals," *Trans. Faraday Soc*., **68**, 236-242 (1972).

Kavitha, V. and Palanivelu, K., "The role of ferrous ion in Fenton and photo-Fenton processes for the degradation of phenol," *Chemosphere,* **55,** 1235-1243 (2004).

Klamerth, N. S., Malato, S., Aguera, A. and Fernand, A., "Photo-Fenton and modified photo-Fenton at neutral pH for the treatment of emerging contaminants in wastewater treatment plant effluents: A comparison", *Water Res.,* **47,** 833-840 (2013).

Klavarioti, M., Mantzavinos, D. and Kassinos, D., "Removal of residual pharmaceuticals from aqueous systems by advanced oxidation processes", *Environ. Int.,* **35,** 402-417 (2009).

Kugelmann, E., Albert, R. C., Bringmann, G. and Holzgrabe, U., "Fenton's oxidation: A tool for the investigation of potential drug metabolites", *J. Pharm. Biomed. Anal.,* **54,** 1047-1058 (2011).

Kummerer, K., Al-Ahmad, A. and Mersch-Sundermann, V., "Biodegradability of some antibiotics, elimination of the genotoxicity and affection of wastewater bacteria in a simple test", *Chemosphere*, **40,** 701–710 (2000).

Knight, R. J. and Sylva, R. N., "Spectrophotometric investigation of iron (III) hydrolysis in light and heavy water at 25°C," *J. Inorg. Nucl. Chem.*, **37,** 779-783 (1975).

Leonidas, A., Perez-Estrada, S. M. and Ana, A. R., "Degradation of dipyrone and its main intermediates by solar AOPs Identification of intermediate products and toxicity assessment," *Catal. Today*, **129,** 207-214 (2007).

Marciniec, B., "Photochemical decomposition of phenazone derivatives. Part 7: Mechanism of decomposition in aqueous solution", *Pharmazie,* **40 (3),** 180-182 (1985).

Oliveira, R., Almeida, M., Santos, L. and Madeira, L., "Experimental design of 2, 4-dichlorophenol oxidation by Fenton's reaction," *Ind. Eng. Chem. Res.*, **45,** 1266-1276 (2006).

Ojha, A. and Rathod, R., "Quantification of 4-methylaminoantipyrine, the active metabolite of dipyrone, in human plasma", *Bioanalysis*, **1,** 293-298 (2009).

Petrovic, M. M., Bianca, F. S., Aleksandra and J. R., "Oxidative transformation of fluoroquinolone antibacterial agents and structurally related amines by manganese oxide," *Chemosphere,* **85,** 1331-1339 (2011).

Pignatello, J. J., Oliveros, E. and MacKay, A., "Advanced oxidation processes for organic contaminant destruction based on the Fenton reaction and related chemistry. Crit. Rev.," *Environ. Sci.Technol.*, **36,** 1-84 (2006).

Saadatjou, M., Taghdiri, R. and Farrokhi, I., "Municipal solid waste landfill leachate treatment by fenton, photo-Fenton and Fenton-like processes: Effect of some variables", *J. Environ. Health Sci. Eng.,* **7(4),** 345-352 (2010).

Sanderson, H., Johnson, D. J., Wilson, C. J., Brain, R.A. and Solomon, K. R., "Probabilistic hazard assess ment of environmentally occurring pharmaceuticals toxicity to fish, daphnids and algae by ECOSAR screening", *Toxicol. Lett.,* **144,** 83-395 (2003).

Shrivastaval, K. S., Rathore1, N. S. and Solanki1, A. K., "Pharmaceutical science and technology today: evolving to reflect the modern industrial life-science environment", *J. Pharm. Sci. Tech.,* **2(3)** 163-170 (2010).

Sohrabi, M. R and Ghavami, M., "Taguchi experimental design used for Nano photo catalytic degradation of the pharmaceutical agent Aspirin," *J. Chem. and Pharm. Res.*, **153(3),** 1235-1239 (2008).

Sykes, P., "A guidebook to mechanism in organic chemistry", 6th ed., Fellow of Christ's College, Cambridge, **320-322** (2005).

Tang,W. Z. and Tassos, S., "Oxidation kinetics and mechanisms of trihalomethanes by Fenton's reagent", *Water Res.,* **31,** 1117-1125 (1997).

Tekin, H., Bilkay, O., Selale, S., and Tolga, H., "Use of Fenton oxidation to improve the biodegradability of a pharmaceutical wastewater", *J. Hazard. Mater.,* **136,** 258–265 (2008).

Teng, W., Liu, R., Li, C. and Zhang, H., "Effect of 4-aminoantipyrine on oxidative stress induced by glutathione depletion in single human erythrocytes using a microfluidic device together with fluorescence imaging", *J. Hazard. Mat.,* **192,** 1766-1771 (2011).

Trovo, A. G., Raquel, F. P., Nogueira, A. A. and Carla, S. A., "Photodegradation of sulfamethoxazole in various aqueous media: Persistence, toxicity and photoproducts assessment", *Chemosphere,* **77,** 1292-1298 (2009).

Waki, K., Zhao, J., Horikoshi, S., Watanabe, M. and Hidaka, H., "Concentrations of polychlorinated dibenzo-p-dioxins and polychlorinated dibenzofurans in soil in the vicinity of a landfill", *Chemosphere,* **41,** 337-342 (2000).

Weber, H. and Bresser, R., "Spectrophotometric and spectrofluorimetric methods for the determination of dothiepin hydrochloride in its pure and dosage forms using Eosin. *Pharmazie*, **51,** 52-155 (1996).

Wessel, J. C., Matyja, M., Neugebauer, M., Kiefer, H., Daldrup, T., Tarbah, F. A. and Weber, H., "Characterization of oxalic acid derivatives as new metabolites of metamizol (dipyrone) in incubated hen's egg and human", *J. Pharmaceut. Sci.,* **28,** 15-25 (2006).

Wiegel, A., Aulinger, R., Brockmeyer, H., Harms, J., Loffler, H., Reincke, R., Schmidt, B., Stachel, W., Tumpling, A. and Wanke, V., "Pharmaceuticals in the river Elbe and its tributaries", *Chemosphere,* **57,** 107–126 (2004).

Zepp, R. G., Faust, B. C., Hoigne, J., "Photoproduction of hydrated electrons from natural organic solutes in aquatin environments", *Environ. Sci. Technol.*, **26,** 313–319 (1992).

Zhou, W. and Moore, D. E., "Photochemical decomposition of sulfamethoxazole," *Int. J. Pharm.,* **110,** 55-63 (2011).

CHAPTER 6

Mixed Drug Decomposition: Comparison to Individual Drug Mineralization, Evolution of Inorganic ions and Toxicity Assay

A comparative degradation study from the mixture (termed as CCD mixture) of Chloramphenicol (CHPL), Ciprofloxacin (CIP) and Dipyrone (DIPY) is investigated in this chapter. Determination and quantification of inorganic ions along with the antimicrobial activity of CCD mixture are also carried out.

6.1 Introduction

Industrial and municipal wastewater contains a number of PhACs rather than a single drug (Table 6.1). There are several reports that PhACs in a mixture could show added toxic effects than a single PhAC. Cleuvers et al. (2003) investigated ecotoxicity of ten pharmaceutical compounds using three different aquatic organisms and most of the compounds exhibited moderate toxic effects. They showed that the mixture of different pharmaceuticals displayed stronger toxicities than likely to be for a single compound. Pomati et al. (2006) studied the effects of mixture of thirteen therapeutic drugs on human embryonic cells. The mixed drug system caused upto 30% reduction in cell proliferation.

In addition, PhACs treatment by AOPs could give different extent of decomposition in mixture and singly. The rate of composition of sulfamethoxazole, oxtetracycline, and

ciprofloxacin is influenced by solution pH when treated singly but not in their mixture by polychromatic UV treatment (Avisar et al., 2010). HCO_3^- and NO_3^- added separately reduced the rate of degradation of five PhACs out of six in UV/H_2O_2 process (Yuan et al., 2013). However, Cl^- did not show any specific impact on the decomposition even through Cl^- acts as a $HO^\bullet$ scavenger and it could also generate chlorine atom ($Cl^\bullet$) and dichloride anion radicals ($Cl_2^{\bullet-}$) (Anipsitakis et al., 2006).

It is prudent that research should be focused on pharmaceutical mixture along with the single compound. Three pharmaceutical compounds i.e., CHPL, CIP and DIPY in continuation of the earlier studies with single system (Chapters 3, 4 and 5) and also based on their occurrence in the environment were selected (Lei et al., 2011; Larsson et al., 2007; Wiegel et al., 2004; Kramer et al., 1984). This work investigates how the mineralization efficiency and antimicrobial activity of CHPL+CIP+DIPY (CCD) could vary when present in a mixture and individually in FP, PFP and UVP. Moreover, the mechanism of their degradation is explored through identification intermediates in mass spectra and inorganic ion formation.

Table 6.1. Concentration and organic loading of pharmaceutical effluents.

Effluent	Compounds/pollutants	Concentrations, mg/L	TOC, mg/L	Sources
STP	Paracetamol, Chloramphenicol and Diclofenac	0.5-30	Avg. 22.5	Mowla et al., 2012
	Camphor, Octocrylene, Ethylhexyl methoxycinnamate, Dipyrone etc	55×10^{-6} - 7.0	48-342	Feldmann et al., 2008; Kupper et al., 2006
	Sulfadiazine, Sulfamethoxazole, Ofloxacin and Chloramphenicol	0.0017-0.0079	10-27	Peng et al., 2006
Hospital	Ciprofloxacin, Hydrochlorthiazide, Ibuprofen, N-acetyl-4-amino antipiryne, Naproxen, Nicotine, Ofloxacin	0.20-0.50	0.4-1.0	Murgolo et al., 2014
	Acetaminophen, Acetylsalicylic acid, 17α-ethinylestradiol, Ibuprofen, Metoprolol and Progesterone	61.7- 83.4	Avg. 50	Musson et al., 2010
	Carbamazepine, Ciprofloxacin, Citalopram hydrobromide hydrochlorothiazide, Metoprolol, Omeprazole, Venlafaxine	87-130	Avg. 9.6	Rosal et al., 2010

6.2 Results and discussion

6.2.1 Drugs removal and mineralization

The reaction condition was selected based on the earlier studies on DIPY decomposition (Chapter 5). The solution pH, Fe^{2+} and H_2O_2 doses were of 3.5, 2.25 mM and 22.5 mM, respectively. The experiments were carried out with an equimolar concentration (0.05 mM) of the individual compound. All individual treatment was performed with 0.15 mM concentration. The same parametric setting was adopted for CIP, CHPL and CCD mixture. The results of drug and TOC removal at 45 min of reaction time are shown in Figures 6.1 to 6.3. The percentage removal of drug in CCD mixture is calculated with respect to the initial concentration of 0.05 mM. The decomposition of drug was somewhat less when present singly than their mixture. Similar results were obtained in case of mineralization.

CHPL degradation of 89.6, 94.7 and 83.7% (Figure 6.1) was noted when treated individually in FP, PFP and UVP, respectively. The decomposition efficiency dropped to 86.2, 91.6 and 79.6% in CCD mixture under identical condition. UV irradiation alone did not show notable effect on its degradation. TOC removal (TOC_{mix}) fell down to 41.6, 44.2 and 41.0% in CCD mixture from 57.4, 61.4 and 47.3% when treated singly (TOC_m) in FP, PFP and UVP, respectively. The decrease in drug and TOC removal is might be due to evolution of different types of inorganic ions and low molecular weight intermediates. Liao et al. (2001) reported that the degradation efficiency of n-chlorobutane (BuCl) was hindered due to production of common ions such as NH_4^+, NO_3^-, HCO_3^- and CO_3^{2-} and low molecular intermediates (Segura et al., 2012). Bennedsen et al. (2011) claimed that increase in Cl^- concentration caused reduction of perchloroethylene due to $HO^\bullet$ scavenging.

CIP and DIPY removal (Figure 6.1) were of 80.1 and 94.6% at 45 min when treated alone in FP. It dropped to 75.8 and 89.0% in CCD mixture (Figures 6.1 to 6.3). FP exhibited TOC removal of 39.3 and 67.1% in individual drug treatment for CIP and DIPY, respectively. Similarly, CIP and DIPY removal were of 90.1 and 98.1% in PFP (Figure 6.2). Removal efficiency fell down to 89.7 and 93.5% in CCD mixture. TOC removal was found to be 49.3 and 71.1% for CIP and DIPY, respectively. UVP gave about 78.4 and 89.7% removal of CIP and DIPY (Figures 6.3) and it decreased to 65.8 and 84.6% in CCD mixture. TOC removal was found to be 36.7 and 63.1% for CIP and DIPY, respectively.

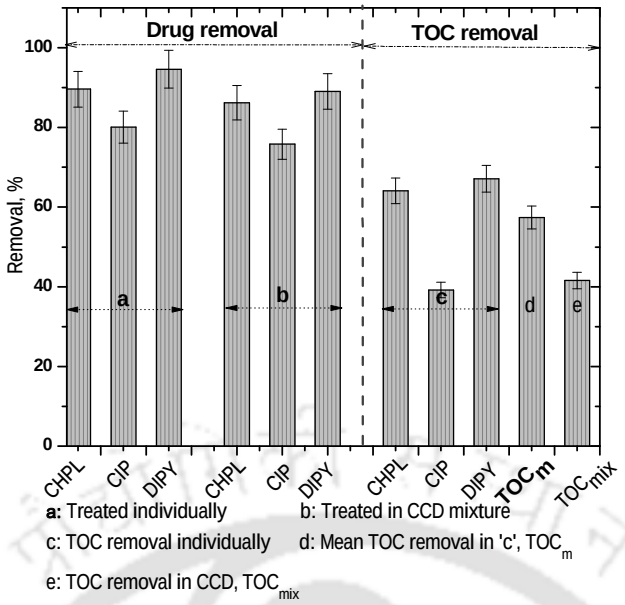

Figure 6.1. Drug and TOC removal with reaction time in FP. Experimental condition: $[\text{Single drug}]_0$ = 0.05 mM, $[\text{CCD}]_0$ = 0.15 mM, Fe^{2+} = 2.25 mM, H_2O_2 = 22.5 mM, pH = 3.5, reaction time = 45 min and temperature = 25°C.

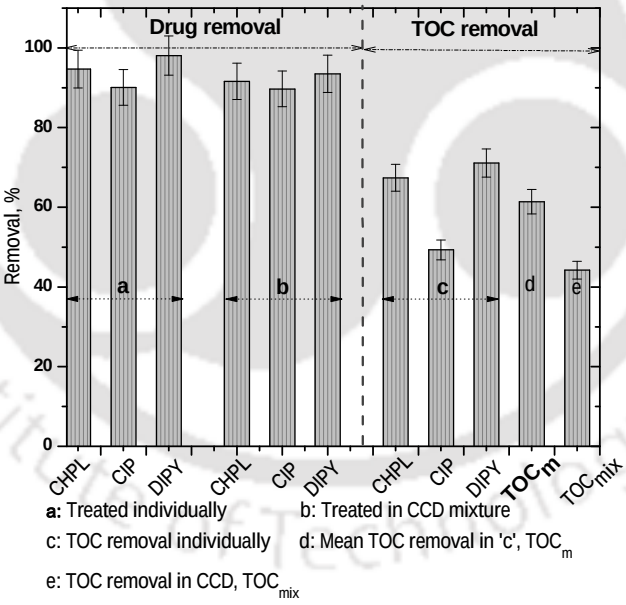

Figure 6.2. Drug and TOC removal with reaction time in PFP. Experimental condition: $[\text{Single drug}]_0$ = 0.05 mM, $[\text{CCD}]_0$ = 0.15 mM, Fe^{2+} = 2.25 mM, H_2O_2 = 22.5 mM, pH = 3.5, reaction time = 45 min and temperature = 25°C. Photo-reaction with an UV lamp of 12 W/m^2 (9 W).

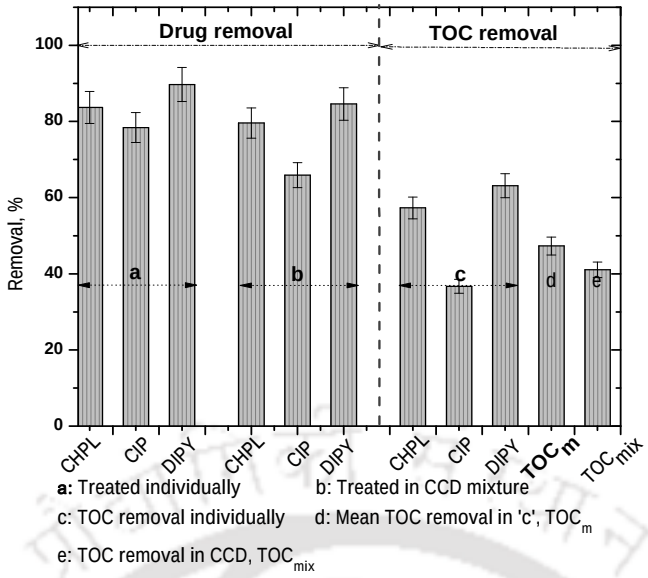

Figure 6.3. Drug and TOC removal with reaction time in UVP. Experimental condition: $[\text{Single drug}]_0$ = 0.05 mM, $[\text{CCD}]_0$ = 0.15 mM, H_2O_2 = 22.5 mM, pH = 3.5, reaction time = 45 min and temperature = 25°C. Photo-reaction with an UV lamp of 12 W/m^2 (9 W).

6.2.2 Effect of foreign anions

Formation of different types of inorganic ions such as Cl^-, F^-, NO_3^- and NH_4^+ could have significant influences on degradation of CHPL, CIP and DIPY. The ion chromatograph obtained in CCD decomposition shows that Cl^-, NO_3^-, F^- and NH_4^+ were the predominant anions (Figure 6.4) and cations (Figure 6.5). In this study, three inorganic anions i.e., Cl^-, NO_3^- and F^- were added one at a time and their effects on drug decomposition was explored.

The results are plotted in Figures 6.6 to 6.8. 10 mM of NaCl, $NaNO_3$ and NH_4F were added to have the same concentration of the anions. CHPL removal was about 89.6, 94.7 and 83.7 % without addition of foreign anion in FP, PFP and UVP, respectively. It decreased to 83.0, 89.1 and 86.9% in FP in presence of Cl^-, NO_3^- and F^-, respectively (Figure 6.6). PFP showed CHPL decomposition of 79.7, 87.0 and 87.3% (Figure 6.7). It was about 71.6, 73.3 and 75.4% in UVP (Figure 6.8). Homolytic cleavage of C-Cl bond could occur in presence of UV-irradiation. The order of Cl^-, F^- and NO_3^- inhibition was as $Cl^- >> NO_3^- > F^-$ in case of CHPL. Cl^-, NO_3^- and F^- exhibited a reduction in CIP degradation of 4.7, 4.8 and 7.6% in FP, 6.4, 4.4 and 12.4% in PFP and, 6.1, 3.1 and 8.3% in UVP determined against 80.1, 89.7 and

57.6% in CCD without addition of anions. Whereas, DIPY decomposition was not affected much in presence of these anions.

It gives an indication that addition of same anion originated upon degradation of the compound inhibited the efficiency moderately. Cl^- and F^- added externally (10 mM) reduced CHPL and CIP decomposition of 11.9 and 12.4%. Yuan et al. (2013) reported that the reaction of Cl^- with $HO^\cdot$ forming $ClOH^-$ is reversible and the increasing concentration of Cl^- inhibites the decomposition reaction by $HO^\cdot$ consumption.

NO_3^- also could hinder degradation efficiency (Sillanpaa et al., 2011). NO_3^- acts more strongly as UV absorber than $HO^\cdot$ scavenger (H_2O_2) (Eqs. 6.1 to 6.5). But the influence was insignificant for CCD mixture. NH_4^+ ions are first formed and then oxidized to NO_3^- (Segura et al., 2012). NH_4^+ concentration was found to be very less (0.019 mg/L). NO_3^- ions also plays an important role in PFP because of its conversion to nitrite (NO_2^-) (Eq. 6.1) (Sillanpaa et al., 2011). NO_3^- photolysis hinders production of $HO^\cdot$ radicals (Eqs. 6.1 to 6.5). The effect of UV shielding of NO_3^- is more significant than formation of $HO^\cdot$ by NO_3^- photolysis (Sillanpaa et al., 2011). Park et al., (2008) reported inhibiting effect of NO_2^- on volatile organic carbon (VOC) degradation during photolysis. Progressive accumulation of NO_2^- causes $HO^\cdot$ depletion.

$$NO_3^- + h\nu \rightarrow NO_2^- + O \quad (6.1)$$

$$NO_3^- + H^+ \rightarrow NO_2^\cdot + HO^\cdot \quad (6.2)$$

$$NO_2^- + HO^\cdot \rightarrow NO_2^\cdot + OH^- \quad (6.3)$$

$$H_2O_2 + HO^\cdot \rightarrow H_2O + H^+ + O_2^{\cdot -} \quad (6.4)$$

$$2NO_2^\cdot + H_2O \rightarrow NO_2^- + NO_3^- + 2H^+ \quad (6.5)$$

The concentration of Cl^-, NO_3^- and F^- ions were found to be 0.47, 1.27 and 0.087 mg/L after 45 min of PFP (Figure 6.4). The same were 0.37, 0.96 and 0.053 mg/L in FP. Cl^-, NO_3^- and F^- of 0.23, 0.87 and 0.036 mg/L were formed in UVP (Figure 6.4). NH_4^+ concentration (Figure 6.5) were found to be 0.0.89, 0.063 and 0.049 mg/L in FP, PFP and UVP, respectively. The concentrations of the ions were calculated from the difference between the initial (if any) and the final amount present in the solution.

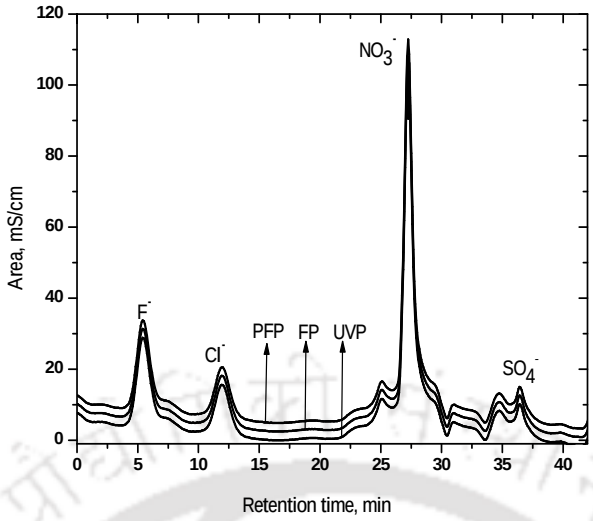

Figure 6.4. Ion chromatograph of an anion during CCD treatment. Experimental condition: $[\text{Single drug}]_0$ = 0.05 mM, $[\text{CCD}]_0$ = 0.15 mM, Fe^{2+} = 2.25 mM (in FP and PFP), H_2O_2 = 22.5 mM (in FP, PFP and UVP), pH = 3.5, reaction time = 45 min and temperature = 25°C. Photo-reaction with an UV lamp of 12 W/m^2 (9 W).

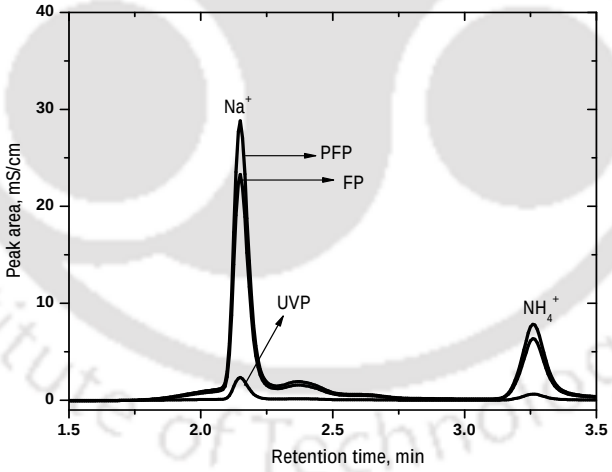

Figure 6.5. Ion chromatograph of cations formed during CCD treatment. Experimental condition: $[\text{Single drug}]_0$ = 0.05 mM, $[\text{CCD}]_0$ = 0.15 mM, Fe^{2+} = 2.25 mM (in FP and PFP), H_2O_2 = 22.5 mM (in FP, PFP and UVP), pH = 3.5, reaction time = 45 min and temperature = 25°C. Photo-reaction with an UV lamp of 12 W/m^2 (9 W).

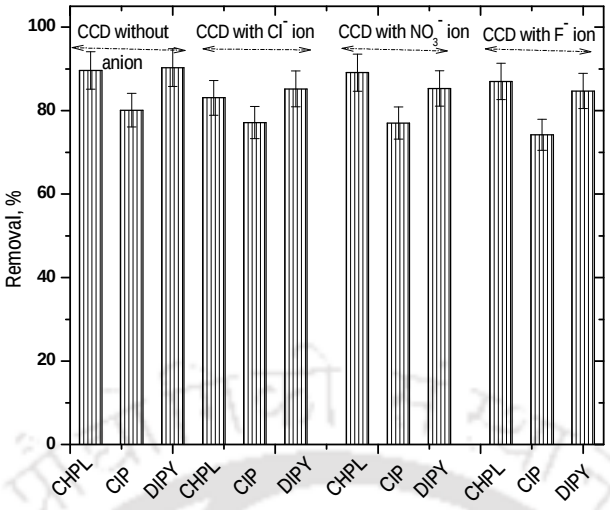

Figure 6.6. Effect of Cl^-, NO_3^- and F^- ions on drug decomposition in FP. Experimental condition: $[Single\ drug]_0$ = 0.05 mM, $[CCD]_0$ = 0.15 mM, Fe^{2+} = 2.25 mM, H_2O_2 = 22.5 mM, pH = 3.5, reaction time = 45 min and temperature = 25°C.

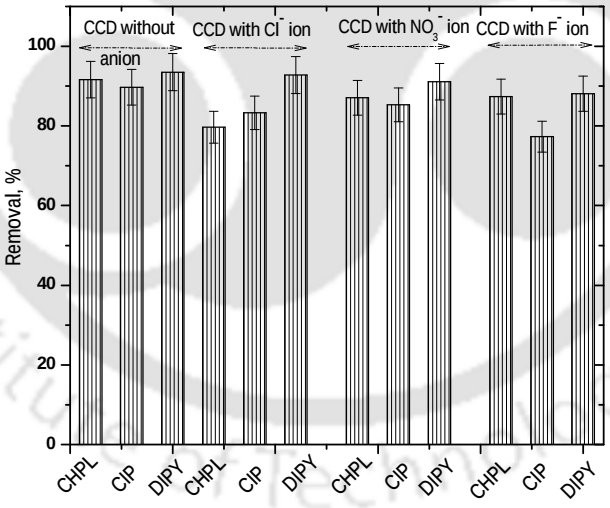

Figure 6.7. Effect of Cl^-, NO_3^- and F^- ions on drug decomposition in PFP. Experimental condition: $[Single\ drug]_0$ = 0.05 mM, $[CCD]_0$ = 0.15 mM, Fe^{2+} = 2.25 mM, H_2O_2 = 22.5 mM, pH = 3.5, reaction time = 45 min and temperature = 25°C. Photo-reaction with an UV lamp of 12 W/m^2 (9 W).

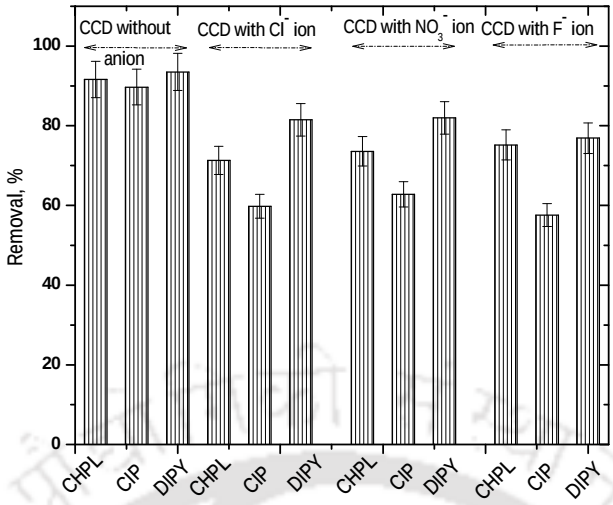

Figure 6.8. Effect of Cl^-, NO_3^- and F^- ions on drug decomposition in UVP. Experimental condition: $[Single\ drug]_0$ = 0.05 mM, $[CCD]_0$ = 0.15 mM, H_2O_2 = 22.5 mM, pH = 3.5, reaction time = 45 min and temperature = 25°C. Photo-reaction with an UV lamp of 12 W/m^2 (9 W).

6.2.3 Degradation pathways and formation of inorganic ions

The mass spectrum of CCD mixture in PFP is shown in Figure 6.9. Figures 6.10 to 6.12 illustrate the formation routes of inorganic ions through cleavage of individual drug in CCD mixture. The discussion is limited to PFP. Likewise, the similar pathways can be developed in FP and UVP. It can be grossly said that the formation of higher molecular weight intermediates were more in CCD mixture than singly (Trovo et al., 2013; Section 3.1 of Chapter 3, Section 4.4.5 of Chapter 4 and Section 5.2.5 of Chapter 5), probably due to enhanced chelation and polymerization.

C_1 and C_2 are the two asymmetry centres of CHPL molecules with weakly bonding to hydrogen atoms (Figure 6.10). It can be easily abstracted by $HO^{\bullet}$ (Csay et al., 2012). The neucleophilicity of both the centres increases due to presence of amide group to C_2 centre (Csay et al., 2012; Finar et al., 2001). Majors routes for CHPL cleavage forming Cl^- and NO_3^- ions are presented in Figure 6.10. D_1 (m/z 302.16), an alkene type compound, yielded by dehydration (Nie et al., 2014) with elimination of –OH group attached to α-carbon with respect to C_2 centre.

D_2 (m/z 279.01) and D_3 (m/z 280.13) molecules could form on cleavage of aliphatic amide side chain (Nie et al., 2014). D_3 molecule was further broken by $HO^{\cdot}$ attack to its carbonyl centre with release of NO_3^- and Cl^- ions. $HO^{\cdot}$ radical attracts Cl^- atom due to its electrophilic nature forming HOCl (Nie et al., 2014). D_4 (m/z 281.14) was formed by hydroxylation of side amide chain of CHPL molecule and simultaneously it get reduced to sequential products (Figure 6.10) with formation of NO_3^- ions. D_5 (m/z 298.03) molecule was originated by hemolytic cleavage of CHPL molecule forming two intermediates of molar mass of 157.11 (p- nitro benzyl alcohol) and 161.0. The later one again was oxidized to release Cl^- and NH_4^+. NH_4^+ ions were converted to NO_3^- to attain the maximum oxidation state of N-atom. p-nitrobenzyl alcohol was reduced to p- amino benzyl alcohol on hydroxylation reaction followed by dehydration reaction. p-nitro benzyl alcohol took part in dimerization reaction (Grither et al., 2012).

On oxidation, p- nitro benzyl alcohol yielded two products i.e., p- nitro benzoic acid (MW 171.4) and p-nitrophenol. First one has greater tendency to take part in intermolecular H-bonding (Finar et al., 2001) and formed D_6 molecule (m/z 361.33). Second compound was originated on oxidation followed by hydroxylation and it was converted to a dimer molecule (D_7) of p-benzoquinone with m/z = 414.20. p-nitrobenzoic acid was decarboxylated forming nitrobenzene. It originated 2-amino phenol and 1, 2-dihydroxy benzyne (catechol) through reduction followed hydroxylation. D_8 and D_9 molecules were chelates of Fe^{3+} with 2-amino phenol and catechol, respectively.

D_{10} to D_{13} products appeared on degradation of CIP molecules (Figure 6.10). Piperazine ring basically takes part in degradation reaction forming such compounds. Piperazine ring is very reactive towards electrophilic attack due to angle strain (Section 4.4.5 of Chapter 4). D_{10} (m/z 303.04) was formed on acidic hydrolysis of CIP molecule followed by partial cleavage of piperazine ring. Zhou et al. (2014) reported a similar pathway of formation of D_{10} molecule (m/z 303.04) during CIP degradation by ferrate (VI) with loss of an ethylene group from piperazine group. Defluorination (breaking of C-F) followed by hydroxylation gave D_{11} (m/z 304.11) with NaF. D_{12} (m/z 362.71) was originated from D_{10} through protonation along with partial piperazine ring breaking. Haddad et al. (2014) proposed an identical formation routes for D_{12} compound. NO_3^- ions were formed on oxidation of ethyl amine with D_{12}. NO_3^- could form on C-N bond breaking of an intermediate

compound having mass number of 239.0 (m/z). The same compound also originated D_{13} compound on dehydradion. It is an ether type compound.

4-MAA (MW 218.11) is a hydrolysis product of DIPY in presence of water soluble sulphonate group (-SO_3H) (Ergun et al., 2004). NH_4^+/NO_3^- ions were evolved on degradation of pyrazolinone structure of DIPY ((Figure 6.12). D_{14} (m/z 279.8) compound was formed by an electrophilic attack of N-hydroxyl amine to N-acyl amine. These two compounds were yielded with an aliphatic ethylamine on C-N bond breaking of pyrazolinone ring. Gomez et al. (2008) also showed the formation of 4-MAA molecule from DIPY with evolution of NH_4^+ / NO_3^- ions. NO_3^- was originated on oxidation of ethyl amine via NH_4^+ oxidation. D_{15} (m/z 467.12), an ether type compound was formed by dimerization of D_{14} followed by dehydration.

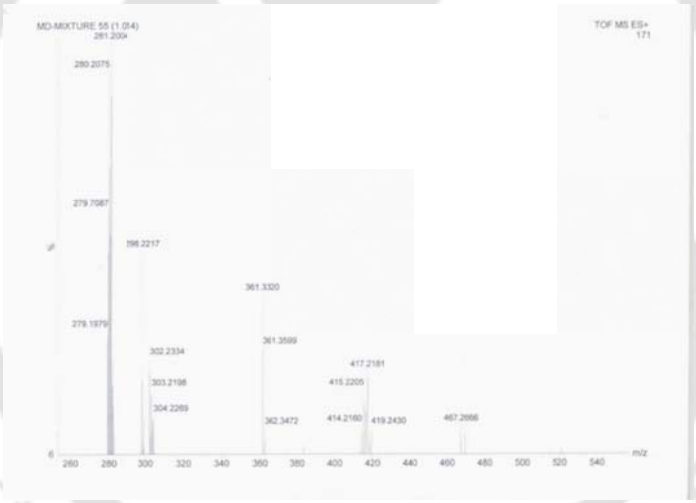

Figure 6.9. Daughter-ion spectra of CCD mixture obtained at 10 min of PFP. Experimental condition: $[Single\ drug]_0$ = 0.05 mM, $[CCD]_0$ = 0.15 mM, Fe^{2+} = 2.25 mM, H_2O_2 = 22.5 mM, pH = 3.5, reaction time = 45 min and temperature = 25°C. Photo-reaction with an UV lamp of 12 W/m^2 (9 W).

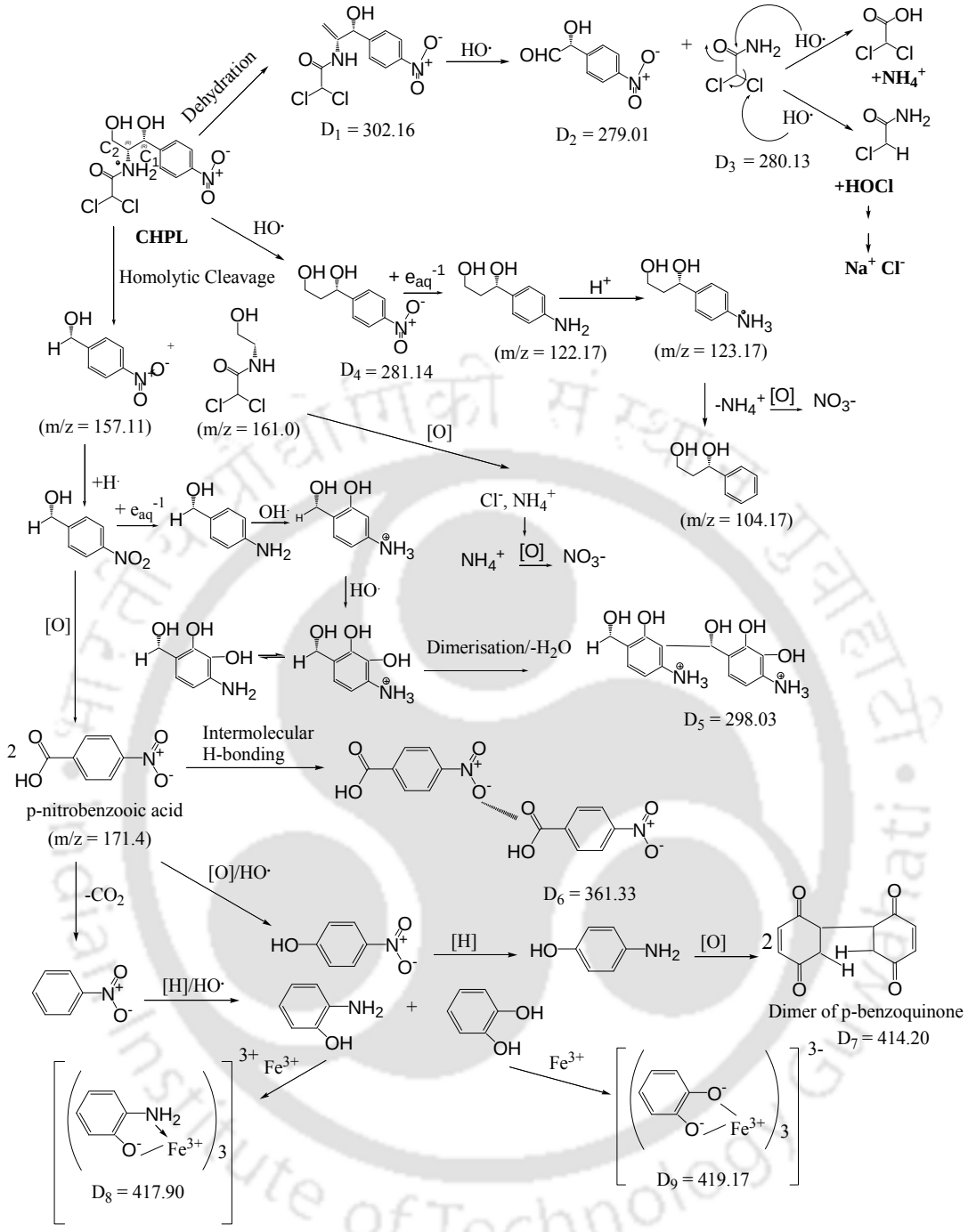

Figure 6.10. Routes of inorganic ion evolution and CHPL decomposition in PFP. Experimental condition: [Single drug]$_0$ = 0.05 mM, [CCD]$_0$ = 0.15 mM, Fe^{2+} = 2.25 mM, H_2O_2 = 22.5 mM, pH = 3.5, reaction time = 45 min and temperature = 25°C. Photo-reaction with an UV lamp of 12 W/m^2 (9 W).

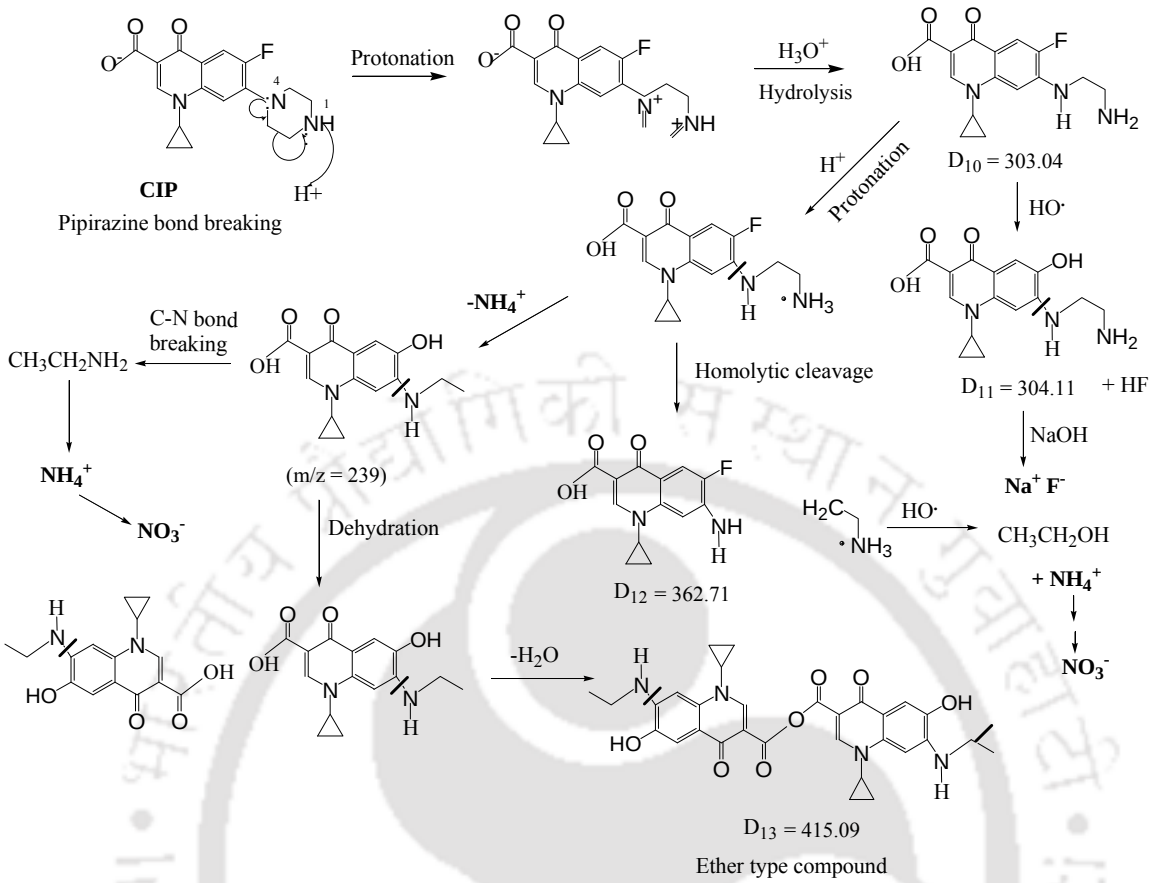

Figure 6.11. Routes of inorganic ion evolution and CIP decomposition in PFP. Experimental condition: $[\text{Single drug}]_0$ = 0.05 mM, $[\text{CCD}]_0$ = 0.15 mM, Fe^{2+} = 2.25 mM, H_2O_2 = 22.5 mM, pH = 3.5, reaction time = 45 min and temperature = 25°C. Photo-reaction with an UV lamp of 12 W/m^2 (9 W).

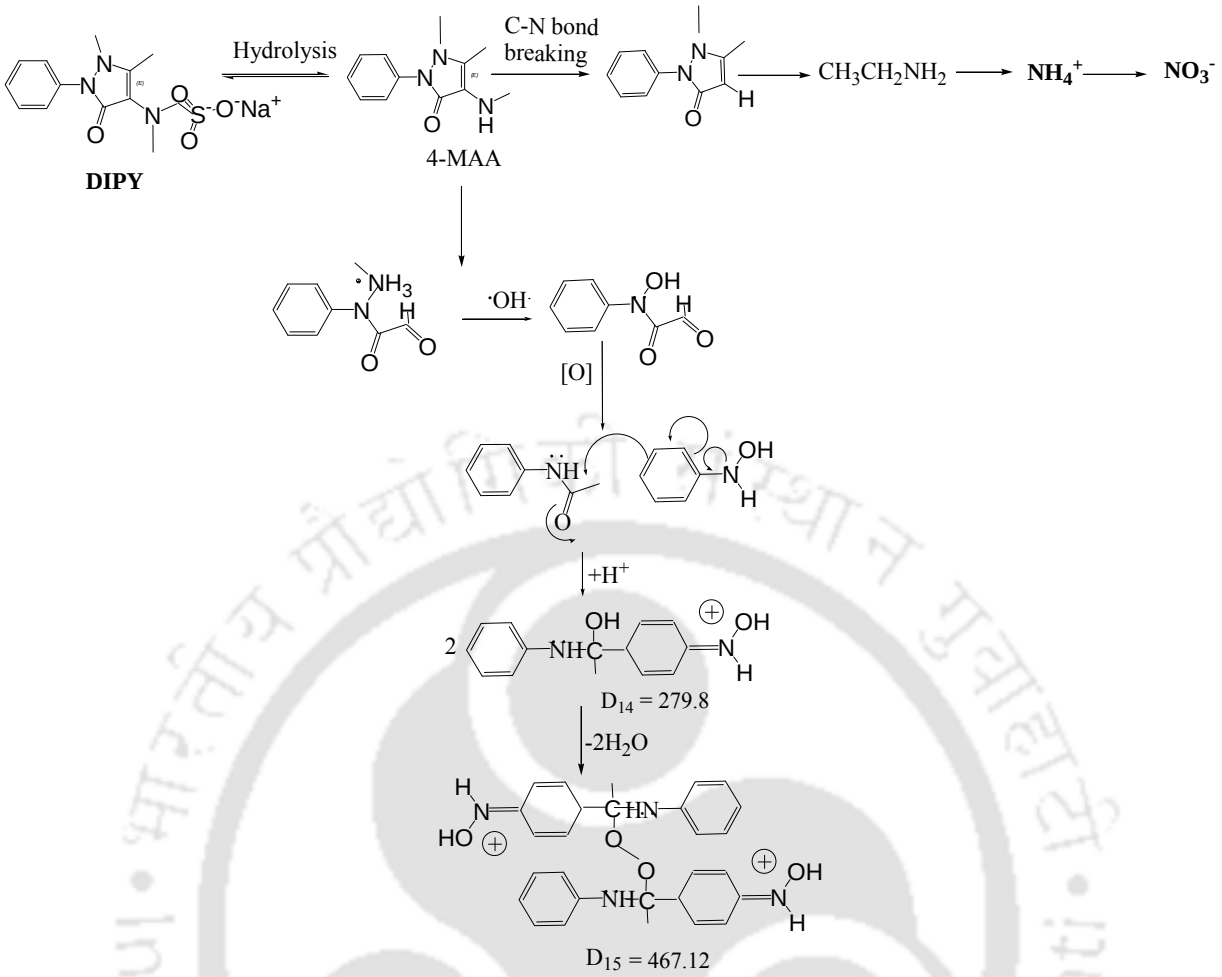

Figure 6.12. Routes of inorganic ion evolution and DIPY decomposition in PFP. Experimental condition: $[\text{Single drug}]_0$ = 0.05 mM, $[\text{CCD}]_0$ = 0.15 mM, Fe^{2+} = 2.25 mM, H_2O_2 = 22.5 mM, pH = 3.5, reaction time = 45 min and temperature =25°C. Photo-reaction with an UV lamp of 12 W/m^2 (9 W).

6.2.4 Antimicrobial activity of drug mixture and its decomposition products

The toxicity of CCD mixture and its intermediates to *E. coli* bacteria in LB media is shown in Table 6.2. The exposure time was 24 h. The growth of *E. coli* was around ~8.13×10^7 CFU/mL in the control media (LB+deionized water). The growth was totally suppressed in 0.05 mM equimolar CCD mixture. The cell count was only about 2.3% (~0.19×10^7 CFU/mL) of the control media. The exposure of *E. coli* in CCD mixture caused about 59.4, 53.2 and 74.1% cell death with respect to the control media in FP, PFP and UVP, respectively.

The results of biodegradability index and antimicrobial activity test of *E. coli* bacteria (also referred as toxicity) outlined in different Chapters are now summarized in Table 6.2. The results imply that untreated drug solutions were essentially non-biodegradable in nature and it caused more than 93% death of *E. coli* bacteria. PFP gave higher biodegradability and lower cell death irrespective to the PhACs used in this study; whereas 4-MAA (DIPY) showed greater biodegradability and less toxicity both in single drug and CCD treatment in PFP compared to CHPL and DIPY. The ease of biodegradability and growth of *E. coli* followed the order as PFP>>FP>UVP>UVPC (only for DIPY) both in single drug and CCD treatment.

Table 6.2. Biodegradability index and antimicrobial activity assay in single drug and CCD treatment.

Process	Single treatment						CCD treatment	
	BI			AMC			BI	AMC
	CHPL	CIP	DIPY	CHPL	CIP	DIPY		
Drug solution	0.17	0.09	0.12	97.6	98.4	93.07	0.21	97.6
FP	0.47	0.44	0.62	55.8	59.4	56.1	0.39	61.2
PFP	0.62	0.53	1.51	35.2	53.2	35.8	0.47	57.0
UVP	0.37	0.33	0.47	63.7	83.7	61.7	0.29	86.7
UVPC	-	-	0.31	-	-	79.0	-	-

BI = Biodegradability index, BOD_5/COD
AMC = Antimicrobial activity, % death

6.3 Major Findings

No significant difference for drug decomposition in single and CCD system of CHPL, CIP and DIPY was noted at pH 3.5, Fe^{2+} 2.25 mM and H_2O_2 22.5 mM with and without UV light illumination in absence of foreign anions. However, mean TOC_{mix} reduction in single drug system was about 16, 17 and 5.7% lower over TOC_{mix} in FP, PFP and UVP, respectively. Prior presence of anions in solution decreased its evolution by drug degradation due to reduction in affinity of $^{\cdot}OH$ radical attack to the more electrophilic centres. Cl^- and F^- addition reduced CHPL and CIP decomposition of 6.5 and 6% in FP against 12 and 12.4% in PFP and 4.2 and 2.2% in UVP, respectively. The mechanism of drug decomposition suggests that the heteroatoms led to formation the respective ions like Cl^-, F^-, NH_4^+ and NO_3^-. The linear intermediates formed due to cleavage of side chain, quinolone moiety and pyrazolinone moiety of CHPL, CIP and DIPY, respectively, was transformed into carboxylic acids or CO_2. The effluent treated in UVP suppressed the bacterial cell growth notably than PFP and FP in CCD treatment.

References

Anipsitakis, G. P., Dionysiou, D. D. and Gonzalez, M. A., "Cobalt-mediated activation of peroxymonosulfate and sulfate radical attack on phenolic compounds. Implications of chloride ions", *Environ. Sci. Technol.,* **40,** 1000-1007 (2006).

Avisar, D., Lester, Y. and Mamane, H., "pH induced polychromatic UV treatment for the removal of a mixture of SMX, OTC and CIP from water", *J. Hazard. Mater.,* **175,** 1068-1074 (2010).

Bennedsen, L. R. and Muff, J., "Influence of chloride and carbonates on the reactivity of activated persulfate", *Chemosphere,* **86,** 1092-1097 (2012).

Cleuvers, M., "Aquatic ecotoxicity of pharmaceuticals including the assessment of combination effects", *Toxicol. Lett.,* **142,** 185-194 (2003).

Csay, T., Racz, G., Takacs, E. and Wojnarovits, L., "Radiation induced degradation of pharmaceutical residues in water: Chloramphenicol", *Rad. Phy. Chem.,* **81,** 1489-1494 (2012).

Ergun, H., Fratarelli, D. and Aranda, J. V., "Characterization of the role of physicochemical factors on the hydrolysis of dipyrone", *J. Pharmaceut. Anal.,* **35,** 479-487 (2004).

Fabre, H., Eddine, N. H., Bressolle, F. and Mandrou, B., "Stability indicating assay for dipyrone-Part I", *Analyst,* **107,** 61-66 (1982).

Feldmann, D. F., Zuehlke, S. and Heberer, T., "Occurrence, fate and assessment of polar metamizole (dipyrone) residues in hospital and municipal wastewater", *Chemosphere,* **71,** 1754 1764 (2008).

Finar, I. L., "Stereochemistry and the Chemistry of Natural Products", Volume 2, fifth ed. Holloway, London. 8-9 (2001).

Gomez, J. M., Sirtory, C. and Mezcua, M., Fernandez-Alba, A. R. and Aguera, A., "Photodegradation study of three dipyrone metabolites in various water systems: Identification and toxicity of their photodegradation products", *Water Res.,* **42,** 2698-2706 (2008).

Grither, W. R., Korang, J., Sauer, J. P., Sherman, M. P., Vanegas, P. L., Zhang, M. and McCulla, R. D., "The effect of nitro substitution on the photochemistry of benzyl benozhydroxamate: Photoinduced release of benzohydroxamic acid", *J. Photochem. Photobiol. A,* **227,** 1-10 (2012).

Hesse, M., Meier, H. and Zeeh, B., "Spectroscopic methods in organic chemistry", second ed. Thieme, New York. 15-17 (2008).

Kramer, W. G., Rensimer, E. R., Ericsson, C. D. and Pickering, L. K., "Comparative bioavailability of intravenous and oral chloramphenicol in adults", *J. Clin. Pharmacol.,* **24,** 181-186 (1984).

Jiao, S., Zheng, S., Yin, D., Wang, L. and Chen, L., "Aqueous photolysis of tetracycline and toxicity of photolytic products to luminescent bacteria", *Chemosphere,* **73,** 377–382 (2008).

Kupper, T., Plagellat, C., Brandli, R. C., de Alencastro, L. F., Grandjean, D. and Tarradellas, J., "Fate and removal of polycyclic musks, UV filters and biocides during wastewater treatment", *Water Res.,* **40,** 2603-2612 (2006).

Larsson, D. G. J., Pedro, C. and Paxeus, N., "Effluent from drug manufactures contains extremely high levels of pharmaceuticals", *J. Hazard. Mater.,* **148,** 751-755 (2007).

Lei, J., Hu, X. L., Yin, D. Q., Zhang, H. C. and Yu, Z. Y., " Occurrence, distribution and seasonal variation of antibiotics in the Huangpu River, Shanghai, China", *Chemosphere,* **82,** 822-828 (2011).

Murgoloa, S., Petronellab, S., Ciannarella, R., Comparellib, R., Agostiano, A. and Currib, M. L., "UV and solar-based photocatalytic degradation of organic pollutantsby nano-sized TiO_2grown on carbon nanotubes", *Catal. Today,* doi.org/10.1016/j.cattod.2014.04.021.

Musson, S. E., Campo, P., Tolaymat , T., Suidan, M. and Townsend, T. G., "Assessment of the anaerobic degradation of six active pharmaceutical ingredients", *Sci. of the Total Environ.,* **408,** 2068-2074 (2010).

Mowla, A., Mehrvar, M. and Dhi, R., "Combination of sonophotolysis and aerobic activated sludge processes for treatment of synthetic pharmaceutical wastewater", *Chem. Eng. J.,* **255,** 411-423 (2014).

Nie, M., Yang, Y., Zhang, Z., Yan, C., Wang, X., Li, H. and Dong, W., "Degradation of chloramphenicol by thermally activated persulfate in aqueous solution", *Chem. Eng. J.,* **246,** 373-382 (2014).

Park, J. H., Kang, S. H., Lee, J. Y., Lim, S. H., Yun, Z., Yim, S. K. and Ko, K. B., "Effects of nitrate on the UV photolysis of H_2O_2 for VOC degradation in an aqueous solution", *Environ. Sci. Technol.,* **29,** 91-99 (2008).

Peng, X., Wang, Z., Kuang, W., Tan, J. and Li, K., "A preliminary study on the occurrence and behavior of sulfonamides, ofloxacin and chloramphenicol antimicrobials in wastewaters of two sewage treatment plants in Guangzhou, China", *Sci. of the Total Environ.,* **371,** 314-322 (2006).

Pomati, F., Castiglioni, S., Zuccato, E., Fanelli, R., Vigetti, D., Rossertti, C. and Calamari, D., "Effects of a complex mixture of therapeutic drugs at environmental levels on human embryonic cells", *Environ. Sci. Technol.,* **40,** 2442-2447 (2006).

Rosal, R., Rodriguez, A., Antonio, P. M. J., Garcia-Calvo, E., Gomez, M. J., Aguera, A. and Amadeo, R., "Occurrence of emerging pollutants in urban wastewater and their removal through biological treatment followed by ozonation", *Water Res.,* **44,** 578-588 (2010).

Segura, S. G., Garrido, A. J., Rodriguez, M. R., Cabot, L. P., Centellas, F., Arias, C. and Enric, B., "Mineralization of flumequine in acidic medium by electro-Fenton and photoelectro-Fenton processes", *Water Res.,* **46,** 2067-2076 (2012).

Sillanpaa, M. E. T., Kurniawan, T. A. and Lo, W., "Degradation of chelating agents in aqueous solution using advanced oxidation process (AOP)", *Chemosphere,* **83,** 1443-1460 (2011).

Trovo, A. G., Paiva, A. B. de. V., Machado, A. E. H., Carlos, A. and Santos, R. O., "Degradation of the antibiotic chloramphenicol by photo-Fenton process at lab-scale and solar pilot plant: Kinetic, toxicity and inactivation assessment", *Solar Energy,* **97,** 596-604 (2013).

Vasconcelos, T. G., Henriques, D. M., Konig, A., Martins, A. F. and Kummerer, K., "Photo degradation of the antimicrobial ciprofloxacin at high pH: identification and biodegradability assessment of the primary by-products", *Chemosphere,* **76,** 487-493 (2009).

Verlicchi, P., Aukidy, M. A. and Zambello, A., "Occurrence of pharmaceutical compounds in urban wastewater: Removal, mass load and environmental risk after a secondary treatment - A review", *Sci. of the Total Environ.,* **429,** 123-155 (2012).

Wessel, J. C., Matyja, M., Neugebauer, M., Kiefer, H., Daldrup, T., Tarbah, F.A. and Weber, H., "Characterization of oxalic acid derivatives as new metabolites of metamizol (dipyrone) in incubated hen's egg and human", *Pharmaceut. Sci.,* **28,** 15-25 (2006).

Yuan, H., Zhou, X. and Zhang, Y., "Degradation of acid pharmaceuticals in the UV/H_2O_2 process: effects of humic acid and inorganic salts", *CLEAN-Soil Air Water*, **348,** 342-347 (2013).

Zhengwei, Z. and Jia-Qian, J., "Reaction kinetics and oxidation products formation in the degradation of ciprofloxacin and ibuprofen by ferrate(VI)", *http://dx.doi.org/10.1016/j.chemosphere.2014.04.006 (2014).*

CHAPTER 7

Conclusions, Limitations and Future Recommendations

In this chapter the salient accomplishments, limitations and major conclusions of the entire work are summarized. The directions for the further extension of the present work are also provided.

7.1 Overall Conclusions

PFP exhibited the highest degradation and mineralization efficiencies over FP, UVP and UVPC for the cleavage CHPL, CIP and DIPY from the aqueous solution. The conclusions based on the present study are:

- ✓ The maximum CHPL degradation was 93.6, 96 and 67.8% in FP, PFP and UVP, respectively. The mineralization was about 6.8 to 21.7% lower. Around 87.1% degradation of FeCHPLCOM occurred in FP and 90.3% in PFP. The cleavage of CIP reached to 74.4, 79.1 and 69.4% against mineralization efficiency of 37.9, 41.7 and 35.2% in FP, PFP and UVP. DIPY was completely hydrolyzed to 4-MAA within 30 min at pH 3.5 and temperature 25°C. The highest 4-MAA decomposition of 94.1, 96.4, 74.4

and 71.2% were noted against mineralization efficiency of 49.3, 58.2, 47 and 24.6% in FP, PFP, UVP and UVPC, respectively.

- ✓ Most of the intermediates were formed by the degradation of side chain of CHPL molecule and aliphatic amide chain was cleaved by $HO^{\bullet}$ attack at C_2 centre. The faster initial rate of TOC reduction was resulted from hydrolysis of amide chain and the slow second stage was associated with the opening of substituted benzene ring.

- ✓ Four primary daughter ions were originated upon cleavage of CIP and MONC increased from 1.27 to 2.1 at the optimal treatment condition. The proposed 2^{nd} order kinetic model for the decomposition of both CIP and degradation products (DP_s) exhibited excellent agreement to the experimental data. The rate constant of CIP and DP_s oxidation was obtained between the range from 2.19×10^3 to 5.07×10^3 and 3.57×10^3 to 6.91×10^3 1/M.s, respectively. The model gave an initial hydroxyl radical concentration of 11.30 to 11.74 µM.

- ✓ UVPC formed more hydroxylated intermediates of DIPY resulted from the attack of $HO^{\bullet}$ at the catalyst surface. Total twenty nine intermediate products appeared in the mass spectra within the mass to charge ratio of 100 to 400 in four oxidation processes from the same parent molecule. The pyrazolinone ring was degraded preceded by cleavage of methyl moieties. The proposed mechanism implies that most of the intermediates were originated by the pyrazolinone ring degradation.

- ✓ Slightly lower mineralization efficiency of CHPL, CIP and DIPY was noted in an equimolar CCD mixture compared to the individual drug degradation. Cl^- and F^- were originated upon degradation of CHPL and CIP and its addition inhibited the decomposition efficiency of CHPL and CIP by about 11.9 and 12.4%, respectively. NO_3^- commonly formed didn't suppress decomposition of drugs both in singly and CCD mixture. Hetero-atoms were converted into their respective ions like Cl^-, F^-, NH_4^+ and NO_3^-. PFP exhibited the 'highest' biodegradability and 'lowest' antimicrobial activity irrespective to the type of drug and treatment process both in singly and CCD mixture.

7.2 Limitations of the Work

- The present study acted on the fixed concentration of individual drug both in single and mixed drug system. The concentration used was much higher than a PhAC commonly present in industrial and municipal wastewater. This is one of the limitations of the work. Even though the concentration of individual PhAC varies from ng/L to µg/L, however, the cumulative concentration is as high as few hundred mg/L (Table 6.1). This was the main reason of taking higher drug concentration so that it could give higher TOC value (Table 6.1). The mechanistic aspects, iron-chelation and kinetic approach elucidated even at high concentration would provide significant information on drug degradation that would be useful for real application and understanding the process.

- The number of compounds present in an industrial effluent is many and it varies from the sites to sites. Also the background ions could alter the treatment efficiency as well as the antimicrobial activity. The percentage death of *E. coli* in treated CHPL, CIP and DIPY solutions was 21.8, 3.8 and 21.2 % lower in PFP compared to CCD system. The mixture of three drugs in presence of common ions could suppress the decomposition efficiency by about 1.2 to 15.1, 0.7 to 16.2 and 1.9 to 35.8 % in FP, PFP and UVP compared to CCD mixture. The background ions added in CCD solution will help to uncover their influence on treatment efficiency that could be anticipated in an industrial effluent.

- It is generally accepted that the state-of-the art electron spins resonance spectroscopy gives a better estimation of $HO^{\bullet}$ radicals over DMSO probe method. Nevertheless, DMSO is highly water soluble and does not form complexes with iron or other metals ions.

7.3 Recommendations for the Future Work

- The present study can be extended for the degradation of ß-blockers, steroids, different classes of antibiotics and antipyretic compounds to understand the cleavage pathways and antimicrobial behavior.

- The degradation mechanisms and, particularly, the kinetics in aqueous solution are quite different to those running in a complex pharmaceutical matrix. The present work can be carried forward for industrial effluent treatment in order to develop some kind of correlations between them.

- The future study should focus on the electronic interactions between other 3d-trasition metals used as catalyst in AOPs and PhACs as a chelating agent.

- The future work may include fabrication of photocatalyst for solar light assisted pharmaceutical wastewater detoxification.

- The studies on AOPs followed by biological treatment of pharmaceutical effluent are also a prudent area of future research.

Publications

Journal Papers

A.S. Giri and A.K. Golder, "Formation of Fe(II)-Chloramphenicol chelate and its decomposition in Fenton and Photo-Fenton: Identification and biodegradability assessment of primary by products", ***Ind. Eng. Chem. Res.*** **doi: 10.1021/ie501508d**.

A.S. Giri and A.K. Golder, "Fenton, Photo-Fenton, H_2O_2-photolysis and TiO_2 photo-catalysis for Dipyrone oxidation: Drug removal, mineralization, biodegradability and degradation mechanism", ***Ind. Eng. Chem. Res.*** 2014, 53 (4), 1351-1358.

A.S. Giri and A. K. Golder, "Ciprofloxacin degradation from aqueous solution by Fenton oxidation: Reaction kinetics and degradation mechanisms", ***RSC Adv.*** 2014, 4, 6738-6745.

A.S. Giri and A. K. Golder, "Kinetics and mechanisms of Ciprofloxacin cleavage in light assisted Fenton reaction***", Int. J. Rec. Res. Sci. Technol.*** 2014, 6(1), 78-82.

A.S. Giri and A. K. Golder, "Drug mixture decomposition in photo-assisted Fenton process: comparison to singly treatment, evolution of inorganic ions and toxicity assay", ***Chemosphere*** (**Under review**).

Conference Publications

A.S. Giri and A.K. Golder, "Degradation of pharmaceutical from wastewater: Oxidative Fenton process", Chemical Engineering Congress (CHEMCON-2011), 27-30th December, 2011, Bangalore, India.

A.S. Giri and A.K. Golder, "Fenton oxidation process for the removal of an antimicrobial drug from wastewater", 2nd International Conference on Advanced Oxidation Processes (AOP 2012), 5-8th October, 2012, Kottayam, Kerala.

A.S. Giri and A.K. Golder, "Oxidative degradation of Dipyrone from wastewater using Fenton reagent", Indian Chemical Engineering Congress (CHEMCON-2012), 27-30th December, 2012, Dr. B.R. Ambedkar National Institute of Technology, Jalandhar, Punjab, India.

A.S. Giri and A.K. Golder, "Dynamics of photo Fenton process for Dipyrone degradation and hydroxyl radical quantification", International Exhibition and Conference on Water Technologies and Environmental Technology and Renewable Energy (OMICS group), 11-14th February, 2013, Mumbai, India.

A.S. Giri and A.K. Golder, "Mechanism and identification of reaction byproducts for the degradation of Chloramphenicol drug in heterogeneous photo-catalytic Process", International Conference on Chemical and Bioprocess Engineering (ICCBPE-2013), 16-17th November, 2013, National Institute of Technology Warangal, Andhra Pradesh, India.

A.S. Giri and A.K. Golder , "Mechanism and identification of reaction byproducts for the degradation of an antibiotic drug in heterogeneous photo-catalysis using TiO_2", International Conference on Frontiers in Chemical Engineering (ICFCE-2013), 9-11th December, 2013, NIT Rourkela, India.

A.S. Giri and A.K. Golder, "Photolytic decomposition of aqueous Ciprofloxacin: Transformation products and mechanisms", Indian Chemical Engineering Congress (CHEMCON-2013), 27-30th December, 2013, Institute of Chemical Technology, Mumbai, India.

A.S. Giri and A.K. Golder, "Kinetics and mechanisms of Ciprofloxacin cleavage in light assisted Fenton reaction", Emerging Challenges and Issues in Environmental Protection, 23-24th January, 2014, Raipur Institute of Technology, Raipur (C.G.), India.

****